

# Supporting Information 1

## Design space for complex DNA structures

Bryan Wei<sup>1,2</sup> Mingjie Dai<sup>1,3</sup> Cameron Myhrvold<sup>1,2</sup> Yonggang Ke<sup>1,4</sup> Ralf Jungmann<sup>1,2</sup> Peng Yin<sup>1,2\*</sup>

Wyss Institute for Biologically Inspired Engineering, Harvard University, Boston, MA 02115<sup>1</sup>,  
Department of Systems Biology, Harvard Medical School, Boston, MA 02115<sup>2</sup>,  
Program in Biophysics, Harvard University, Boston, MA 02115<sup>3</sup>,  
Dana Farber Cancer Institute, Boston, MA 02215<sup>4</sup>  
E-mail address\*: py@hms.harvard.edu

### Contents

<b>SI1 Self-assembly of structures from different motifs</b>	<b>S1</b>
SI1.1 Agarose gel electrophoresis results . . . . .	S1
SI1.2 Effect of annealing conditions on the assembly of structures of different motifs . . . . .	S2
SI1.3 AFM imaging results . . . . .	S4
SI1.4 Structure conformation variation . . . . .	S37
SI1.5 Distance measurements . . . . .	S38
<b>SI2 Curvature design and characterization</b>	<b>S39</b>
SI2.1 Curvature: design and modeling . . . . .	S39
SI2.1.1 Domain shift . . . . .	S39
SI2.1.2 Parallel helix design . . . . .	S39
SI2.1.3 Corrugation design . . . . .	S40
SI2.2 Agarose gel electrophoresis results . . . . .	S43
SI2.3 AFM imaging results . . . . .	S44
SI2.4 TEM imaging results . . . . .	S49
SI2.5 AFM-based landing assay results . . . . .	S52
SI2.6 Summary . . . . .	S55
<b>SI3 Twist analysis</b>	<b>S55</b>
SI3.1 AFM imaging results . . . . .	S55
SI3.2 TEM imaging results . . . . .	S58

## SI1 Self-assembly of structures from different motifs

### SI1.1 Agarose gel electrophoresis results

Fig. SI1 shows the results of native agarose gel electrophoresis for structures of different motifs. The annealed samples (or gel-purified samples after annealing, as explained below) were subjected to AFM imaging shown in Fig. SI5 to Fig. SI35.

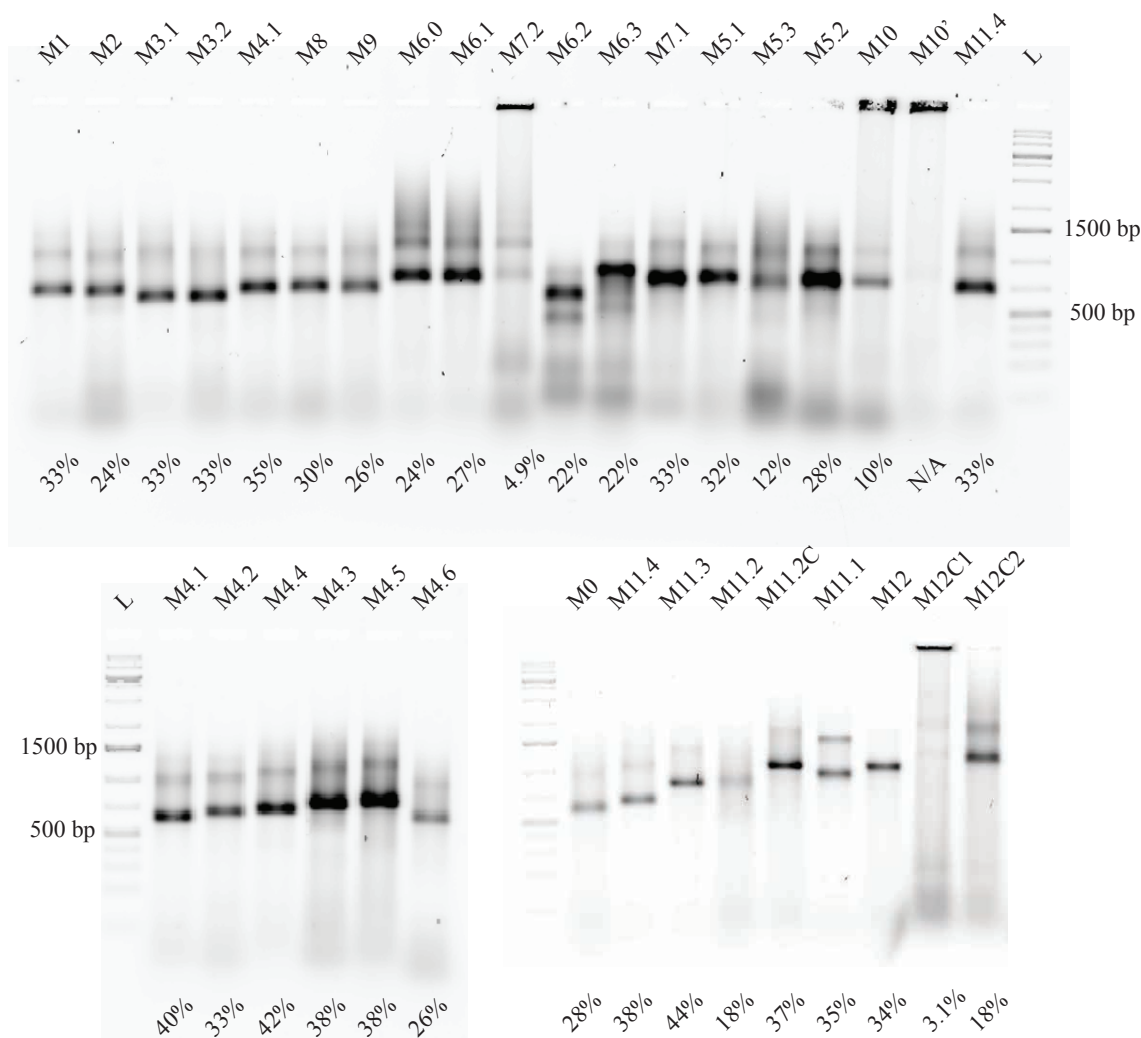


**Figure SI1. Agarose gel electrophoresis analysis for different motifs.** Labels above gel lanes indicate motifs for the structures (e.g. M0 refers to motif 0). M10' refers to a variation of motif 10 that failed to assemble; M11.2C refers to motif 11.2, with the addition of complementary strands to the linker sequence during annealing; M12C1 refers to motif 12, with the addition of complementary strands to the linker sequence during annealing; M12C2 refers to motif 12, with the addition of complementary strands to the linker sequence after annealing. Numbers at the bottom indicate assembly yields. Mixtures containing 200 nM of each component strand were annealed in  $0.5\times$  TE buffer supplemented with 15 mM  $MgCl_2$  from  $90^\circ C$  to  $25^\circ C$  over 17 hours. In the case of M11.2C or M12C1, the concentration of the complementary strand to the linker sequence was set at  $10.8\ \mu M$  because there were 54 linker domains for a respective structure. In the case of M12C2,  $6\ \mu L$  of complementary strand to the linker sequence ( $100\ \mu M$  in double distilled water) was added in  $50\ \mu L$  sample of M13 after annealing with 1 h incubation at room temperature. Then, a  $15\ \mu L$  sample (mixed with  $3\ \mu L$   $6\times$  bromophenol blue loading dye) was loaded into a 2% native agarose gel and subjected to electrophoresis in an ice water bath with  $0.5\times$  TBE running buffer (supplemented with 10 mM  $MgCl_2$ ).

Most motifs assembled into desired structures with decent yield except for motifs 5.3, 7.2 and 10. These structures were gel purified prior to AFM imaging. The structure from motif 11.2 (lane M11.2 in Fig. SI1) formed with low yield, likely due to exposure of the single-stranded, non-poly-T, linker domains. When the component strands were mixed with the complementary strands to the linker sequences, this structure formed with high yield using the same annealing

protocol.

The structure from motif 12 was floppy and difficult to image. To facilitate imaging, we introduced 10 nt poly-A strand to complement the 10 nt poly-T linker either during or after annealing (M12C1 and M12C2). Poly-A strands were expected to form duplexes with the poly-T linkers and thus enhance the rigidity of the structure. Agarose gel electrophoresis results showed the addition after annealing led to a structure formation with high yield.

## SI1.2 Effect of annealing conditions on the assembly of structures of different motifs

We tested the effect of  $Mg^{2+}$  concentration and annealing time on the assembly yield for different motifs. For a typical motif (e.g. motif 4.1) that assembled with high yield, relatively low  $Mg^{2+}$  concentration (5-10 mM) was usually enough for structure formation; higher  $Mg^{2+}$  concentration did not lead to an apparent increase in yield. For a motif (e.g. motif 4.6) that did not assemble with high yield, higher  $Mg^{2+}$  concentration (up to 40 mM) usually resulted in an increase of the yield. For all structures, longer annealing time (up to 72.5 hours in our test) generally resulted in higher yield.

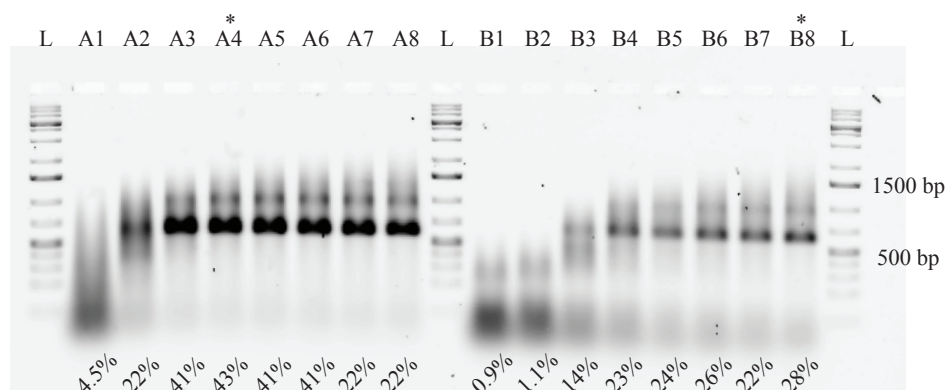


**Figure SI2. Agarose gel electrophoresis results of structures from motifs 4.1 and 4.6 annealed in different  $Mg^{2+}$  concentration for 17 hours.** Lane L: 1 kb DNA ladder; lanes A1 and B1: sample annealed in 0 mM  $Mg^{2+}$ ; lanes A2 and B2: 2 mM  $Mg^{2+}$ ; lane A3 and B3: 5 mM  $Mg^{2+}$ ; lanes A4 and B4: 10 mM  $Mg^{2+}$ ; lanes A5 and B5: 15 mM  $Mg^{2+}$ ; lanes A6 and B6: 20 mM  $Mg^{2+}$ ; lanes A7 and B7: 25 mM  $Mg^{2+}$ ; lanes A8 and B8: 40 mM  $Mg^{2+}$ . Lanes A1 to A8: structures from motif 4.1; lanes B1-B8: structures from motif 4.6. Asterisk (\*) above lane A4 or B8 indicates the highest observed yield for motif 4.1 or 4.6, respectively. Numbers at the bottom indicate assembly yields. Samples (200 nM) were annealed in  $0.5\times$  TE buffer (5-40 mM  $MgCl_2$ ) from  $90^\circ C$  to  $25^\circ C$  in 17 hours. Then, a  $15\ \mu L$  sample (mixed with  $3\ \mu L$   $6\times$  bromophenol blue loading dye) was loaded into a 2% native agarose gel and subjected to electrophoresis in an ice water bath with  $0.5\times$  TBE running buffer (10 mM  $MgCl_2$ ).

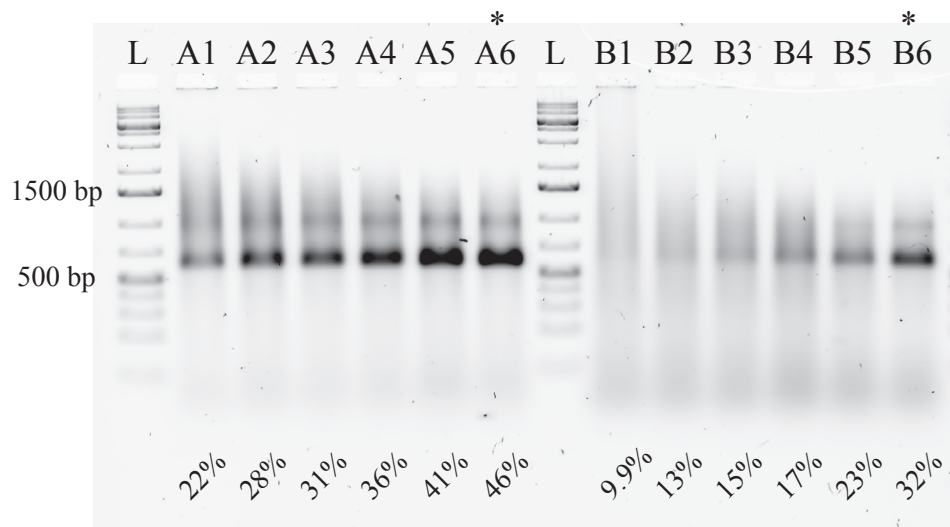


**Figure S13. Time course yield study of structures from motifs 4.1 and 4.6 using agarose gel electrophoresis.** The first ramp (from 90°C down to 61°C) was kept at a constant speed (5 minutes per °C). The second ramp (from 60°C down to 25°C) varied in speed: the waiting time per °C was 5, 10, 20, 30, 60, and 120 minutes, respectively. The total annealing time was 5.4 (lanes A1, B1), 8.3 (A2, B2), 14.1 (A3, B3), 20 (A4, B4), 37.5 (A5, B5) and 72.5 (A6, B6) hours, respectively. Lane L: 1 kb DNA ladder. Lanes A1 to A8: structures from motif 4.1. Lanes B1 to B8: structures from motif 4.6. Asterisks (\*) over lanes A6 and B6 indicate highest yields for respective motifs. Numbers at the bottom indicate assembly yields. Samples (200 nM) were annealed in 0.5× TE buffer (5-40 mM MgCl<sub>2</sub>) from 90°C to 25°C for 5 to 73 hours. Then, a 15 μL sample (mixed with 3 μL 6× bromophenol blue loading dye) was loaded into a 2% native agarose gel and subjected to electrophoresis in an ice water bath with 0.5× TBE running buffer (10 mM MgCl<sub>2</sub>).

### SI1.3 AFM imaging results

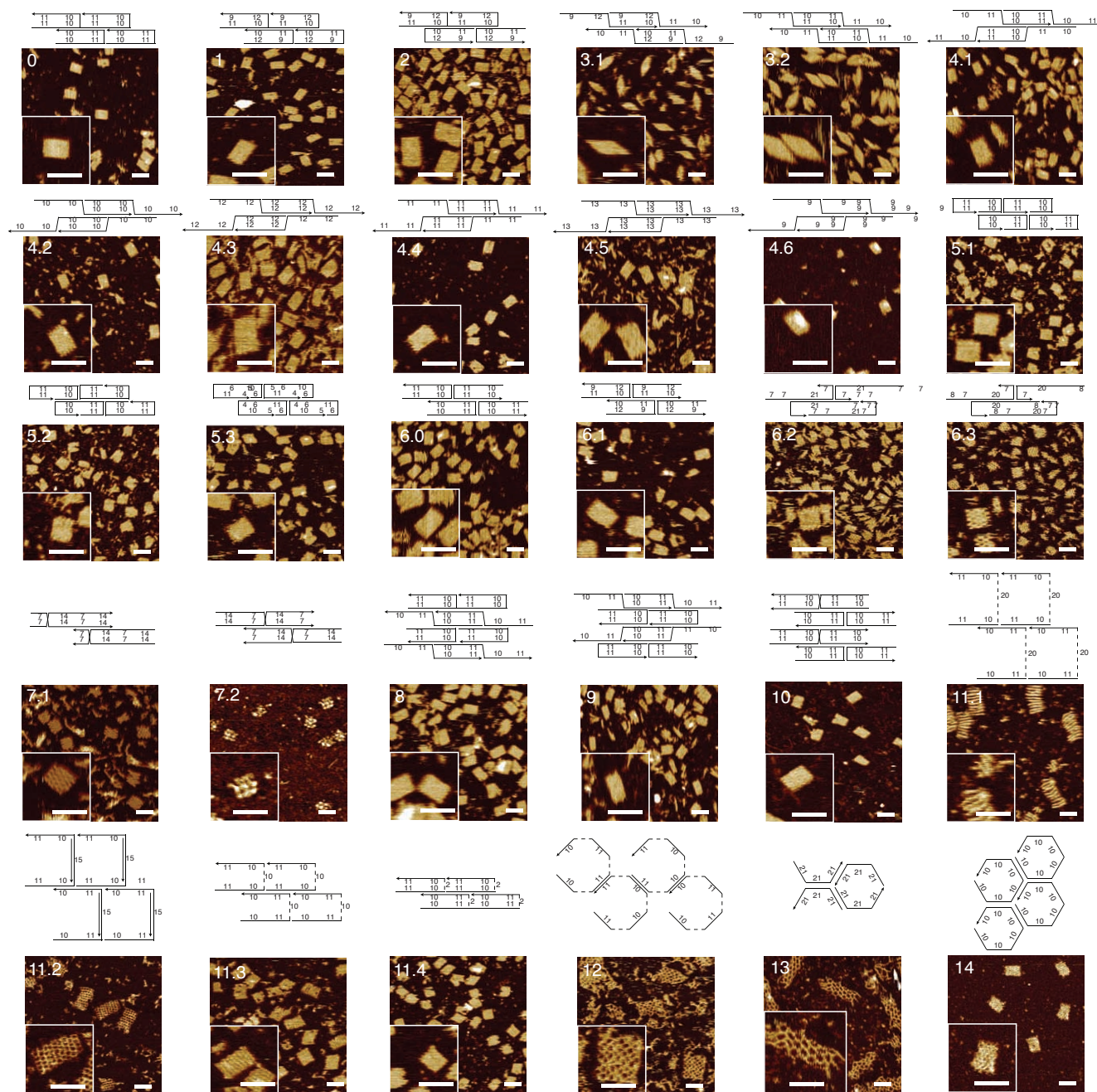


**Figure SI4. Strand diagrams and AFM images of structures made from different motifs** Top panel: strand diagram of a  $2 \times 2$  or  $2 \times 4$  unit containing 4 or 8 SSTs. Dashed lines represent poly-T linkers. Numbers indicate domain lengths. Bottom panel: AFM images. Scale bars: 50 nm.

Figs. SI4 show the strand diagrams and AFM images for structures made from different motifs. Figs. SI5-SI35 show large AFM images for structures made from different motifs.

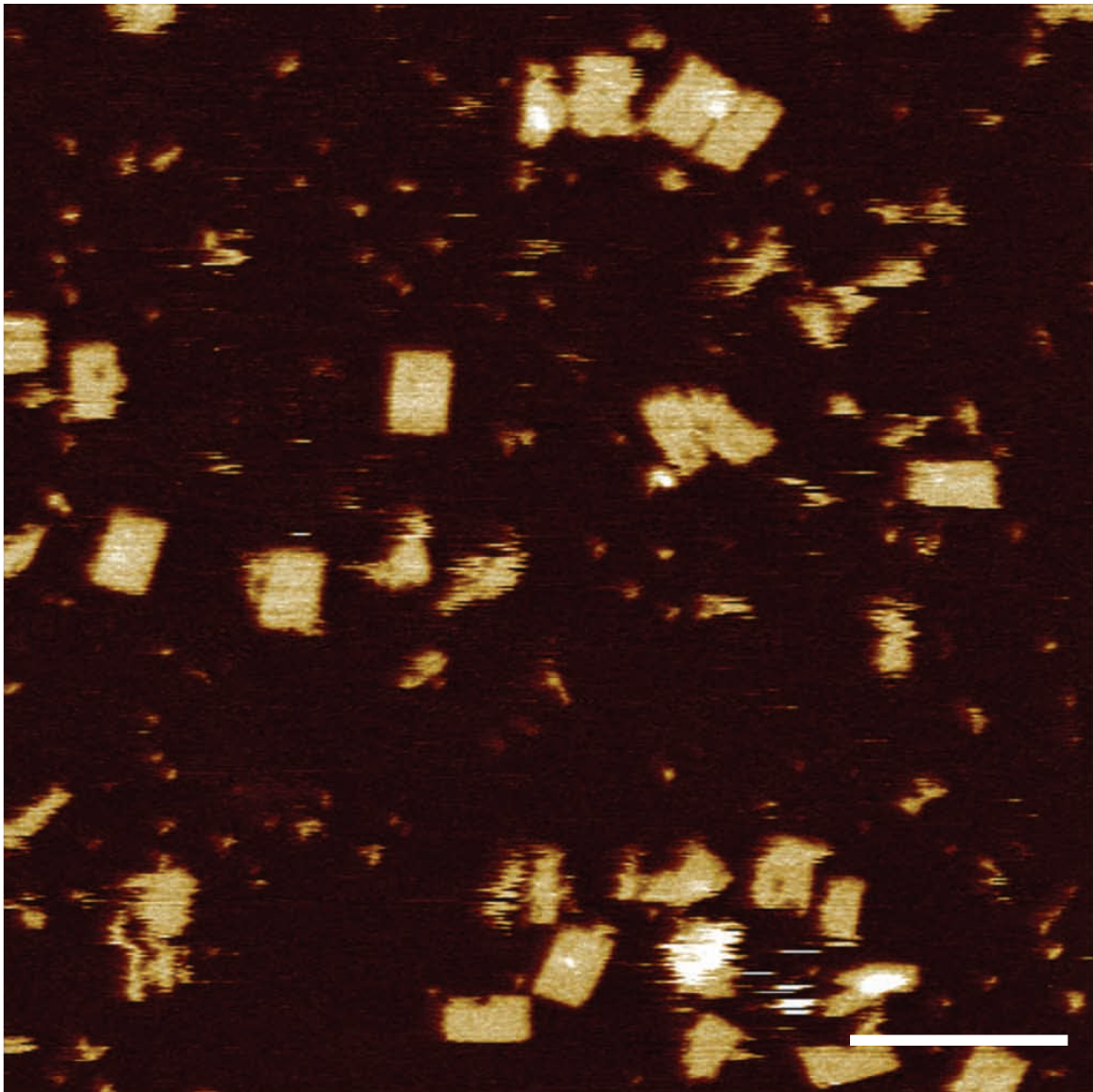


**Figure S15. AFM image of the  $10H \times 11T$  structure made from motif 0 (scale bar: 100 nm).**

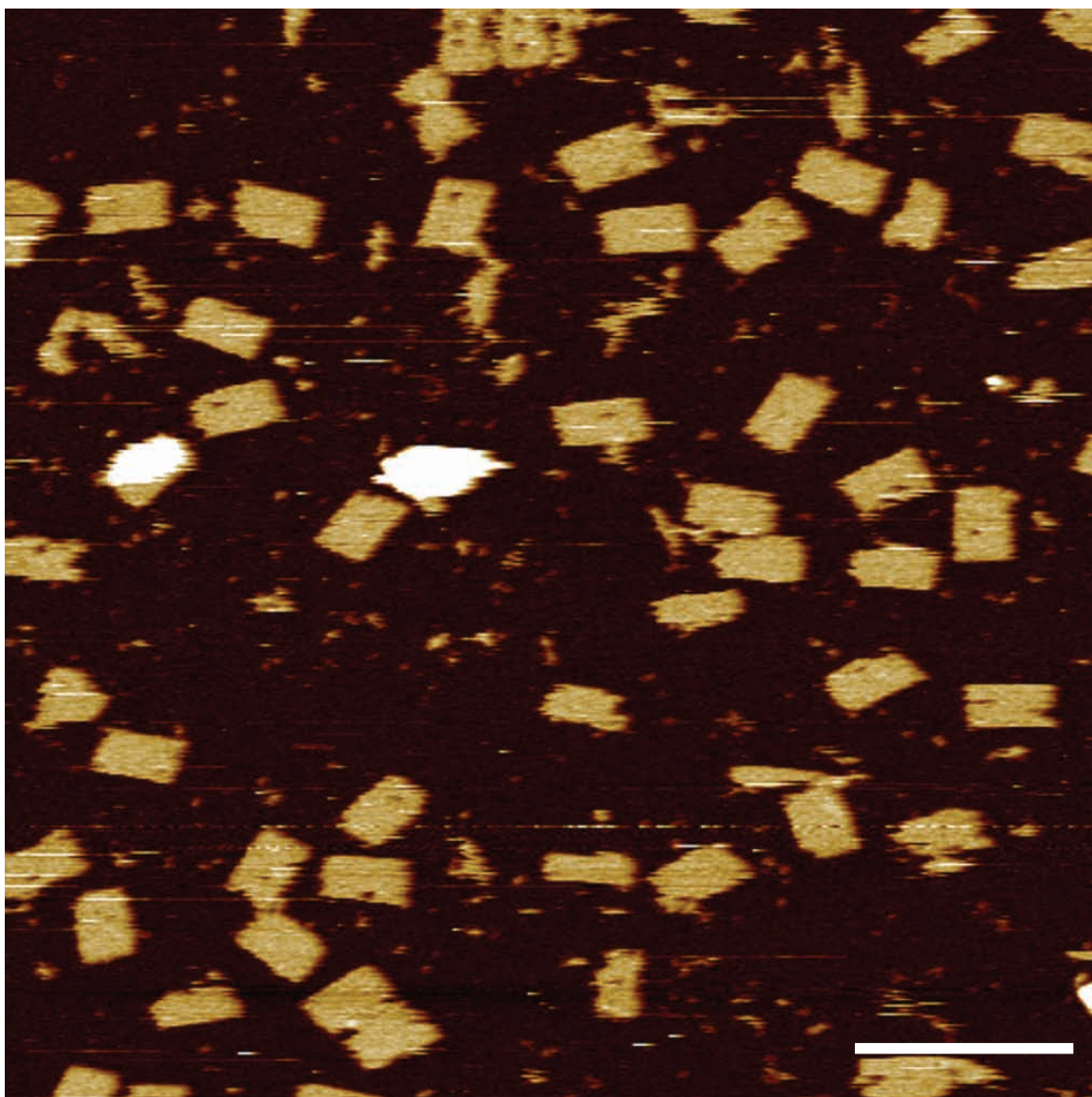


**Figure S16. AFM image of the 10H×11T structure made from motif 1 (scale bar: 100 nm).**

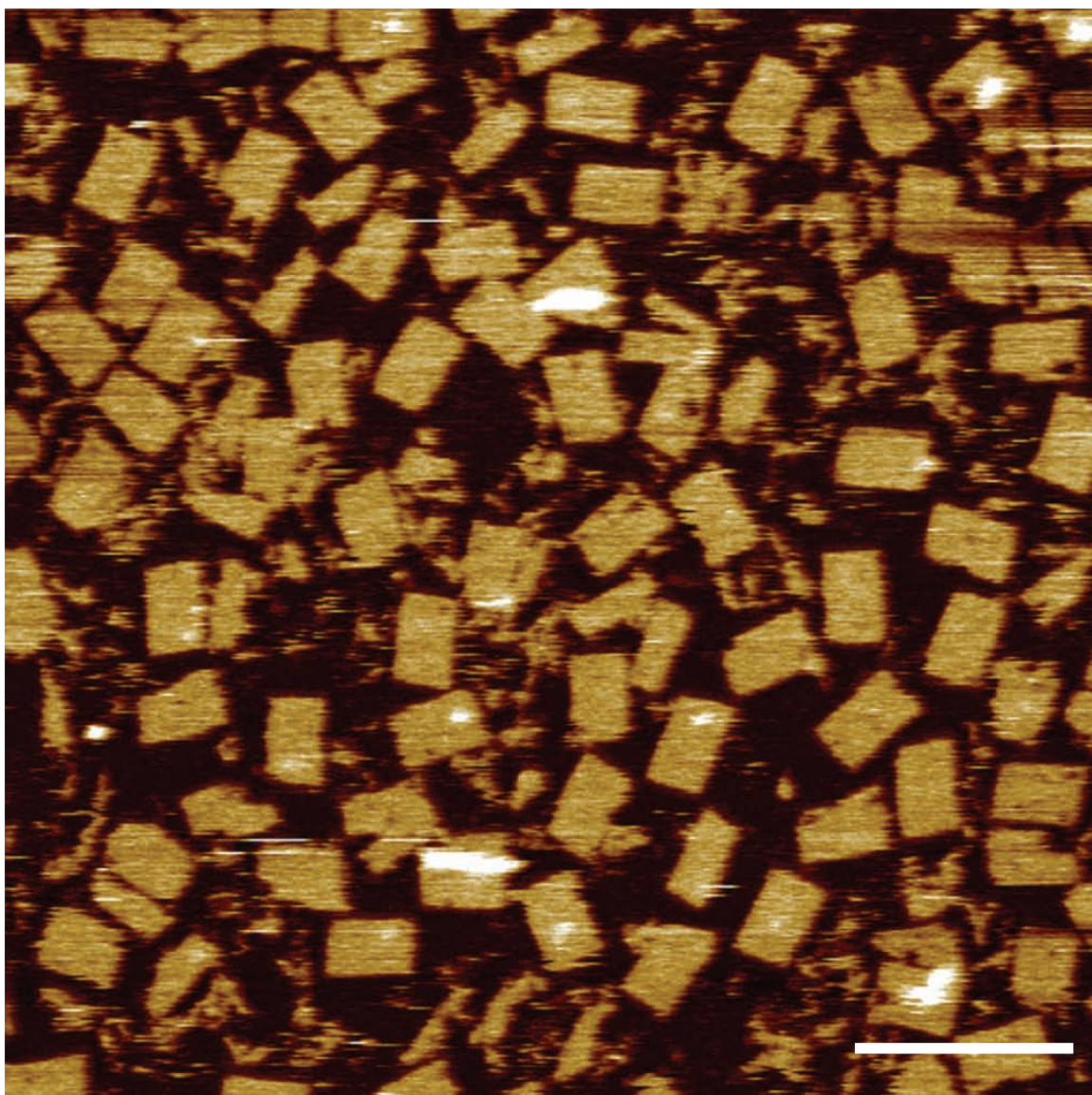


**Figure S17. AFM image of the 10H×11T structure made from motif 2 (scale bar: 100 nm).**

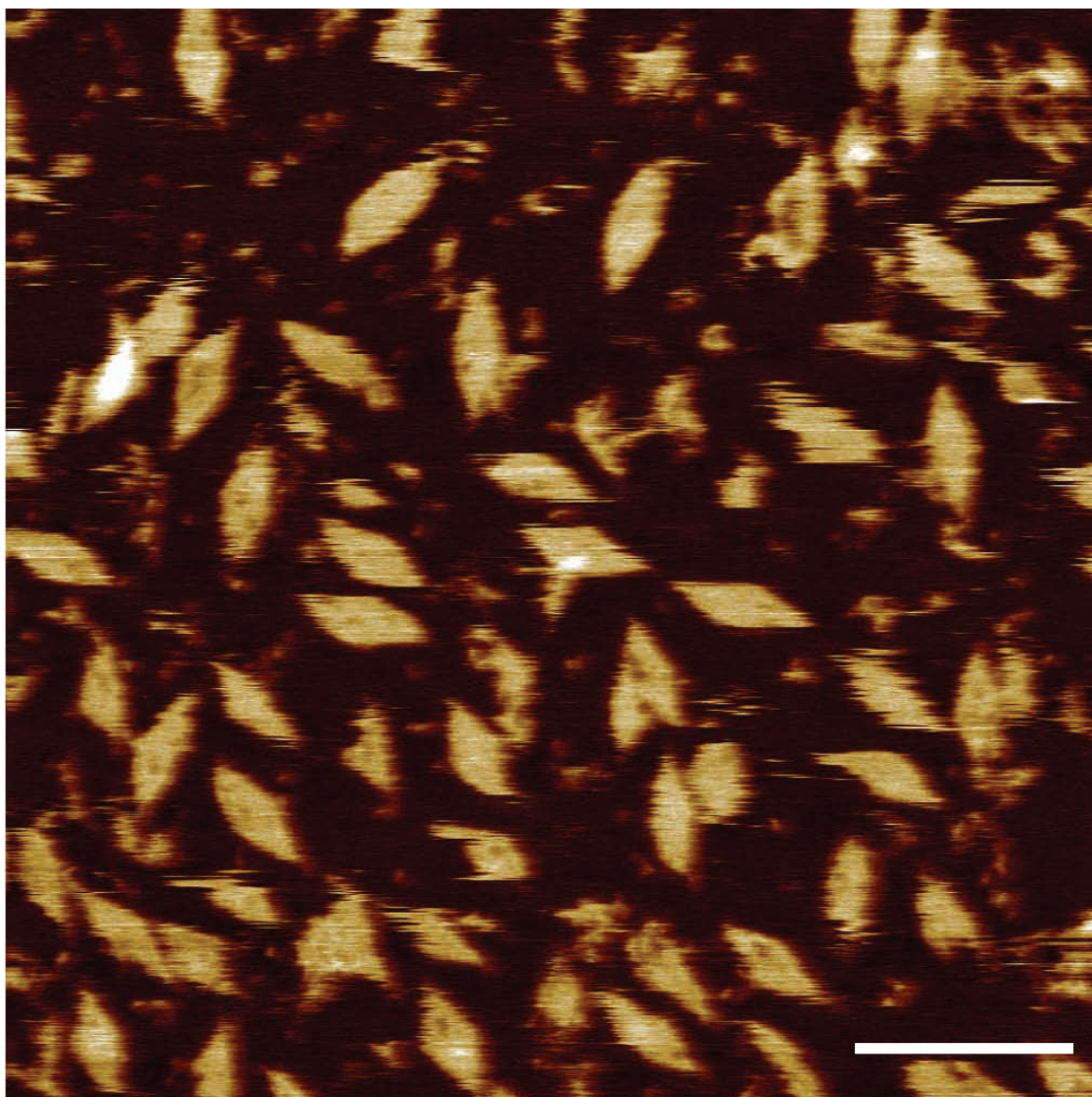


**Figure S18. AFM image of the  $10H \times 11T$  structure made from motif 3.1 (scale bar: 100 nm).**

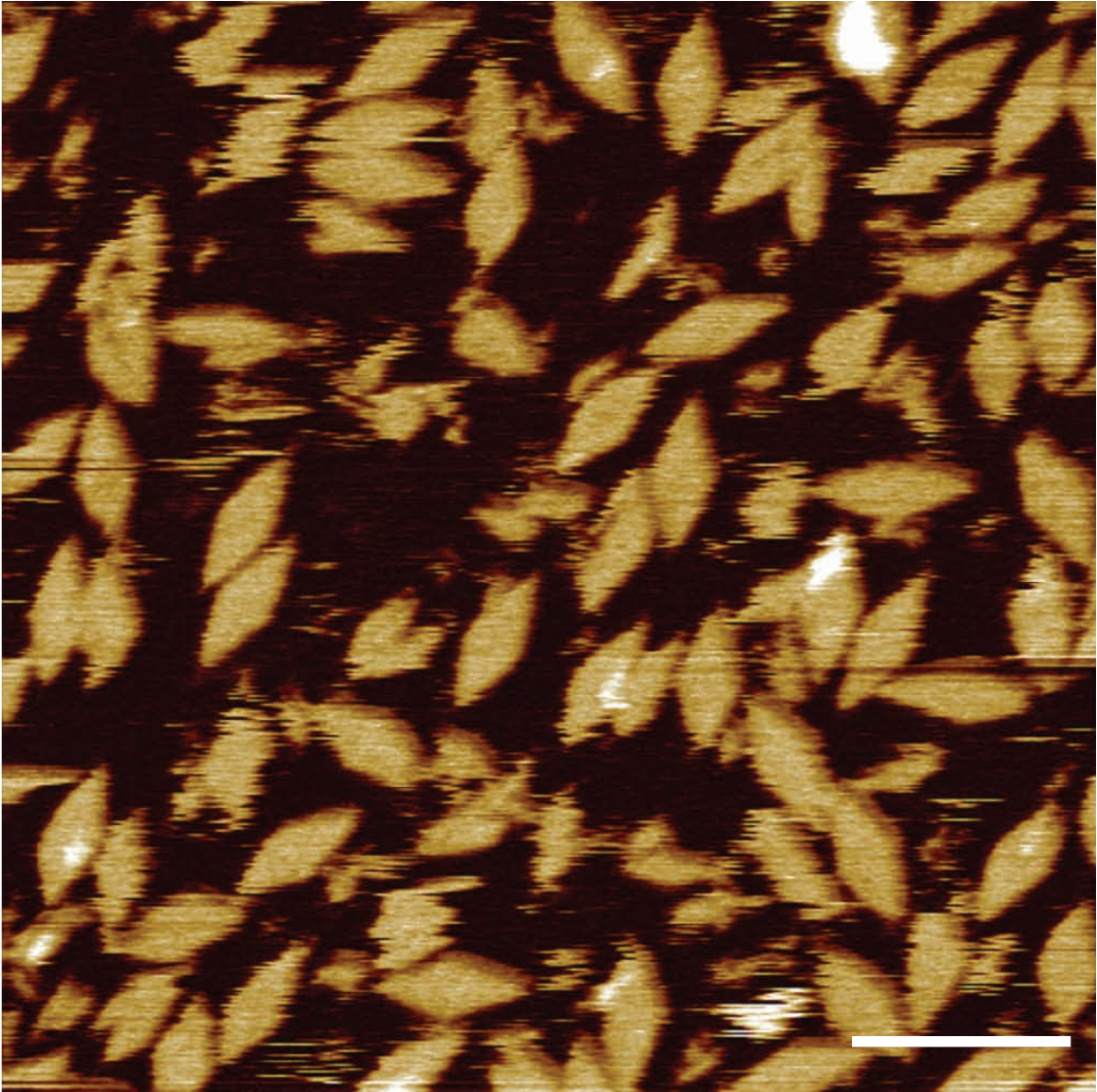


**Figure SI9. AFM image of the 10H×11T structure made from motif 3.2 (scale bar: 100 nm).**

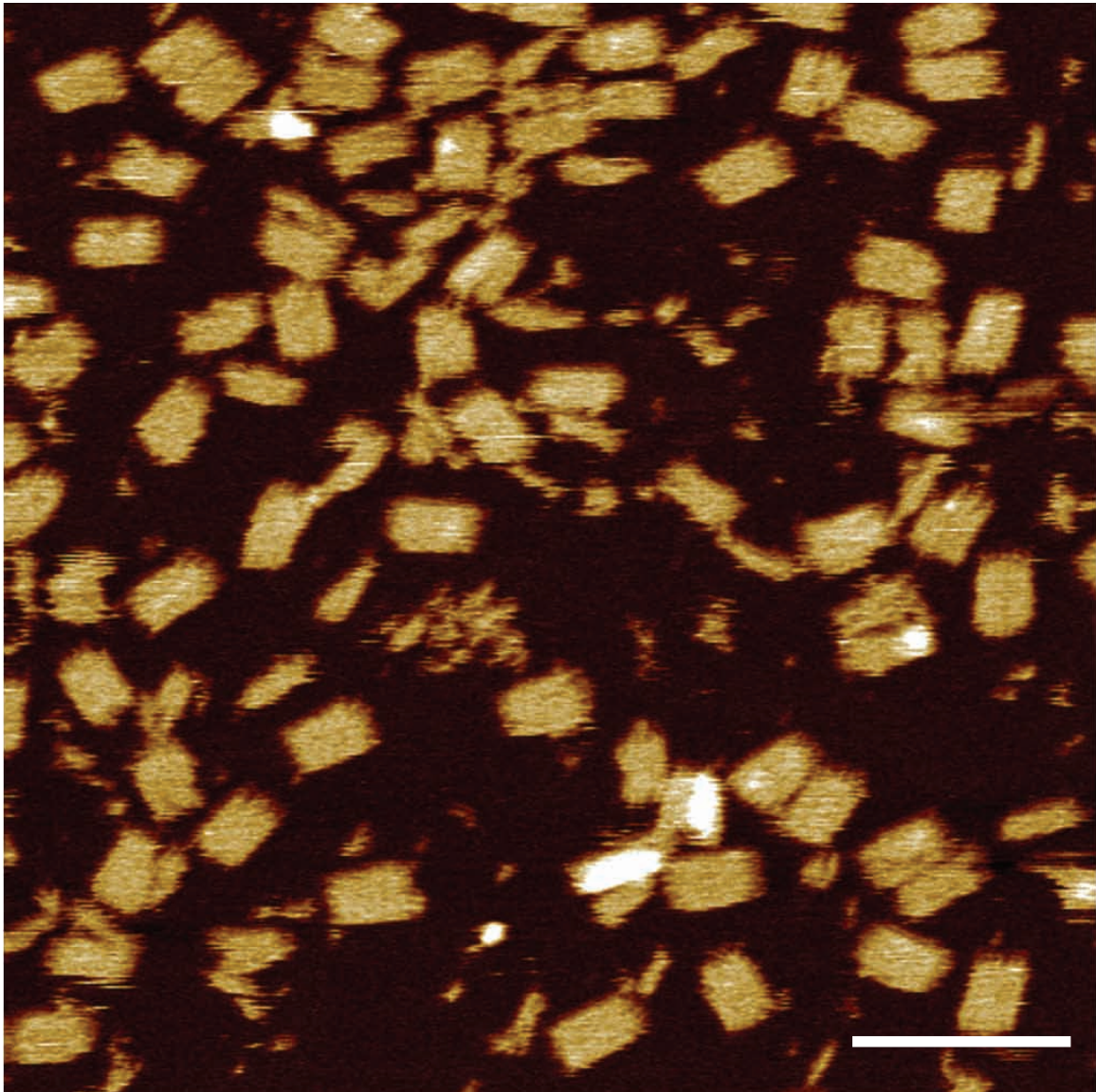


**Figure S10. AFM image of the 10H×11T structure made from motif 4.1 (scale bar: 100 nm).**

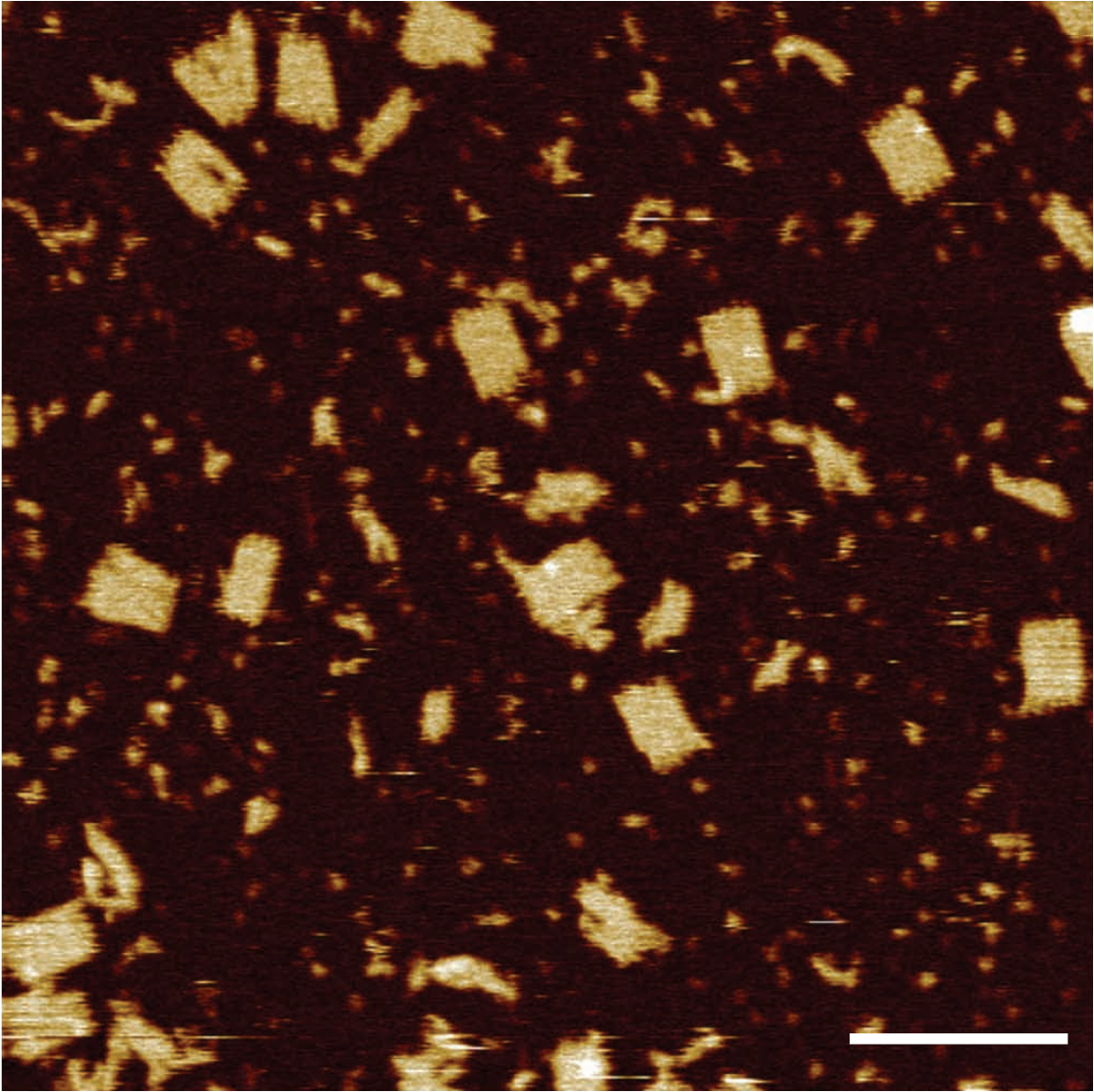


**Figure S11. AFM image of the 10H×11T structure made from motif 4.2 (scale bar: 100 nm).**

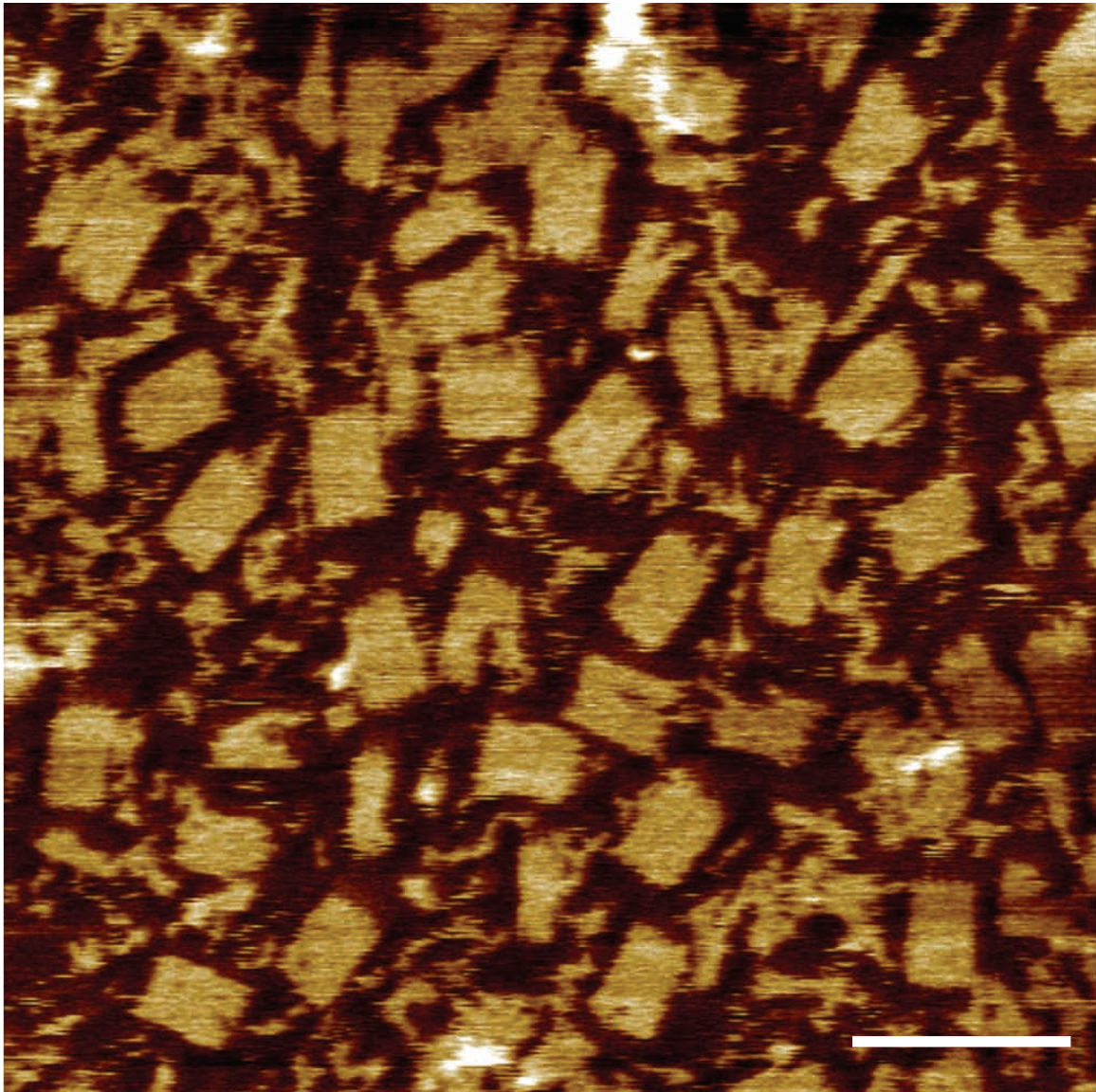


**Figure SI12. AFM image of the 10H×11T structure made from motif 4.3 (scale bar: 100 nm).**

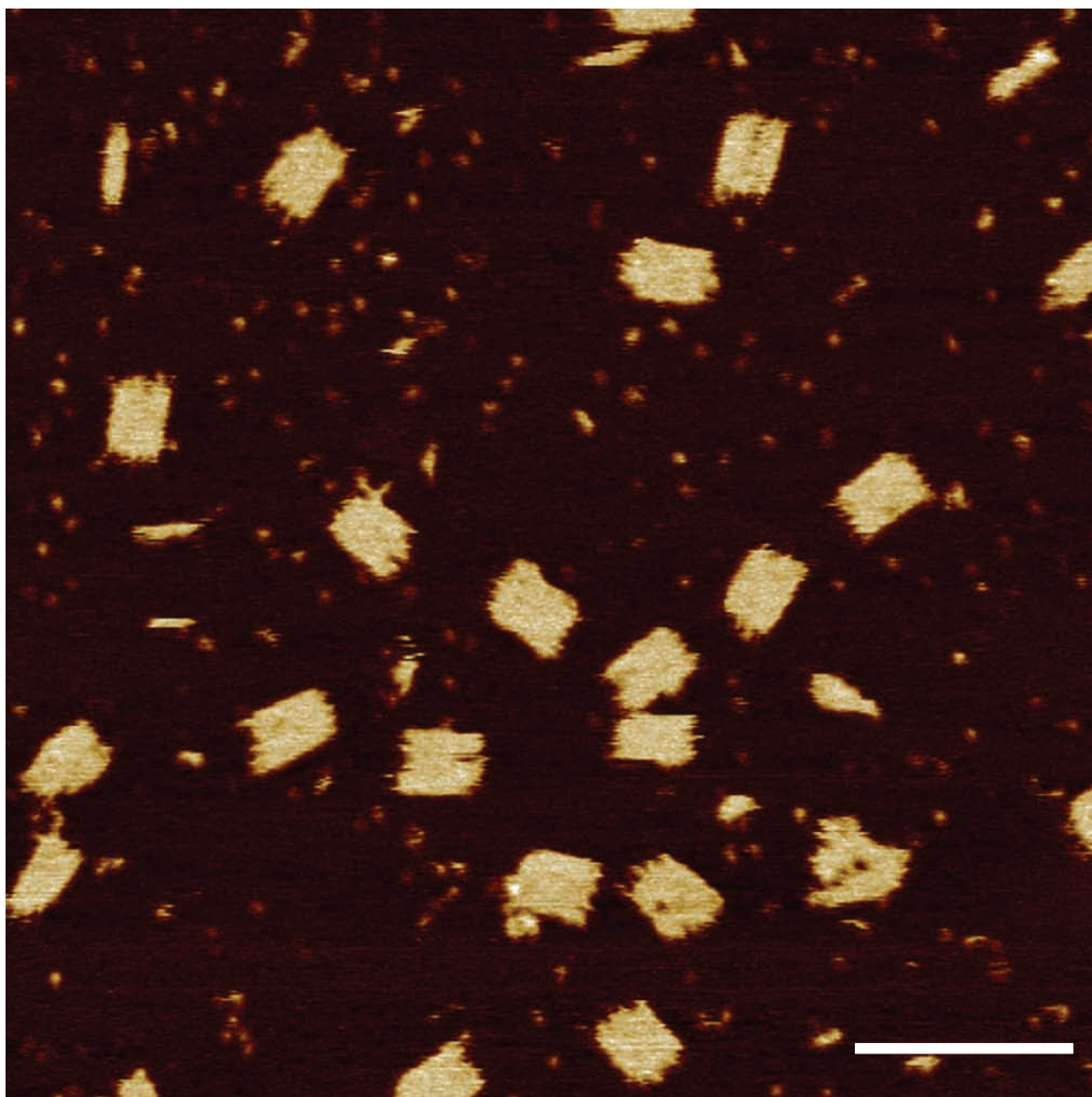


**Figure S13. AFM image of the 10H×11T structure made from motif 4.4 (scale bar: 100 nm).**

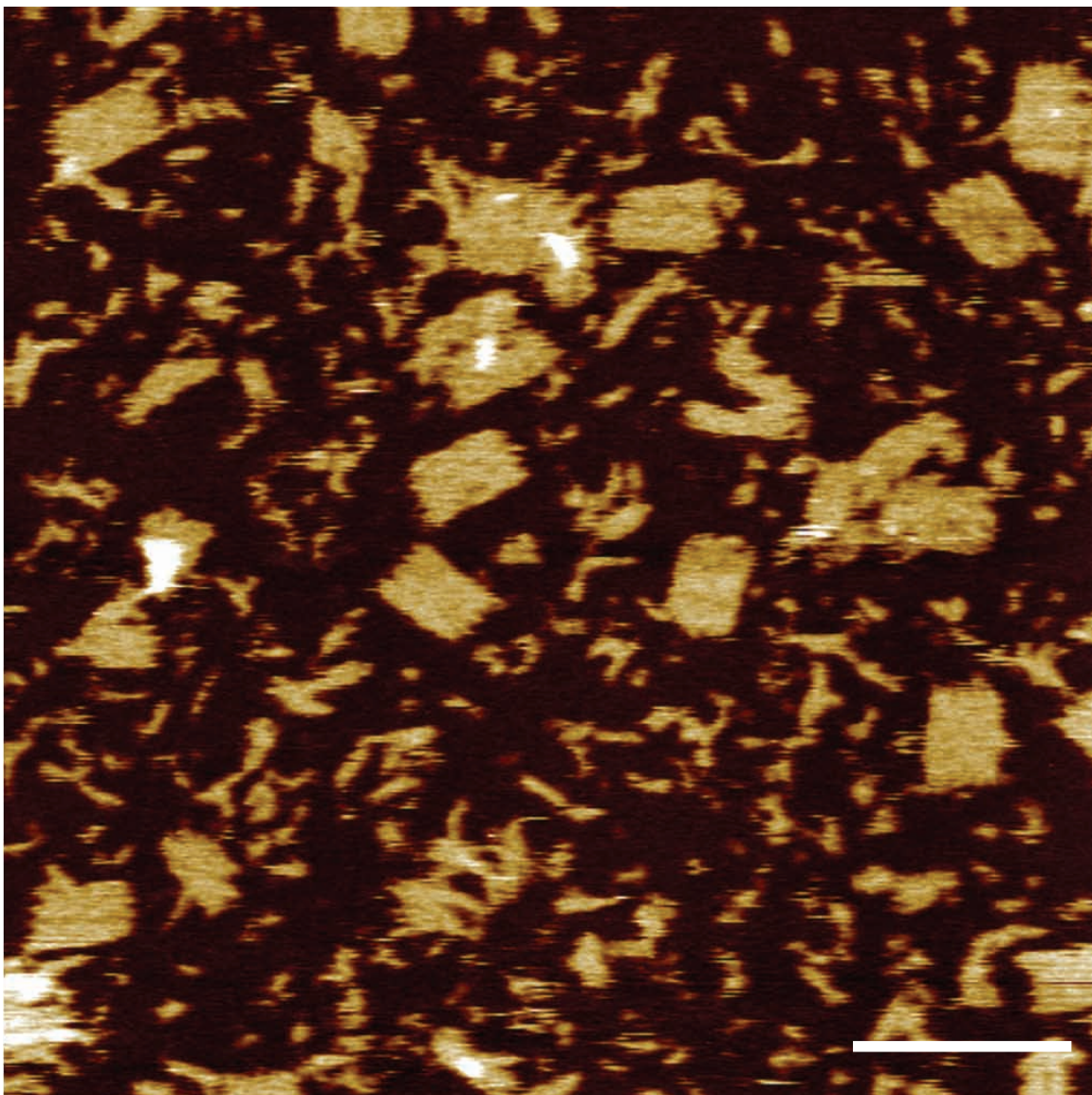


**Figure SI14. AFM image of the 10H×11T structure made from motif 4.5 (scale bar: 100 nm).**

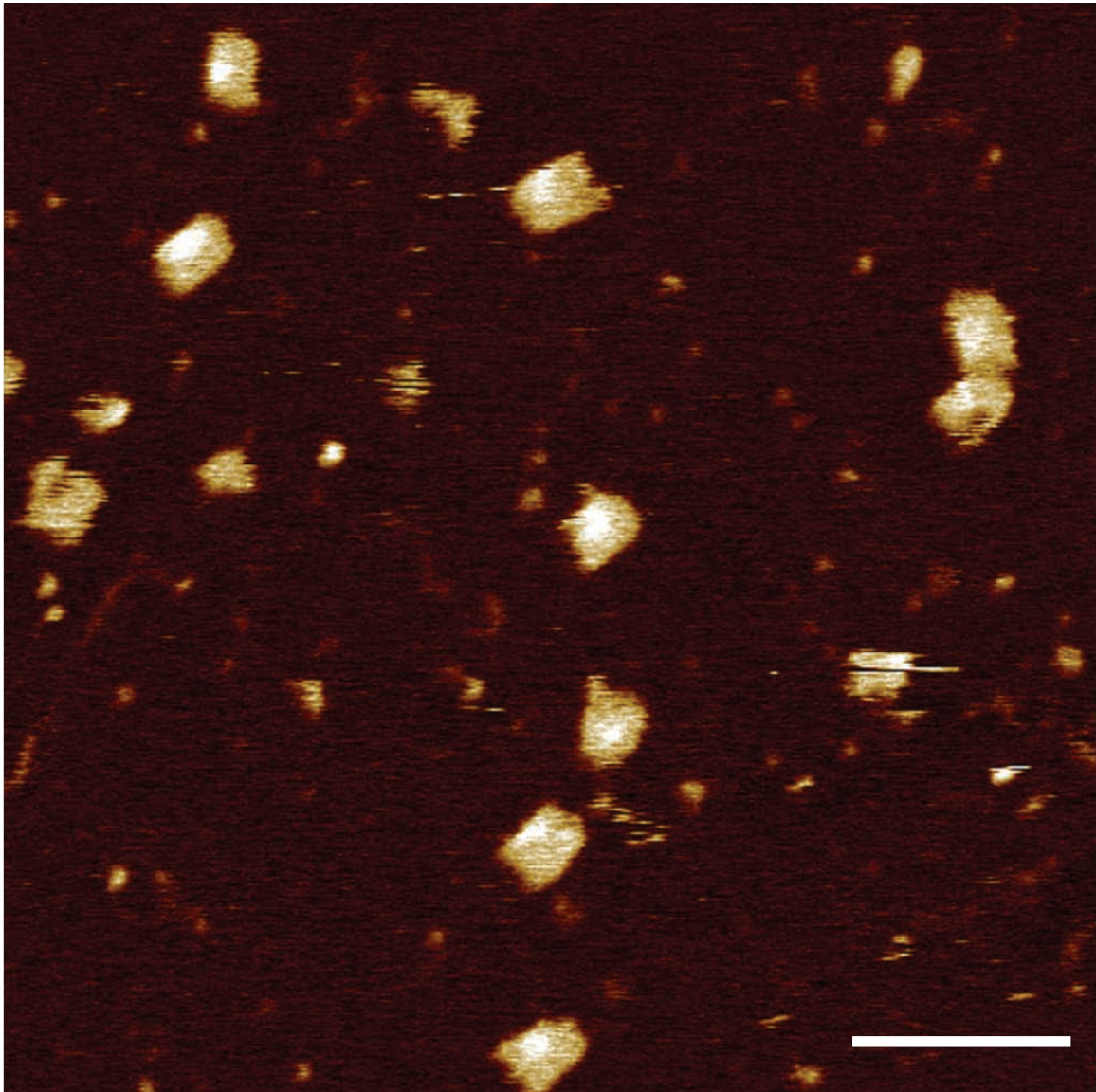


**Figure S15. AFM image of the 10H×11T structure made from motif 4.6 (scale bar: 100 nm).**

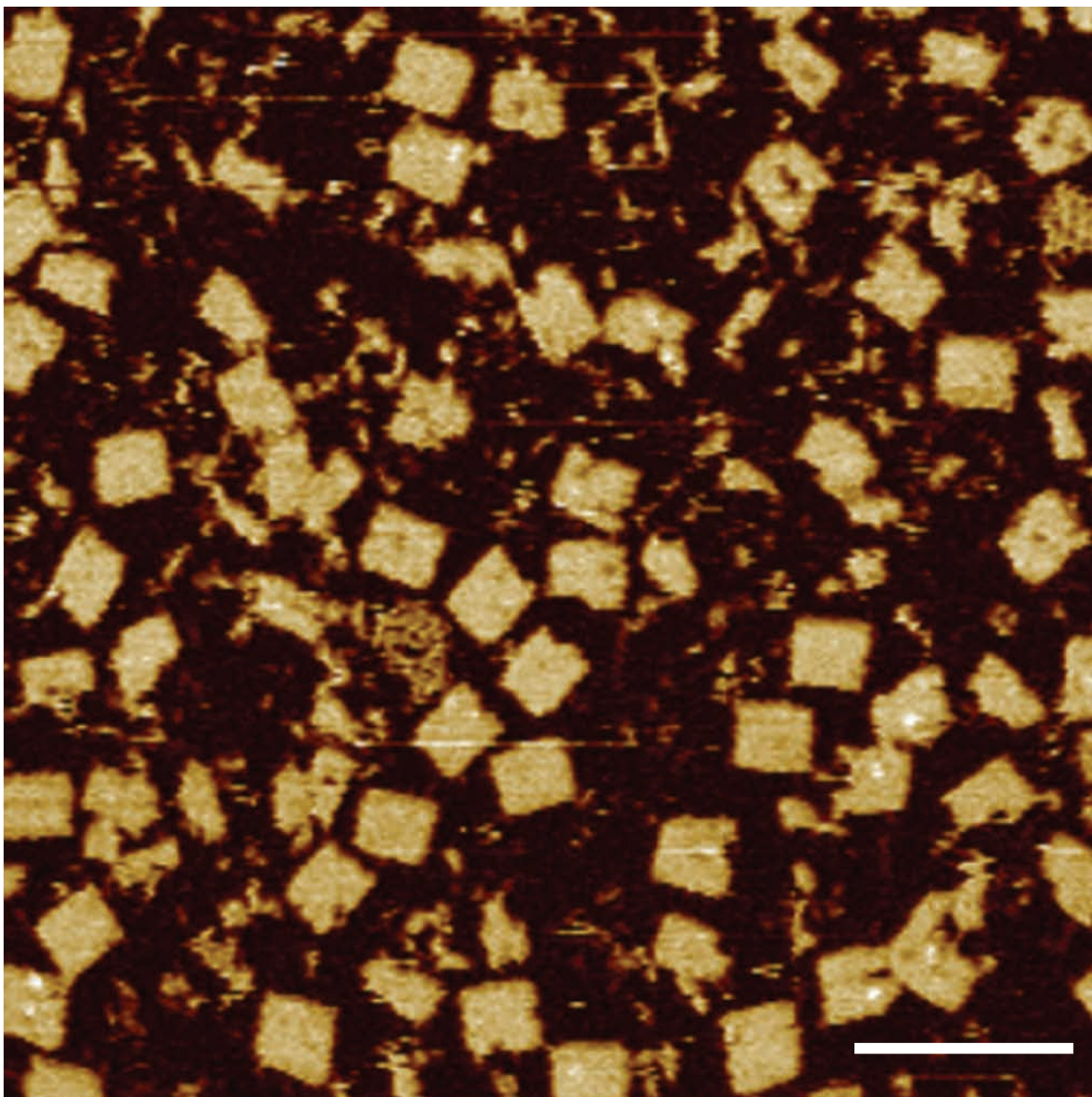


**Figure S16. AFM image of the 10H×11T structure made from motif 5.1 (scale bar: 100 nm).**

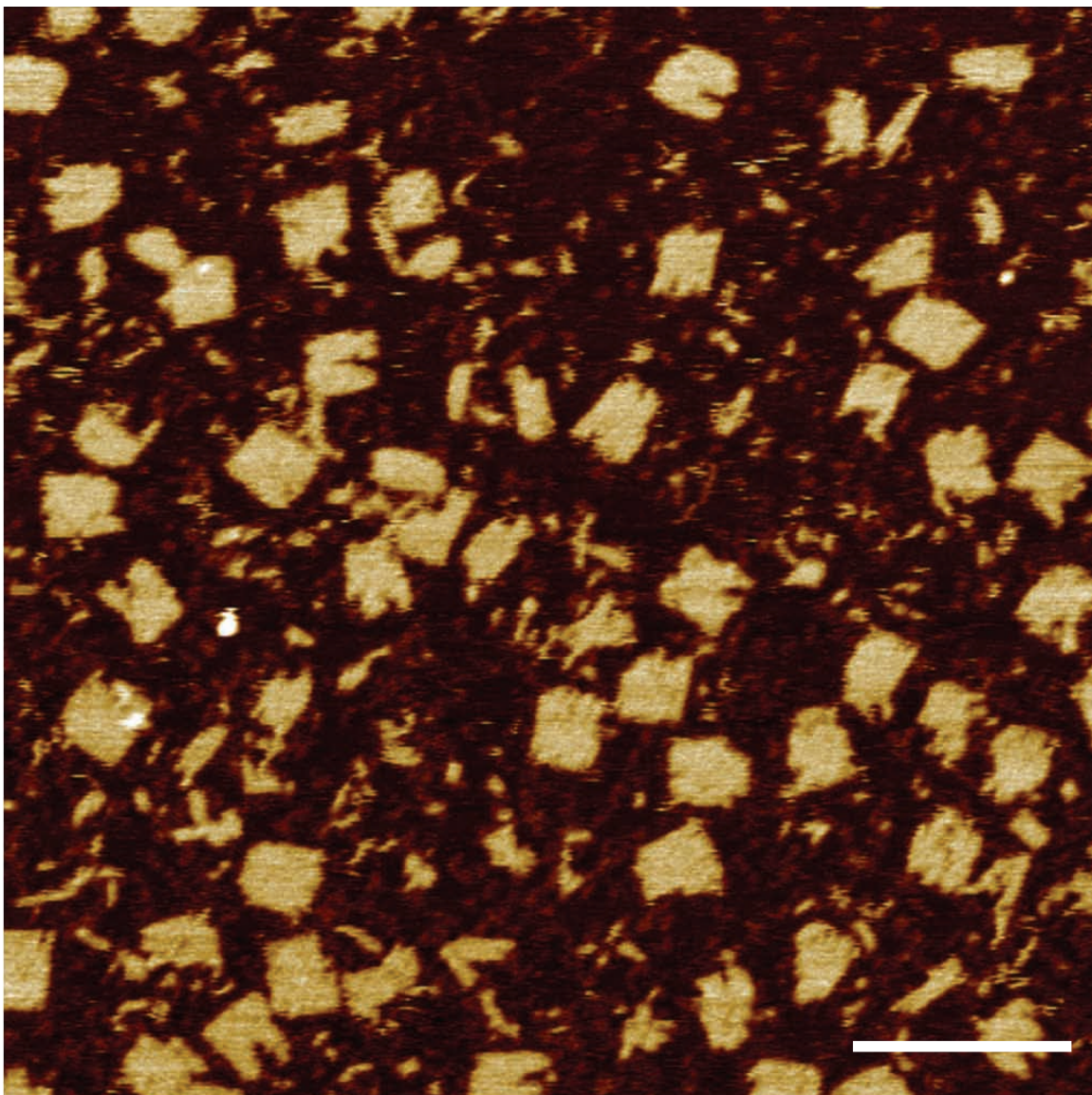


**Figure S17. AFM image of the 10H×11T structure made from motif 5.2 (scale bar: 100 nm).**

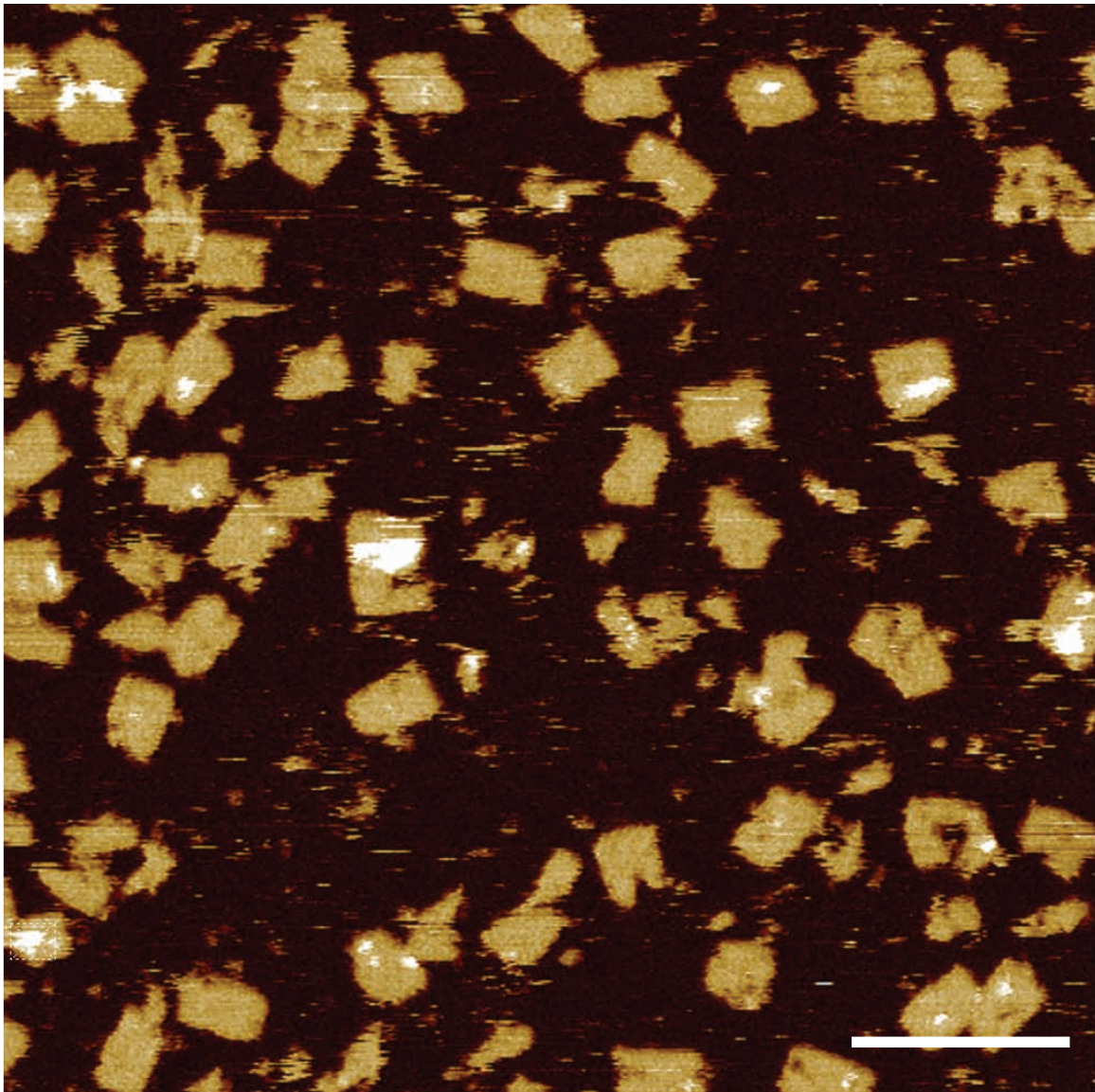


**Figure S118. AFM image of the 10H×11T structure made from motif 5.3 (scale bar: 100 nm).**

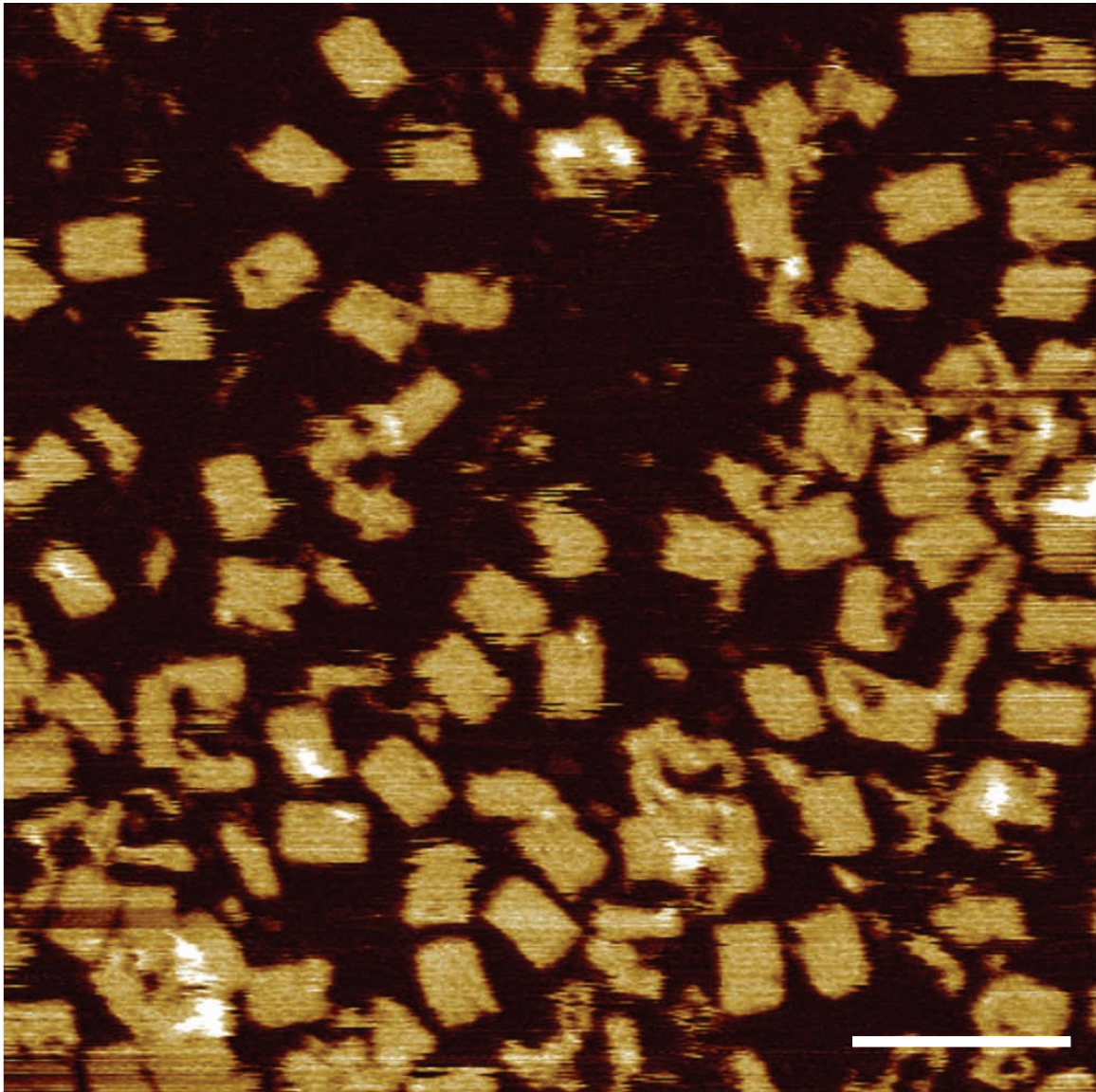


**Figure SI19. AFM image of the 10H×11T structure made from motif 6.0 (scale bar: 100 nm).**

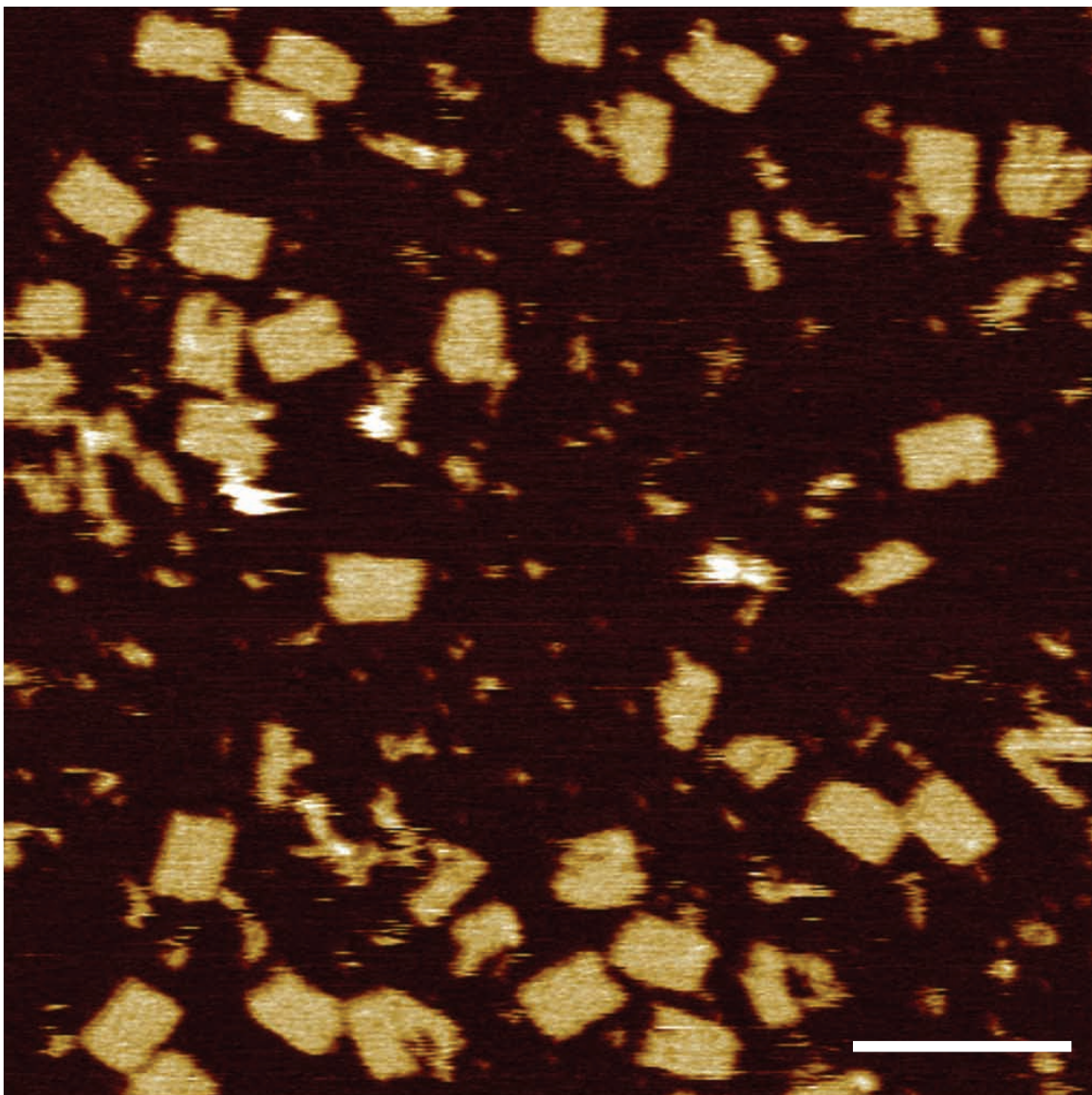


**Figure SI20. AFM image of the 10H×11T structure made from motif 6.1 (scale bar: 100 nm).**

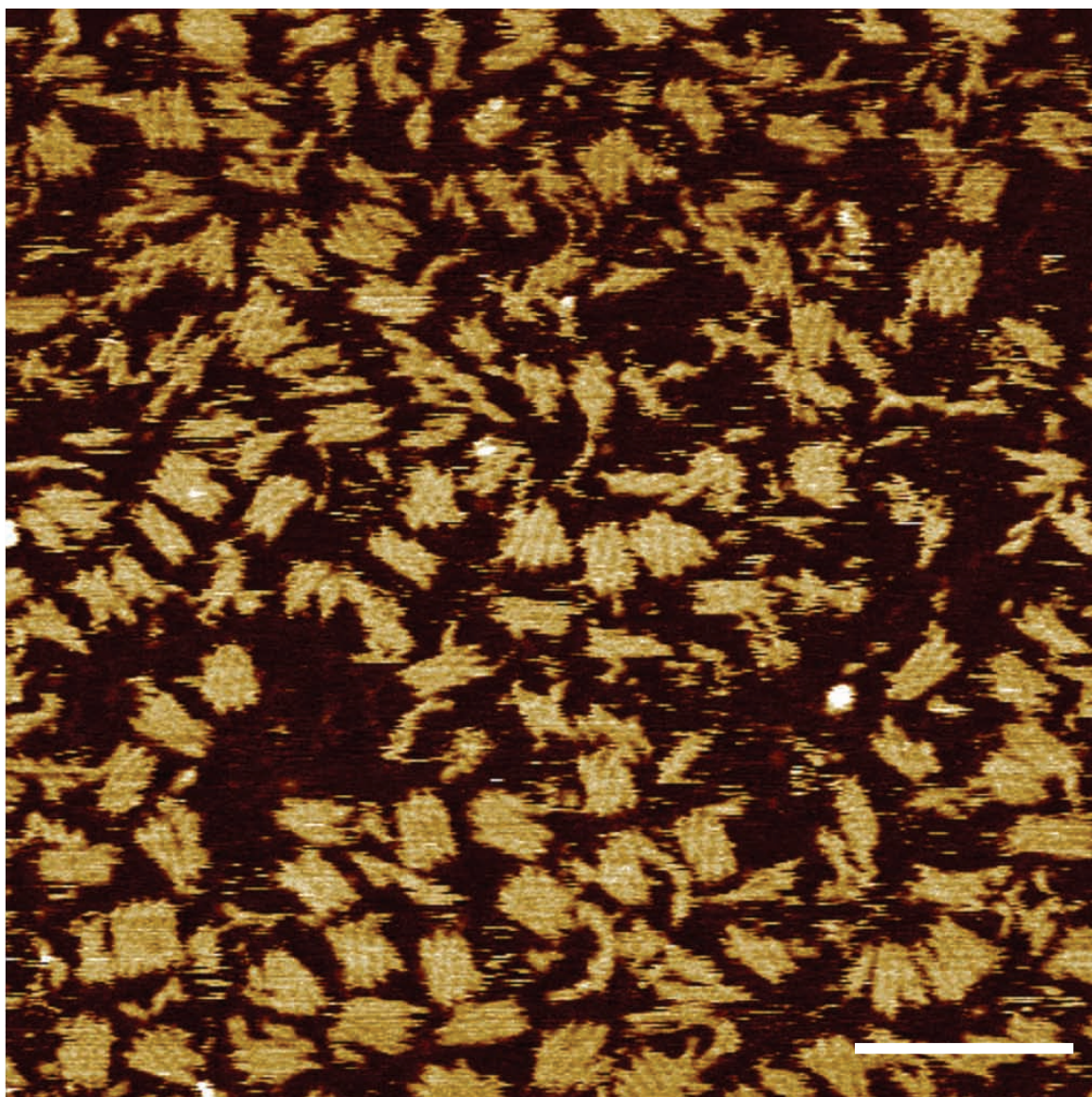


**Figure SI21. AFM image of the 10H×11T structure made from motif 6.2 (scale bar: 100 nm).**

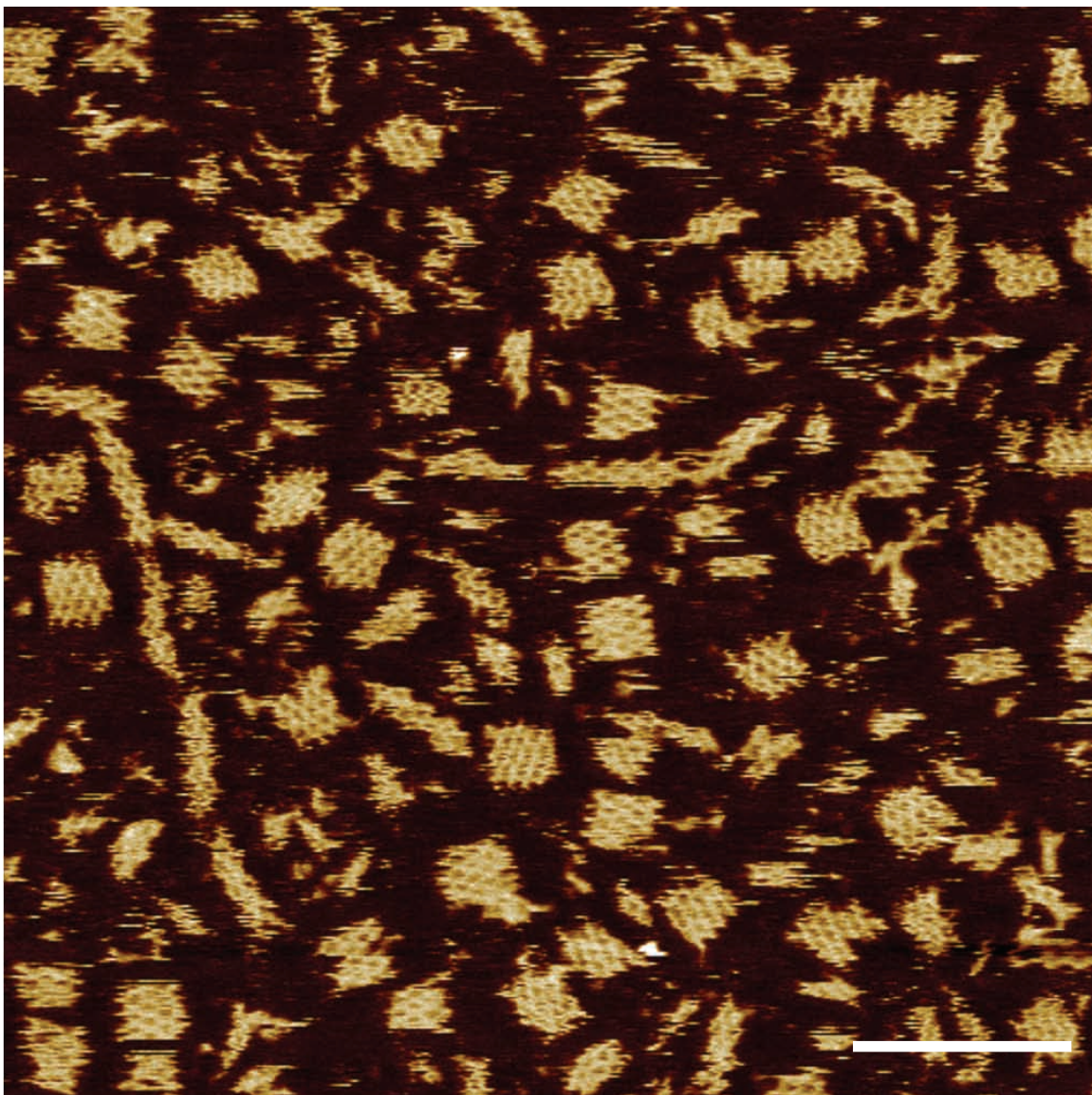


**Figure SI22. AFM image of the  $10H \times 11T$  structure made from motif 6.3 (scale bar: 100 nm).**

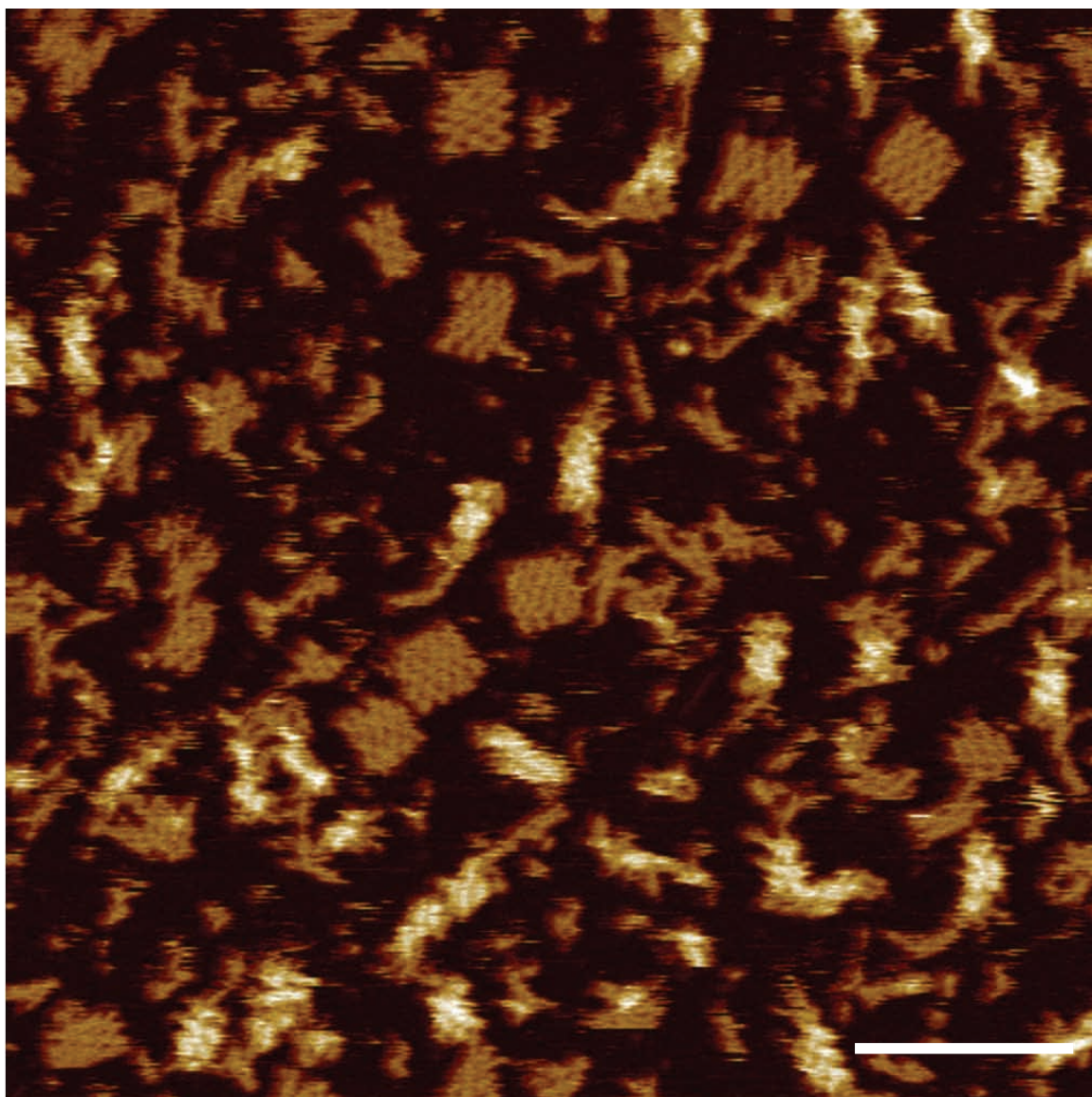


**Figure SI23. AFM image of the 10H×11T structure made from motif 7.1 (scale bar: 100 nm).**

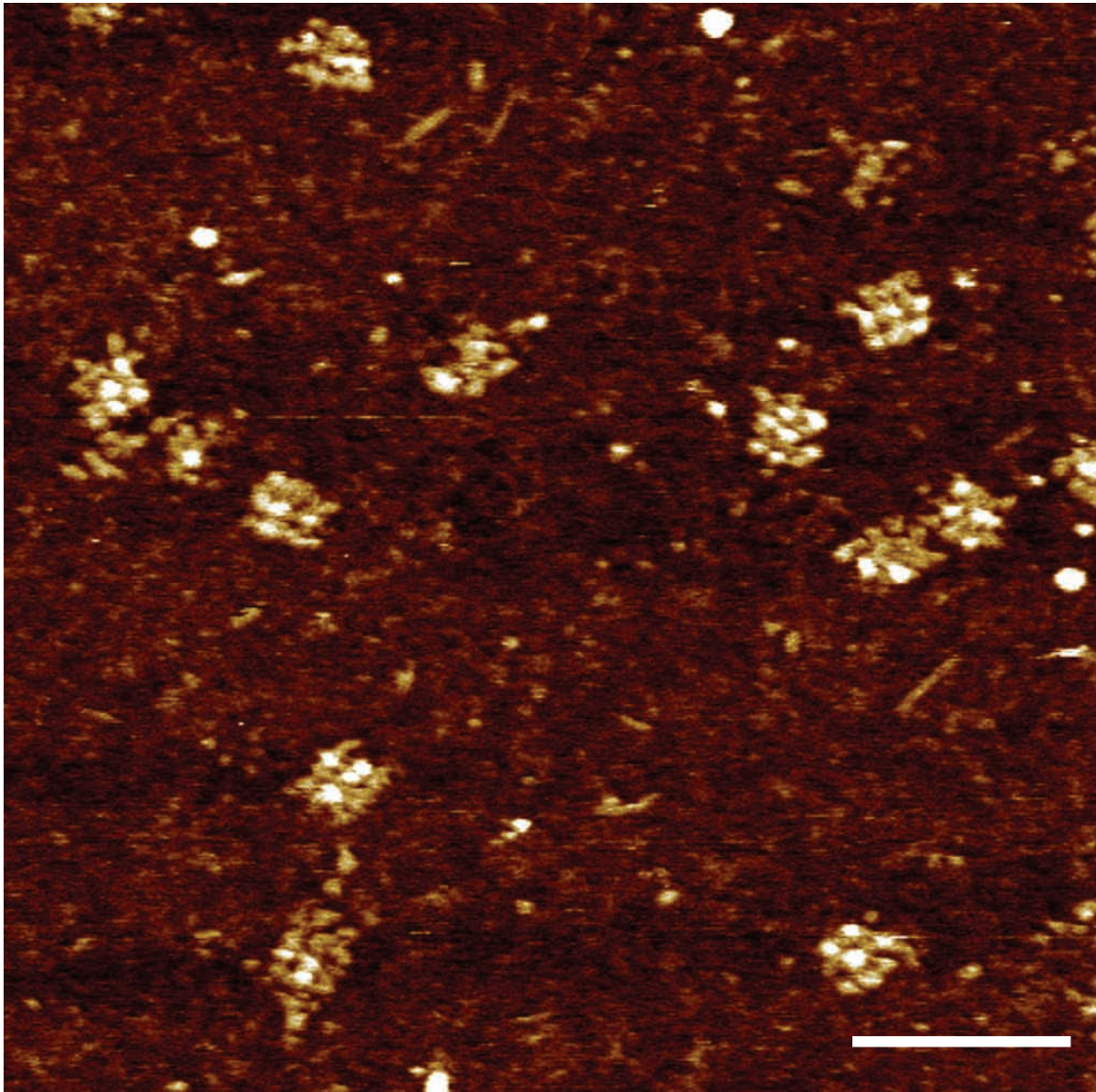


**Figure SI24. AFM image of the 10H×11T structure made from motif 7.2 (scale bar: 100 nm).**

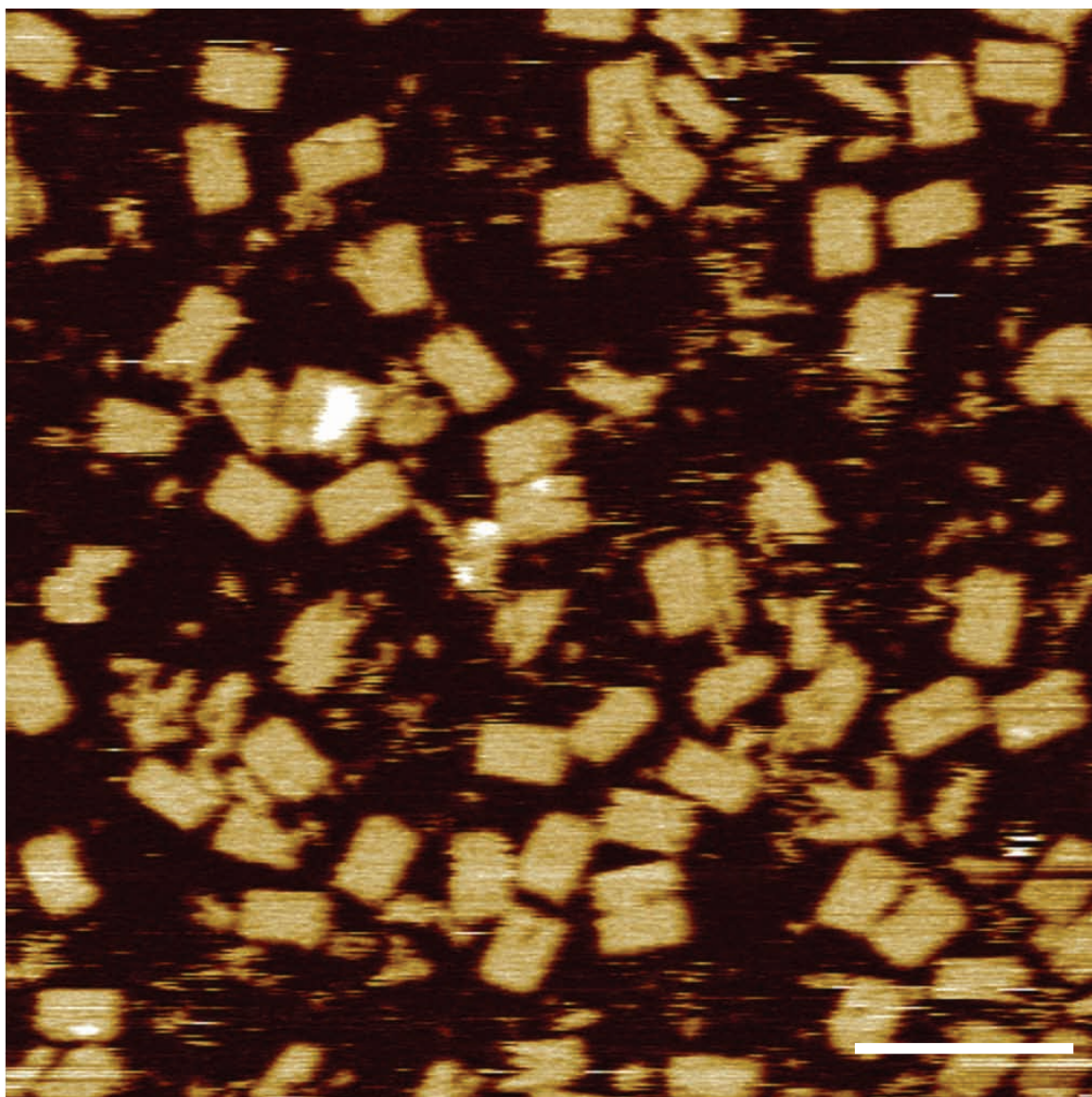


**Figure S125. AFM image of the 10H×11T structure made from motif 8 (scale bar: 100 nm).**

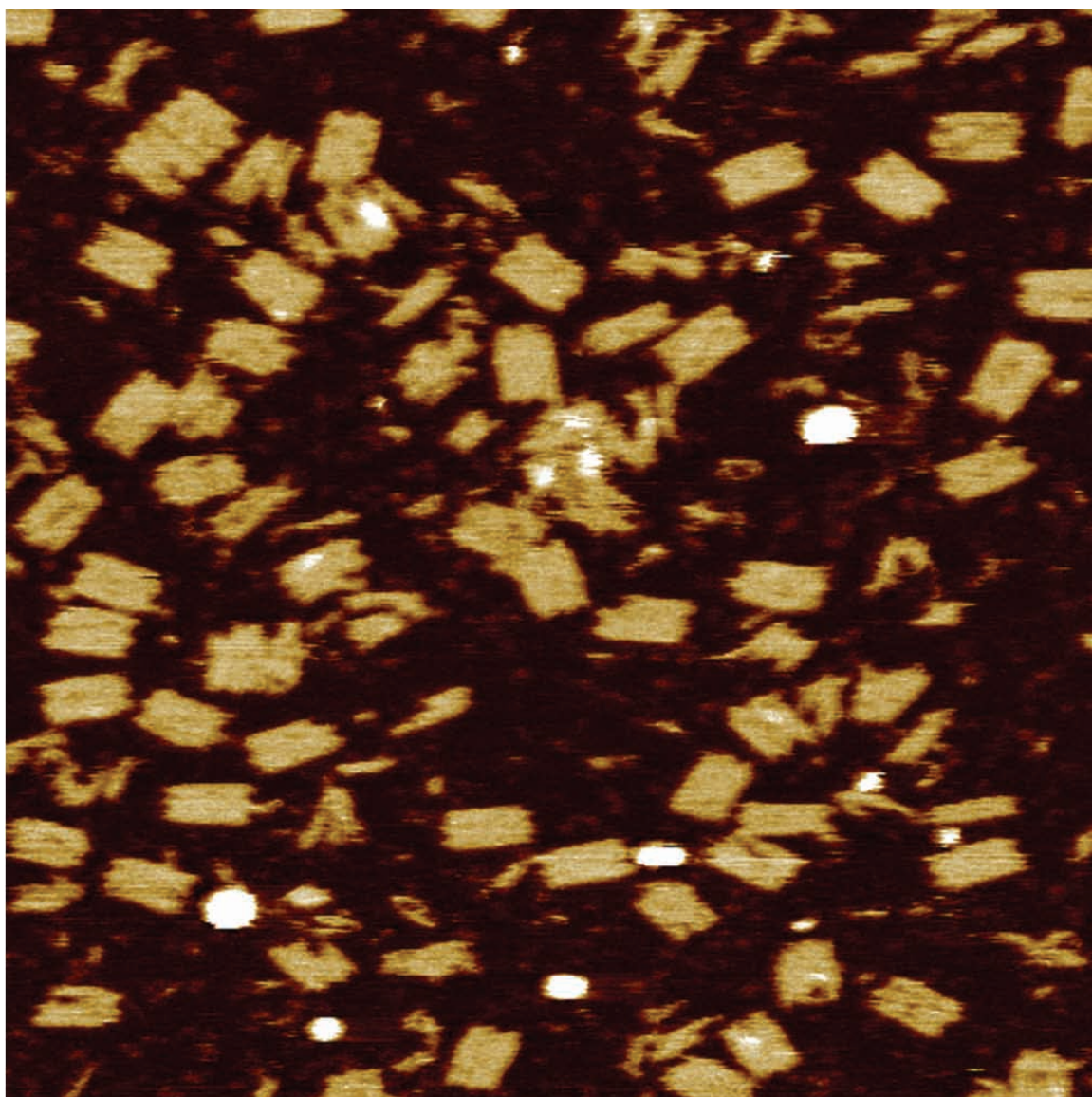


**Figure S126.** AFM image of the 10H×11T structure made from motif 9 (scale bar: 100 nm).

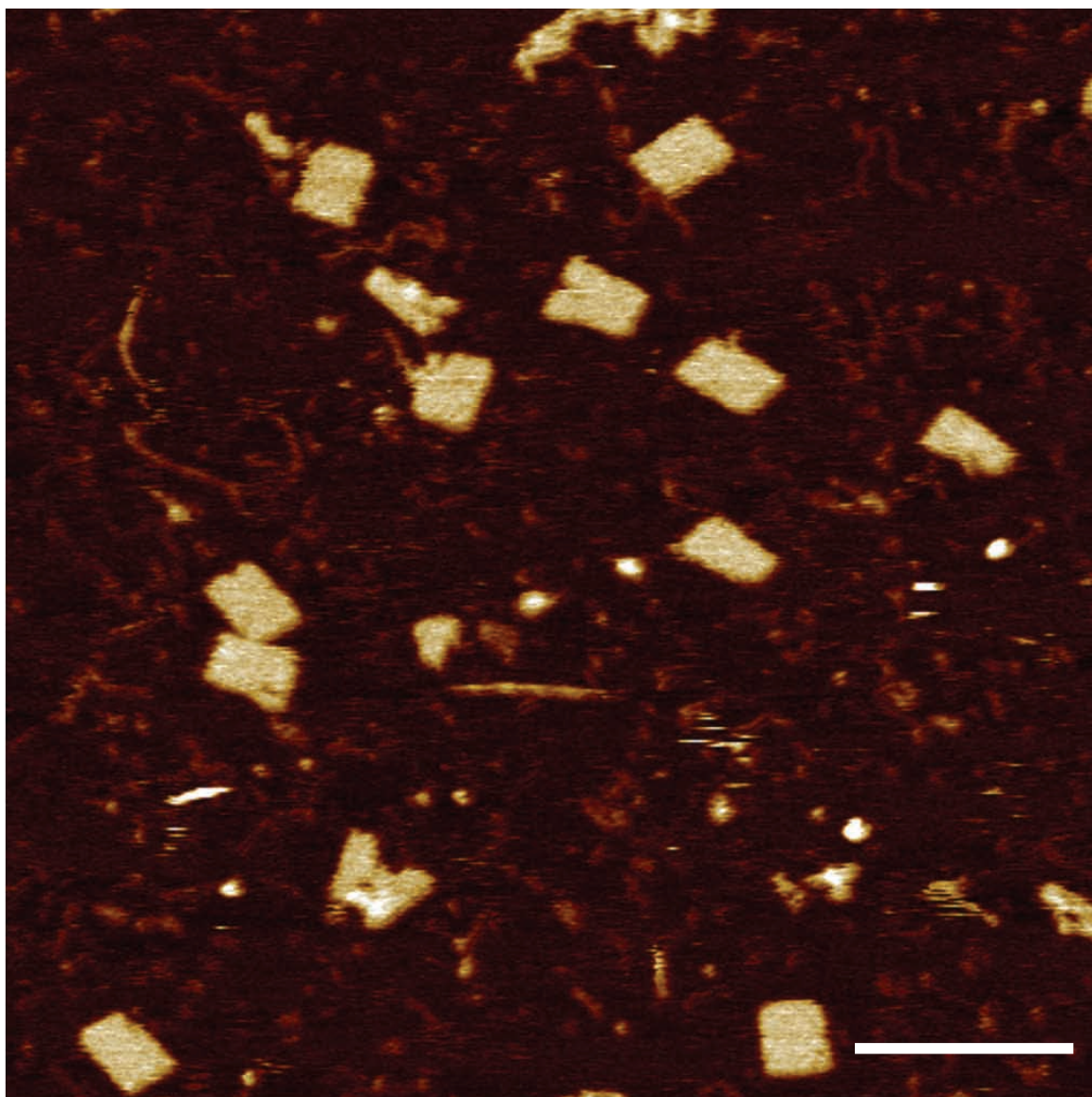


**Figure SI27. AFM image of the 10H×11T structure made from motif 10 (scale bar: 100 nm).**

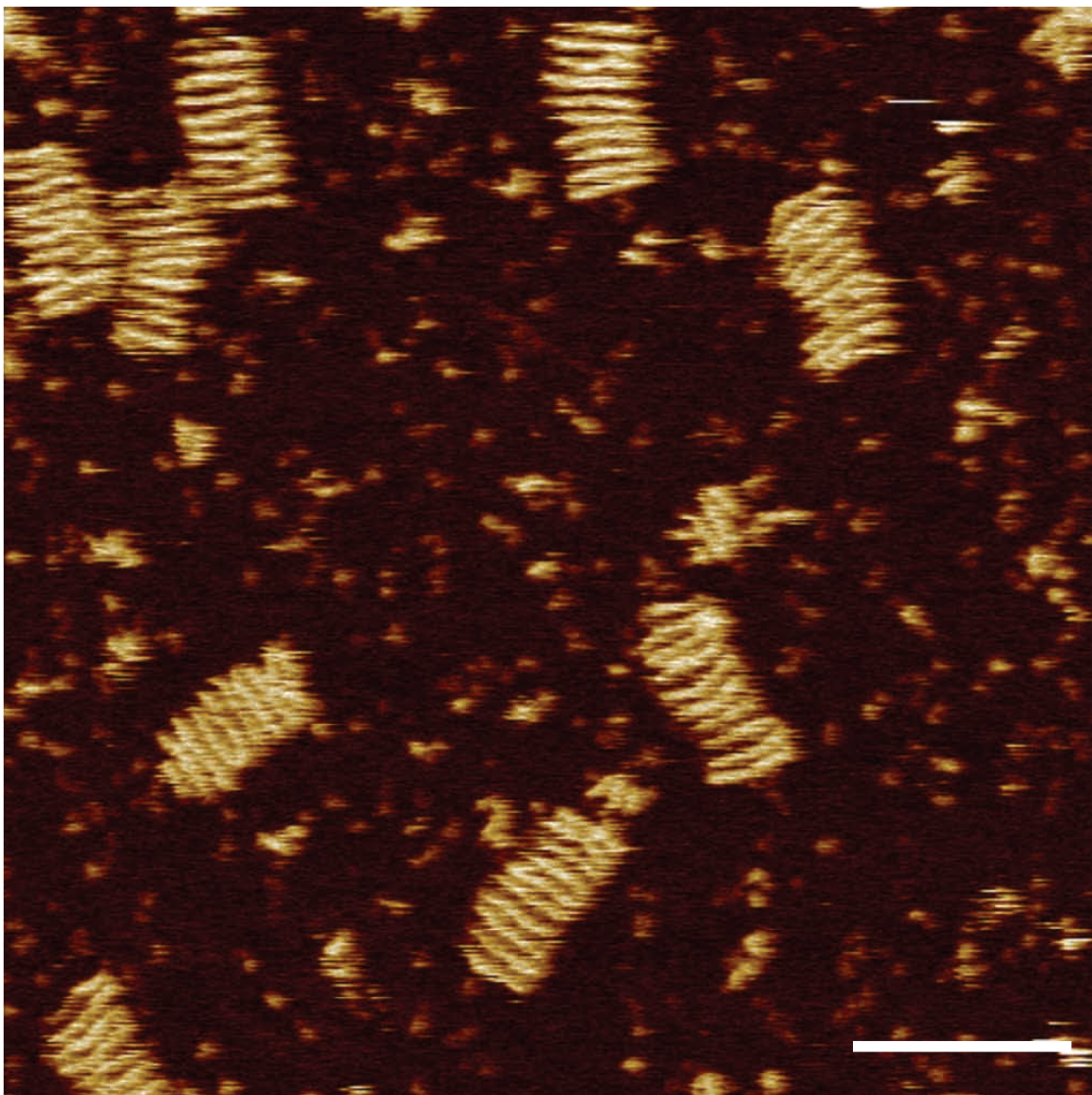


**Figure S128. AFM image of the 10H×11T structure made from motif 11.1 (scale bar: 100 nm).**

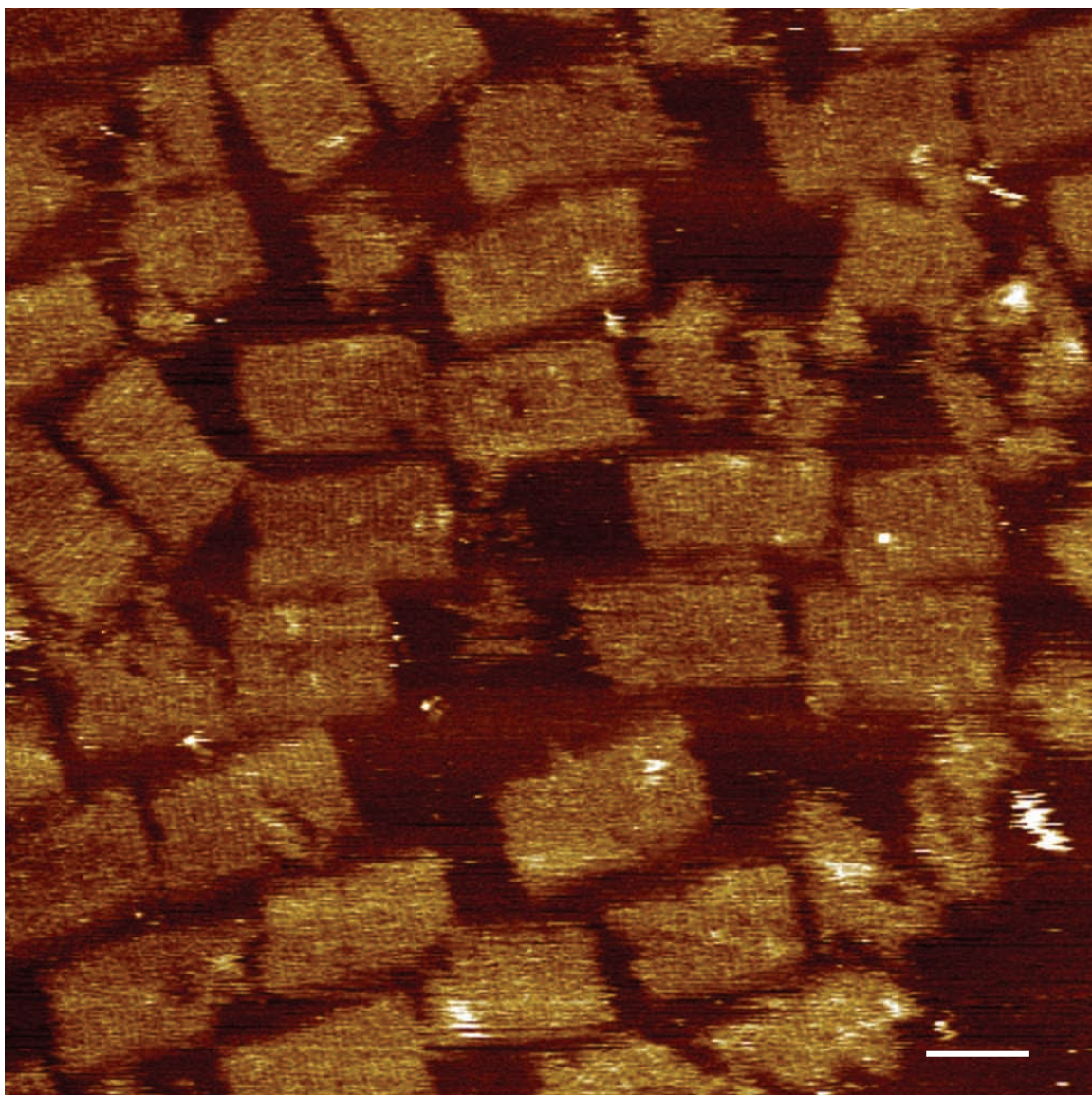


**Figure S129.** AFM image of the 24H×29T structure made from motif 11.1 (scale bar: 100 nm).

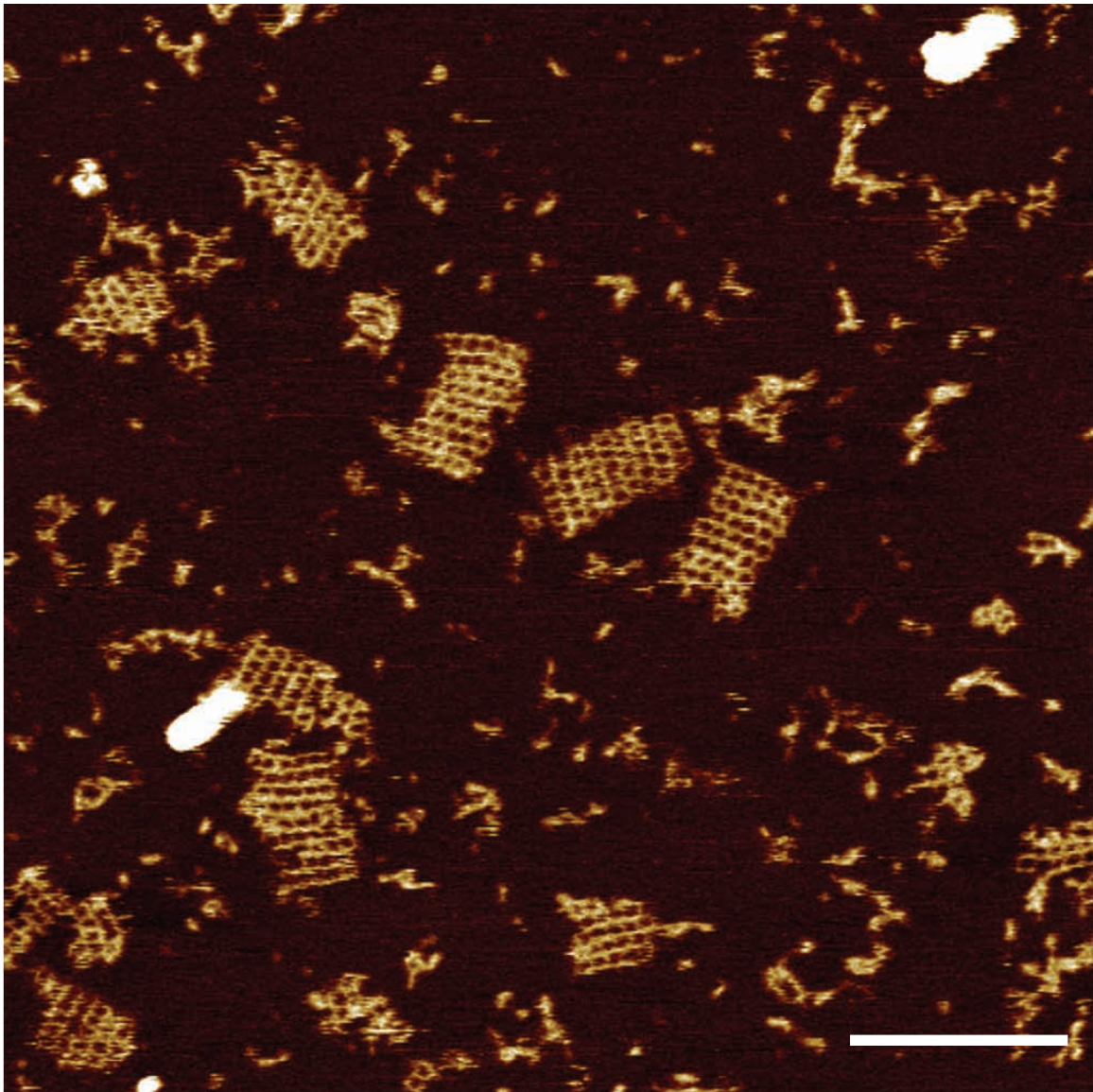


**Figure S130. AFM image of the 10H×11T structure made from motif 11.2 (scale bar: 100 nm).**

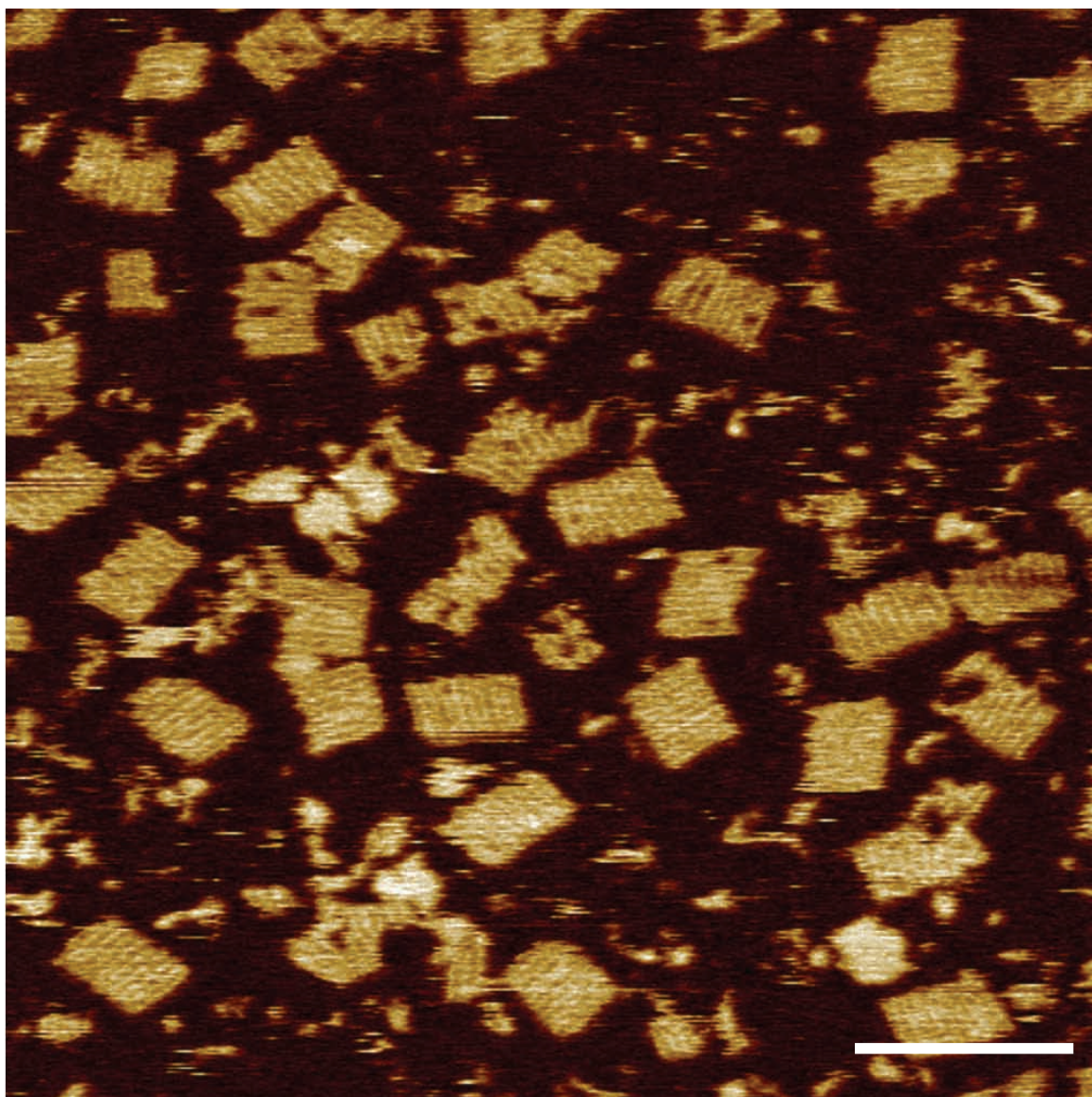


**Figure S131. AFM image of the 10H×11T structure made from motif 11.3 (scale bar: 100 nm).**

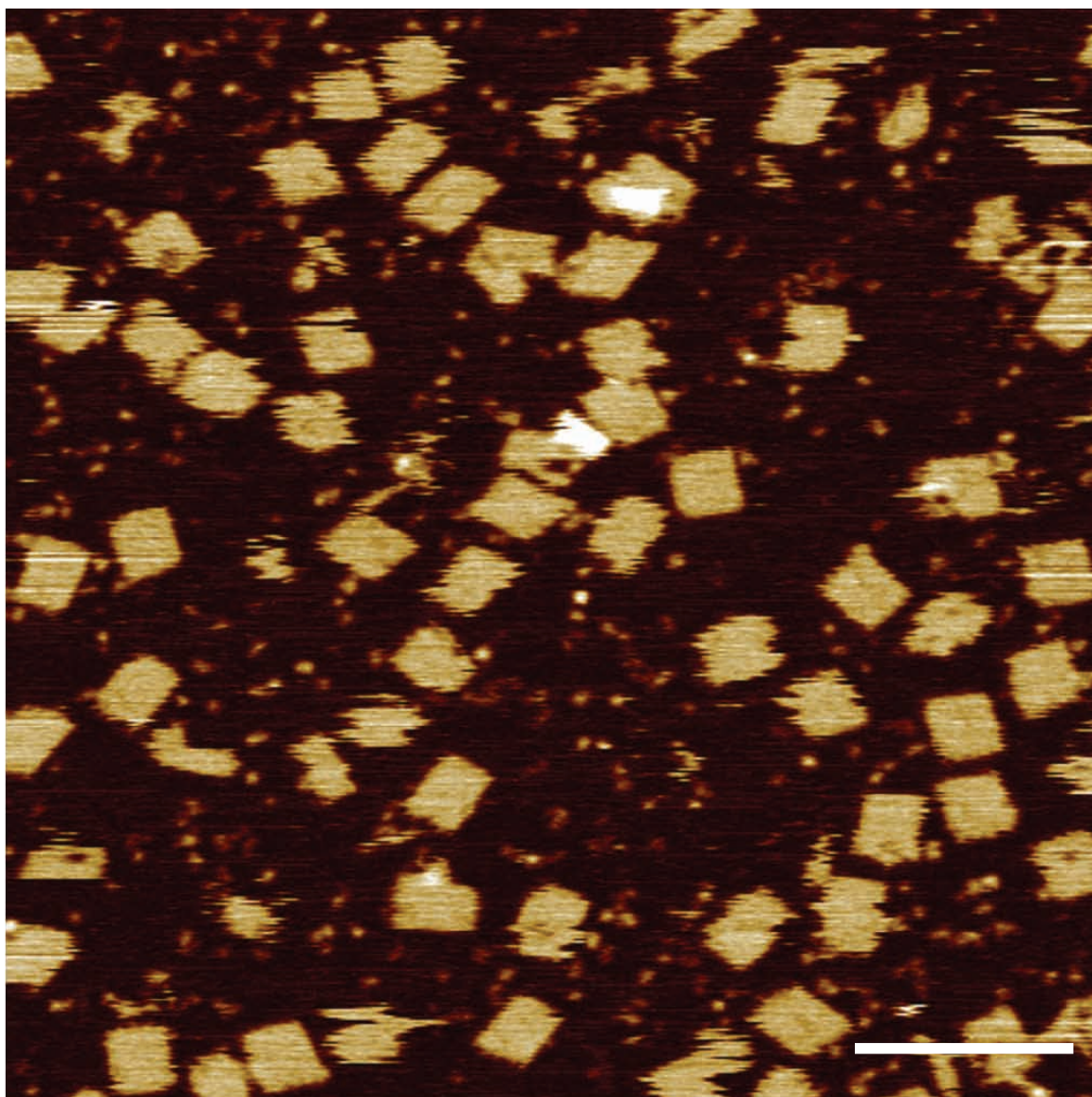


**Figure S132. AFM image of the 10H×11T structure made from motif 11.4 (scale bar: 100 nm).**

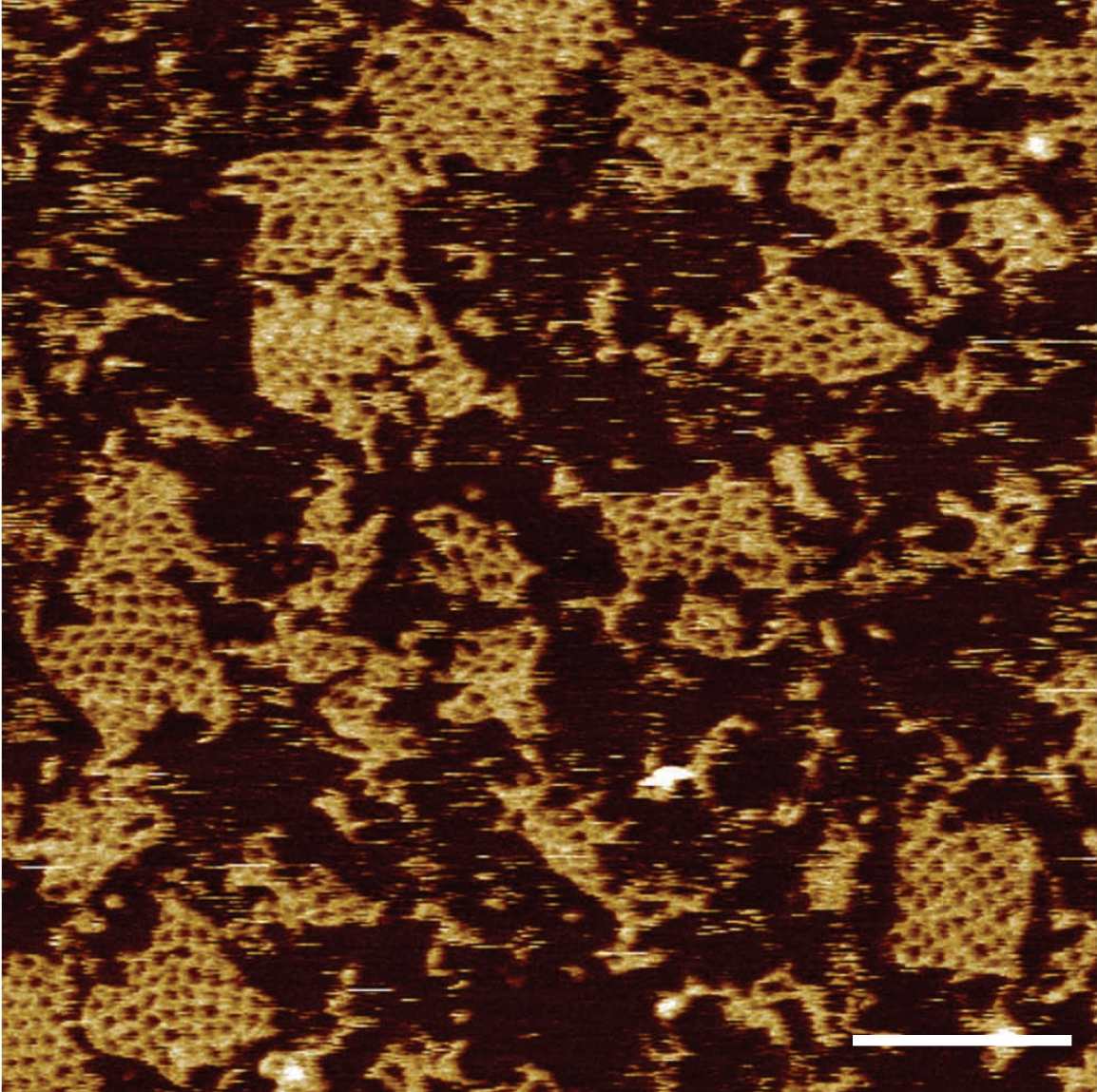


**Figure SI33. AFM image of the 5 square  $\times$  5 square structure made from motif 12** (scale bar: 100 nm). Before imaging, excessive poly-A strands were added to the annealed sample and incubated for 2 hours at 4°C . The sample was deposited on mica surface at 4°C in a cold room. The purpose of the excessive poly-A and low temperature treatment was to prevent the dissociation of poly-A strands from poly-T linker s.

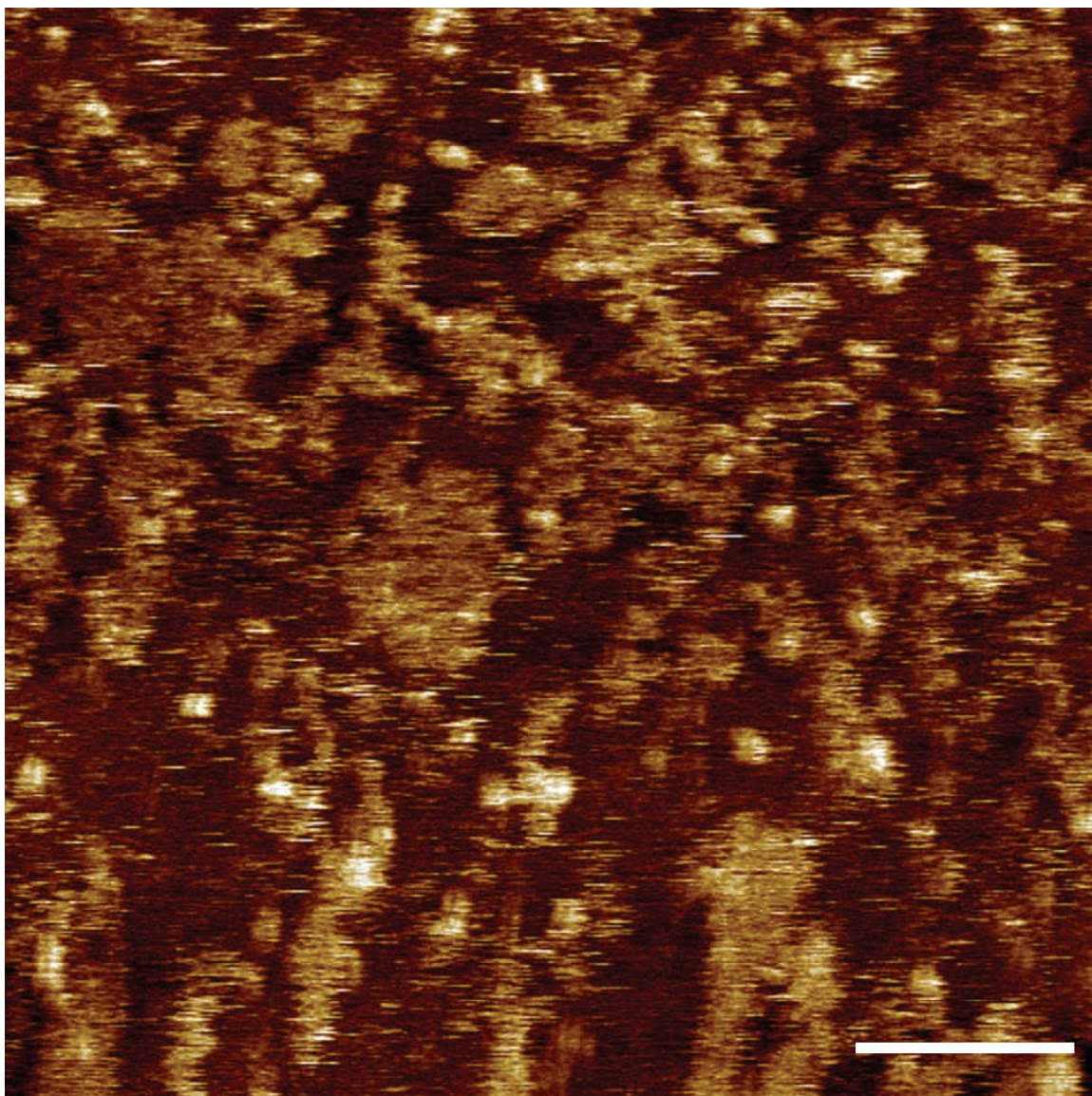


**Figure SI34. AFM image of the 5 square  $\times$  5 square structure made from motif 12** (scale bar: 100 nm). When structure made from motif 13 was imaged without applying the poly-A strand to pair with the poly-T linker, only amorphous structures was observed.

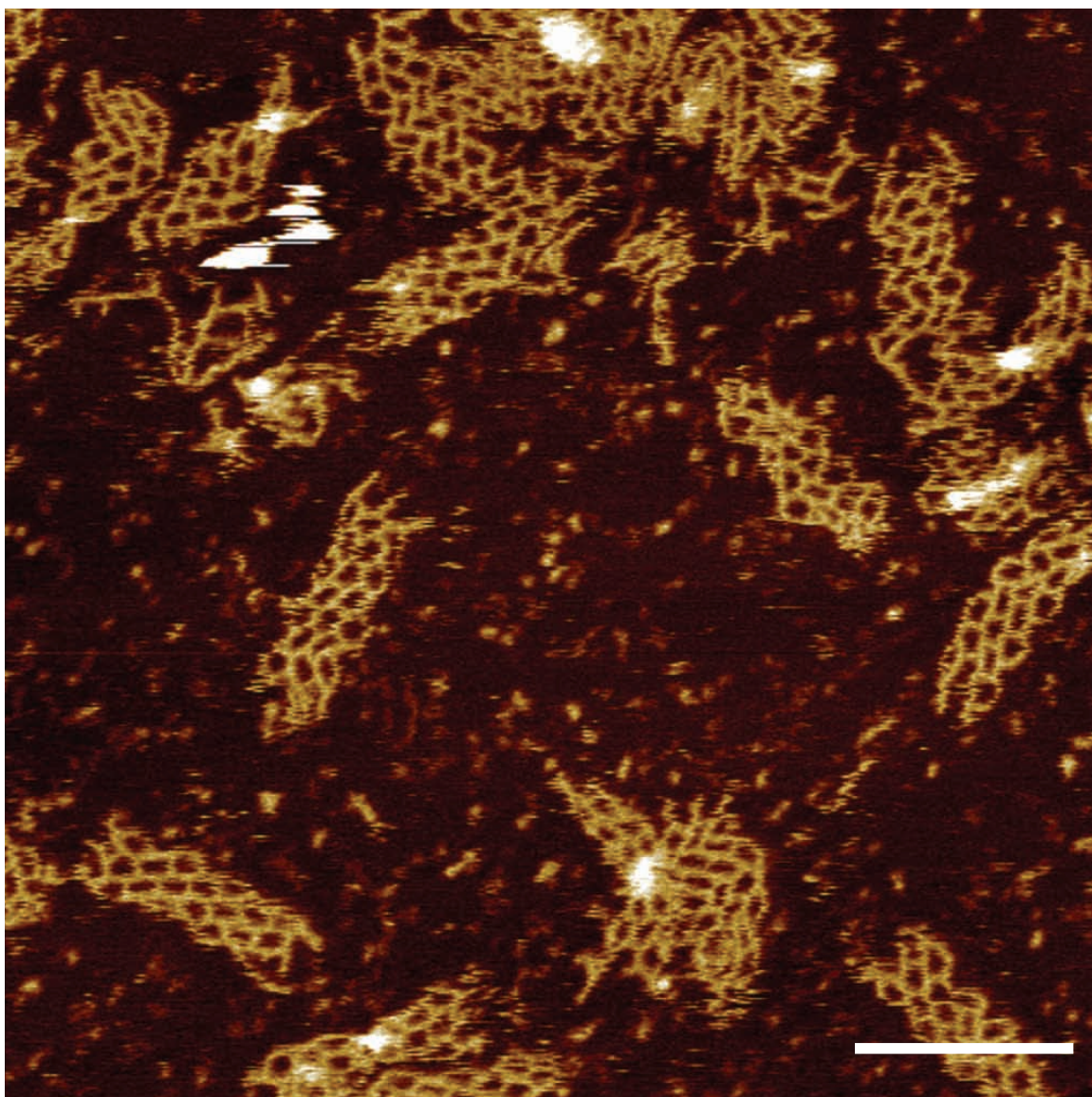
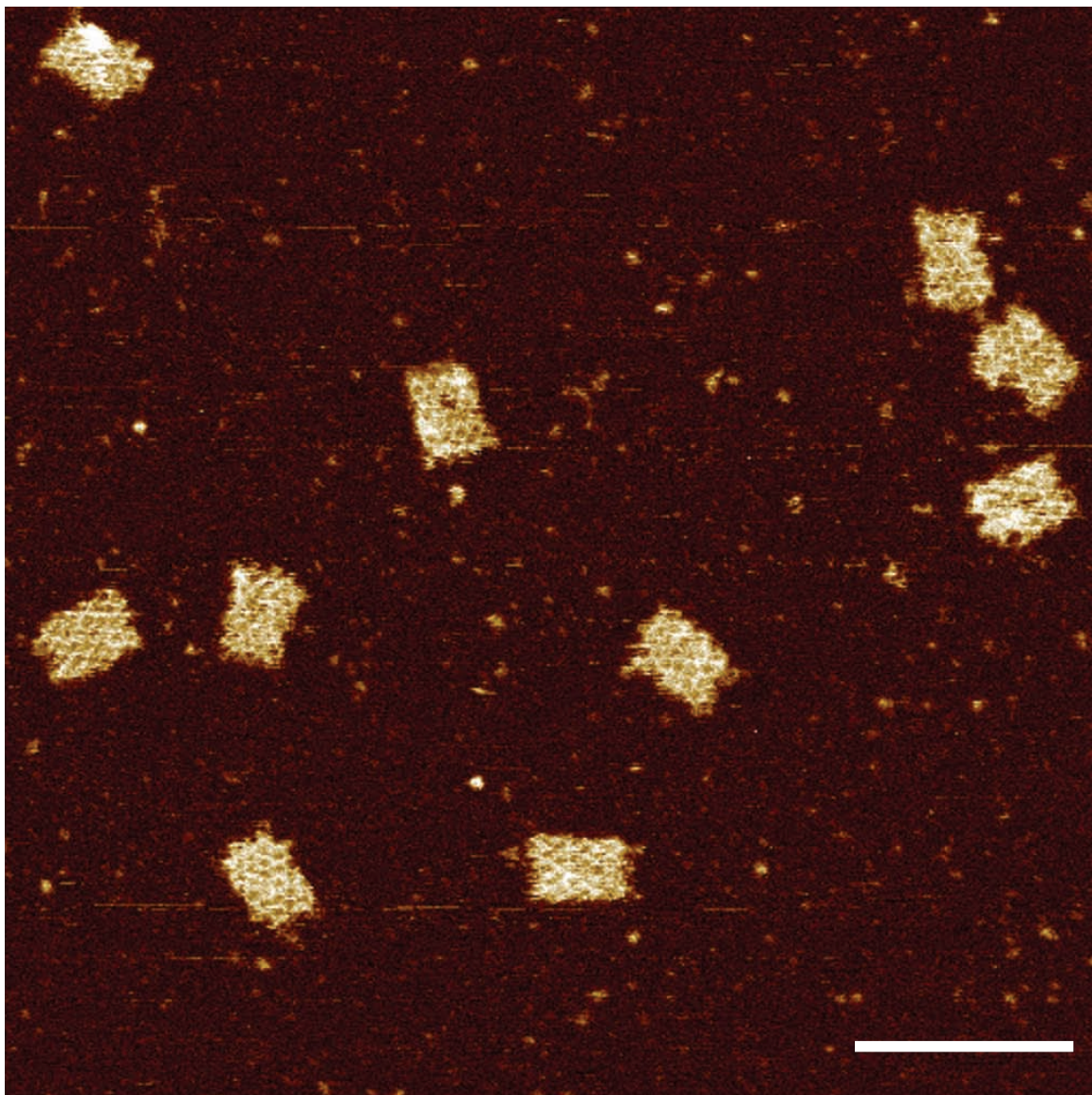
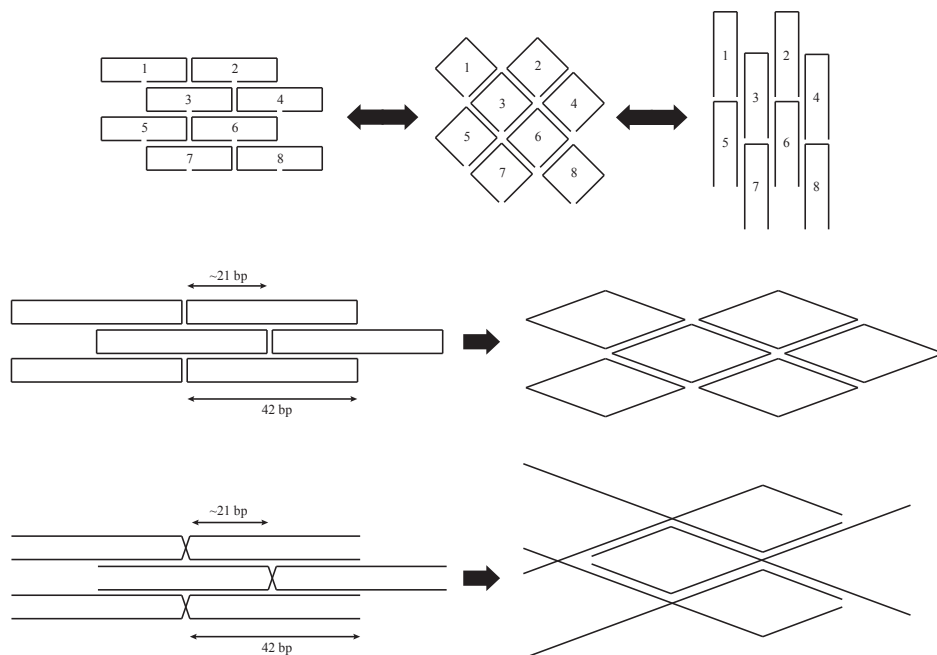


Figure SI35. AFM image of the 3 hexagon  $\times$  7 hexagon structure made from motif 13 (scale bar: 100 nm).



**Figure SI36. AFM image of the 4 hexagon  $\times$  6 hexagon structure made from motif 14 (scale bar: 100 nm).**

## SI1.4 Structure conformation variation



**Figure SI37. Conformation variation of structures.**

We noticed that some structures took with slightly different conformation from the original design. Fig. SI37 shows some examples of such conformation variations.

The top panel of Fig. SI37 shows three possible conformations for motifs 5.1, 5.2, and 5.3. The middle panel shows variation from closely packed parallel helices to wire-frame, fish-net like pattern. This was observed for motifs 6.2 and 6.3, but not for 6.1. Similar reconfiguration for motif 7.1 is shown in the bottom panel.

## SI1.5 Distance measurements

motif	<b>0</b>	<b>1</b>	<b>2</b>	<b>3.1</b>	<b>3.2</b>	<b>4.1</b>	<b>4.2</b>	<b>4.3</b>
dimension	10H×11T	10H×11T	10H×11T	10H×11T	10H×11T	10H×11T	~10H×11T	~10H×11T
width (nm , N=6)	33±2	21±2	27±1	24±2	27±2	23±2	27±1	31±1
length (nm , N=6)	45±2	41±2	42±1	42±5	44±3	40±2	40±1	50±2
yield	28%	33%	24%	33%	33%	35%	33%	38%
motif	<b>4.4</b>	<b>4.5</b>	<b>4.6</b>	<b>5.1</b>	<b>5.2</b>	<b>5.3</b>	<b>6.0</b>	<b>6.1</b>
dimension	~10H×11T	~10H×11T	~10H×11T	10H×11T	10H×11T	10H×11T	10H×11T	~10H×10T
width (nm , N=6)	27±1	32±2	26±2	N/A	N/A	N/A	29±1	29±2
length (nm , N=6)	37±1	47±2	36±3	N/A	N/A	N/A	40±1	43±2
yield	42%	38%	26%	32%	28%	12%	24%	27%
motif	<b>6.2</b>	<b>6.3</b>	<b>7.1</b>	<b>7.2</b>	<b>8</b>	<b>9</b>	<b>10</b>	<b>11.1</b>
dimension	~10H×11T	~10H×10T	~10H×11T	10H×10T	10H×11T	10H×11T	10H×11T	10H×11T
width (nm , N=6)	N/A	N/A	N/A	N/A	28±2	25±2	28±1	74±5
length (nm , N=6)	N/A	N/A	N/A	N/A	41±2	39±2	38±2	37±3
yield	22%	22%	33%	4.9%	30%	26%	10%	34.6%
motif	<b>11.2C</b>	<b>11.3</b>	<b>11.4</b>	<b>12</b>	<b>13</b>	<b>14</b>		
dimension	10H×11T	10H×11T	10H×11T	10H×11T	4×6, 10bp	3×7, 21bp		
width (nm , N=6)	68±6	50±3	28±1	N/A	32±2	31±3		
length (nm , N=6)	37±2	32±3	34±2	N/A	47±2	102±8		
yield	37%	44%	33%	34%				

**Figure SI38. Distance measurements and gel yields.** The table summarizes the designed dimensions, measured widths and lengths, and the measured gel yields for the structures formed from 30 different motifs. Measurements were not available for some motifs: the dimensions for structures from motifs 5.1, 5.2, 5.3, 6.2, 6.3 and 7.1 were not uniform presumably due to the structural variation shown in Fig. SI37; structures from motifs 12, 13 and 14 were also flexible thus the dimensions were not uniform; the imaging quality for structures from motif 7.2 was not good enough for distance measurement.

The AFM images were analyzed using Nanoscope Analysis (version 1.20). Lengths and widths of the rectangles were measured; 6 data points of lengths and widths for each shape were used for statistical analysis in Fig. SI38.

## SI2 Curvature design and characterization

### SI2.1 Curvature: design and modeling

The strand weaving pattern of the strands can affect the curvature of the structure. We performed a case study below to test a number of motifs to design a flat 24H×29T rectangle structure.

#### SI2.1.1 Domain shift

Working towards our goal of controlling curvature and design flat structure, we first attempted to reduce curvature by adjusting the domain length of the canonical U-shaped SST motif. Assuming that the crossover points of adjacent double helices are collinear with the centers of the adjacent helices, our model predicts an average curvature of 30° per double helix for the motif 0 and hence 720° for the 24H×29T rectangle. The calculation is described in detail below (Fig. SI39a).

A B-DNA double helix is modeled as having 10.5 base pairs per helical turn ( $360^\circ/10.5 = 34.3^\circ$  each bp) and a minor groove angle of 150°. For motif 0 (Fig. SI39a),  $\theta_a = 150^\circ + 360^\circ/10.5 \times a$  (150° is the minor groove angle from top helix to bottom helix;  $a = 10$  indicates 10 nt between crossover points across helices shown in red and cyan lines) =  $493^\circ \cong 133^\circ$  ( $0^\circ \leq \theta \leq 360^\circ$ ), the curvature  $\delta$  can be defined as  $\delta = 180^\circ - \theta$  ( $-180^\circ \leq \delta \leq 180^\circ$ ), so  $\delta_a = 180^\circ - \theta_a = 180^\circ - 133^\circ = 47^\circ$ . Similarly,  $\theta_b = 150^\circ + 360^\circ/10.5 \times b$  (150° is the minor groove angle from top helix to bottom helix;  $b = 11$  indicates means 11 nt between crossover points across helices shown in cyan and green lines) =  $527^\circ \cong 167^\circ$ , and  $\delta_b = 180^\circ - \theta_b = 13^\circ$ .  $\delta_a + \delta_b = 47^\circ + 13^\circ = 60^\circ$ . Because there are 24 helices for the structure, the overall curvature  $C_{M0} = 12 \times 60^\circ = 720^\circ$  (Fig. SI40a).

By adopting a domain length of 9/12 nt (motif 1) instead of the canonical 10/11 nt in motif 0, we were able to reduce the calculated average curvature per double helix from 30° to -4° and hence -96° for the 24H rectangle. The details are described below.

In order to reduce curvature, we made adjustment for domain lengths  $a$  and  $b$ . For motif 1, when  $a = 11$  and  $b = 12$ ,  $\theta_a = 150^\circ + 360^\circ/10.5 \times 11 = 527^\circ \cong 167^\circ$  and  $\theta_b = 150^\circ + 360^\circ/10.5 \times 12 = 561^\circ = 201^\circ$ , then  $\delta_a = 180^\circ - \theta_a = 13^\circ$  and  $\delta_b = 180^\circ - \theta_b = -21^\circ$ , and  $\delta_a + \delta_b = 13^\circ - 21^\circ = -8^\circ$ , so  $C_{M1} = 12 \times (-8^\circ) = -96^\circ$  (Fig. SI40b).

However, a 2D structure (such as that formed by motif 0 or motif 1) designed with anti-parallel crossovers will always possess a minor groove side that displays minor grooves at crossovers and a major groove side that displays major grooves at crossovers. As such, the curvature will not be perfectly counterbalanced for anti-parallel helix based structures designed from U-shaped motifs.

#### SI2.1.2 Parallel helix design

Next, we hypothesize that curvature induced by the asymmetric arrangement of major and minor grooves at the crossovers on the two sides of the structures would be negated in parallel-helix-based structures formed from Z-shaped motifs: here, on either side of the structure, the crossovers display major and minor grooves in an alternating fashion. Like in the U-shaped motif, we assume the crossover points of adjacent double helices are collinear with the centers of the adjacent helices, and designed a Z-shaped motif (motif 3.1) based structure that is expected to be perfectly flat. The calculation details are described below (Fig. SI39b).

For motif 3.1 (Fig. SI39b, left panel),  $\theta_a = 150^\circ + 360^\circ/10.5 \times a$  (150° is the minor groove angle from top helix to bottom helix;  $a = 10$  indicates 10 nt between crossover points across helices shown in red and cyan lines) =  $493^\circ \cong 133^\circ$  and  $\theta_b = -150^\circ + 360^\circ/10.5 \times b$  (-150° is the minor groove angle from bottom helix to top helix;  $b = 11$  indicates 10 nt between crossover points across helices shown in red and cyan lines) =  $227^\circ$ , then  $\delta_a = 180^\circ - \theta_a = 47^\circ$  and  $\delta_b = 180^\circ - \theta_b = -47^\circ$ , and  $\delta_a + \delta_b = 0^\circ$ .

Thus, according to our model, the structures of motif 3.1 should be flat. However, our experimental data revealed significant curvature in the structure. The discrepancy between our model and experiments led us to revise the previous assumption that the crossover points of adjacent double helices are collinear with the centers of the adjacent helices. Although our experimental results from U-shaped motifs (motifs 0 and 1) did not invalidate such an assumption, the results from Z-shaped motifs were clearly incompatible with this collinear assumption. To reconcile this discrepancy between the model and the experimental results, we introduced an offset angle  $\alpha$  formed between a base at the crossover

and the two center points of the adjacent helices (Fig. SI39b, middle). In a structure formed from motif 3.1, this offset angle at the crossover always appears on the same side of the structure, resulting in an accumulative curvature for this otherwise flat structure.

Incidentally, another structure based on a Z-shaped motif with different domain length (Motif 3.2) appeared approximately flat in our experiments. Assuming this structure (motif 3.2) has  $0^\circ$  curvature, we back-calculated an approximate value for the offset angle  $\alpha$  ( $8.5^\circ$ ). Using this  $\alpha$  value, the 24H $\times$ 29T structure formed from Motif 3.1 was expected to have significant curvature, consistent with experimental observation of a curved structure. The detailed calculation is described below (Fig. SI39c).

As we can see in the model for motif 3.2 (Fig. SI39c),  $\theta'_a = \theta_a + 2\alpha$  and  $\theta'_b = \theta_b + 2\alpha$ , as long as  $\theta_a = 150^\circ + 360^\circ/10.5 \times a$  ( $150^\circ$  is the minor groove angle from top helix to bottom helix;  $a = 10$  indicates 10 nt between crossover points across helices shown in red and cyan lines) =  $493^\circ \cong 133^\circ$  and  $\theta_b = -150^\circ + 360^\circ/10.5 \times b$  ( $-150^\circ$  is the minor groove angle from bottom helix to top helix;  $b = 10$  indicates 10 nt between crossover points across helices shown in red and cyan lines) =  $193^\circ$ ,  $\theta'_a = 133^\circ + 2\alpha$  and  $\theta'_b = 193^\circ + 2\alpha$ , then  $\delta_a = 180^\circ - \theta'_a = 47^\circ - 2\alpha$  and  $\delta_b = 180^\circ - \theta'_b = 13^\circ - 2\alpha$ , and  $\delta_a + \delta_b = 34^\circ - 4\alpha$ . If we suppose the structures are more or less flat, then  $34^\circ - 4\alpha = 0^\circ$ , so  $\alpha = 8.5^\circ$ . We can fit the value of  $\alpha$  back to the structure of motif 3.1, in which  $\delta_a + \delta_b = 0^\circ - 4 \times 8.5^\circ = -34^\circ$  (Fig. SI39b, middle), so the overall curvature  $C_{M3.1} = 12 \times (-34^\circ) = -408^\circ$ . It is consistent with our experimental results for the rolled up structures (curving down).

### SI2.1.3 Corrugation design

We next devised a corrugated design (motif 4.1) where the offset angle  $\alpha$  appears alternately on the two sides of the structure and thus its effect would cancel out (independent of its value, Fig. SI39d). As we can see in the model for motif 4.1 (Fig. SI39d),  $\theta_a = 150^\circ + 360^\circ/10.5 \times a$  ( $a = 10$ ) =  $493^\circ \cong 133^\circ$  and  $\theta_b = -150^\circ + 360^\circ/10.5 \times 11$  ( $b = 11$ ) =  $227^\circ$ . Because of the corrugation,  $\theta'_a = \theta_a$  and  $\theta'_b = \theta_b$ ,  $\delta_a + \delta_b = 180^\circ - 133^\circ + 180^\circ - 227^\circ = 0^\circ$ . Therefore, the structure is flat according to our calculation (Fig. SI40c). The experimental results are consistent with our theoretical calculation.

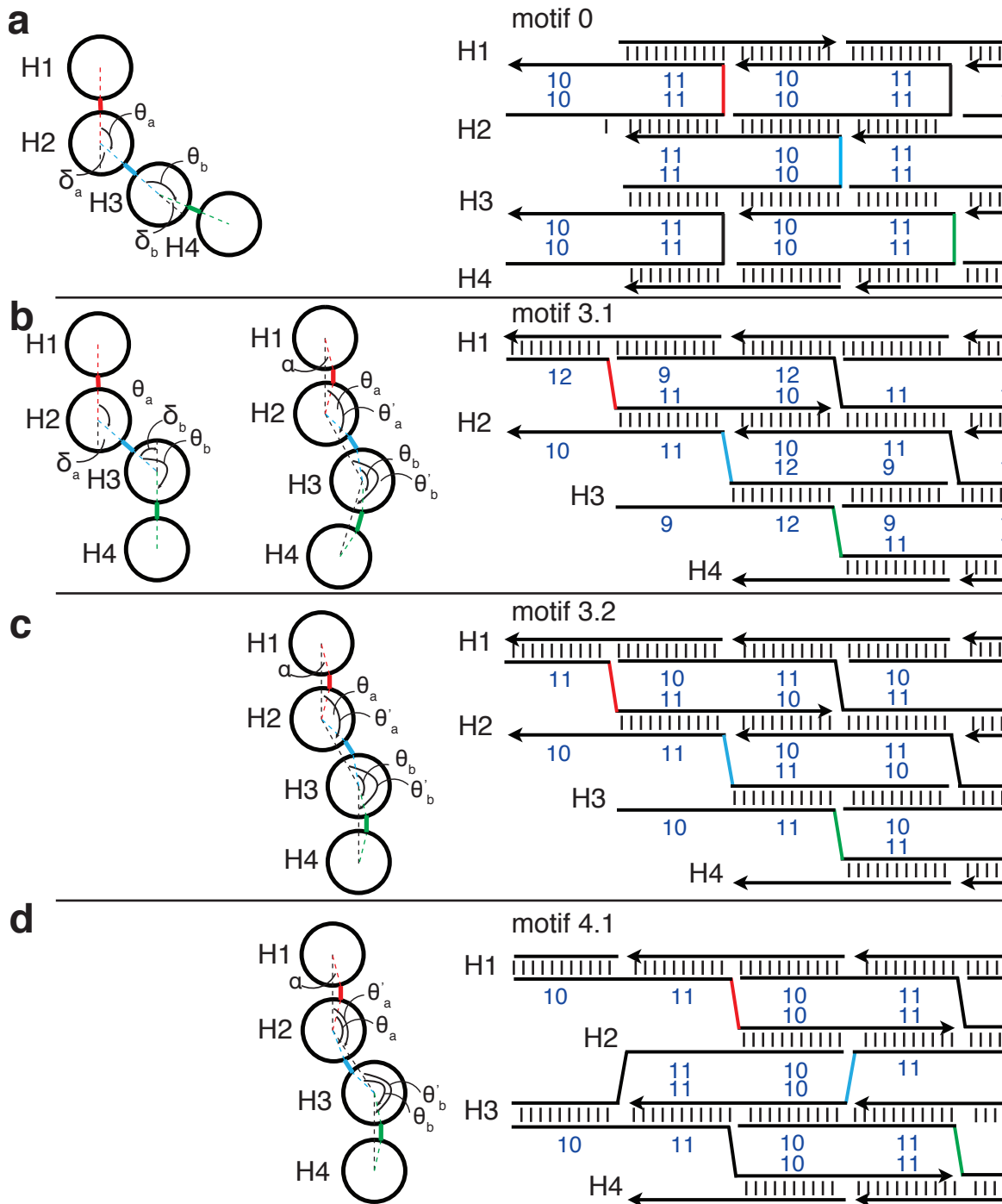


**Figure SI39. Models for curvature calculation.** **a** Curvature model for U-shaped motif. **b** Curvature models for motif 3.1 without parameter  $\alpha$  and with parameter  $\alpha$ . **c** Curvature model for motif 3.2 with parameter  $\alpha$ . **d** Curvature model for motif 4.1. Dihedral angle  $\theta_a$  is formed by three adjacent helices H1, H2 and H3; the next dihedral angle  $\theta_b$  is formed by helices H2, H3 and H4. Numbers indicate domain lengths.

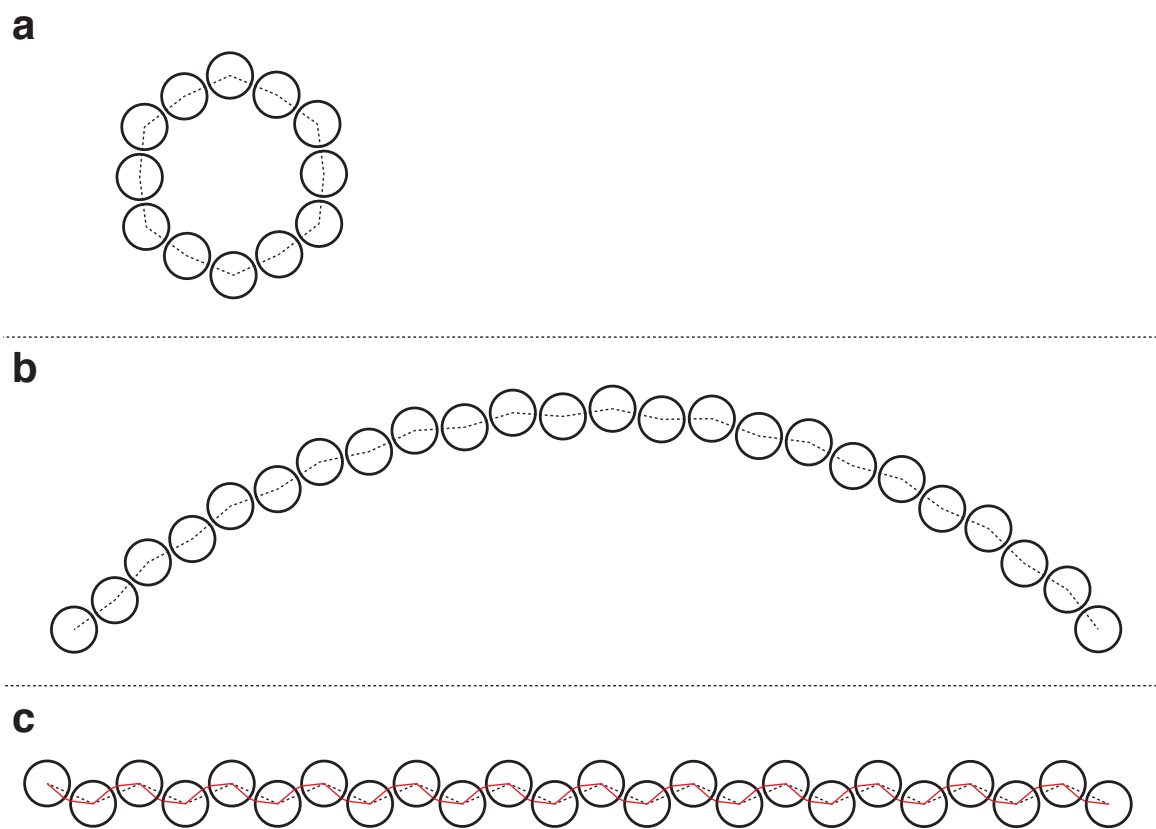


**Figure SI40. Curvature models for structures in cross-section view.** **a** Model for motif 0. Note that the full structure curves with  $720^\circ$  instead of  $360^\circ$ . **b** Model for motif 1. **c** Model of motif 4.1 (red lines indicate the offset positions for crossover points (see details in Sect. SI2.1.3).

## SI2.2 Agarose gel electrophoresis results

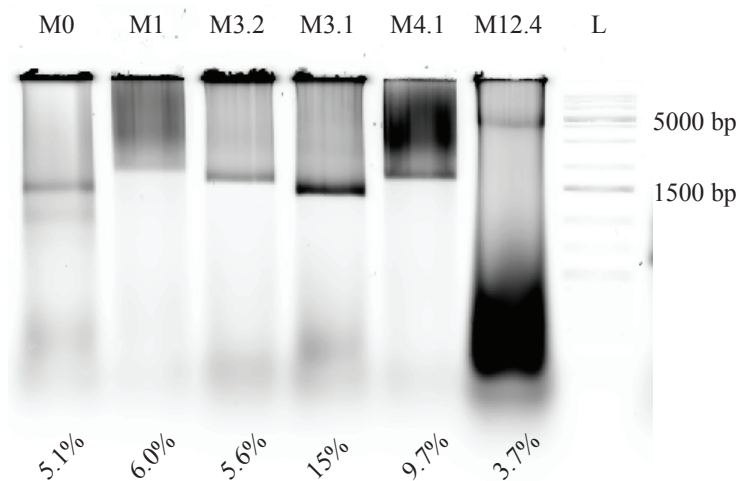


**Figure SI41. Agarose gel electrophoresis analysis for 24H×29T structures used for curvature study.** Labels above a gel lane indicates the corresponding motif (lane L: 1 kb DNA ladder). For example, M0 refers to the structure made from motif 0. Samples (100 nM) were annealed in 0.5× TE buffer (25 mM MgCl<sub>2</sub>) from 90°C to 25°C over 17 hours. Then, a 15 μL sample (mixed with 3 μL 6× bromophenol blue loading dye) was loaded into a 2% native agarose gel and subjected to electrophoresis in an ice water bath with 0.5× TBE running buffer (10 mM MgCl<sub>2</sub>).

Fig. SI41 shows the result of native agarose gel electrophoresis for structures used for the curvature study. The purified samples were then imaged with AFM (Fig. SI42 to Fig. SI46).

### SI2.3 AFM imaging results

Figs. SI42-SI46 show the AFM images of structures made from different motifs with a size of  $24\text{H}\times 28\text{T}$  (motif 0) or  $24\text{H}\times 29\text{T}$  (motifs 1, 3.1, 3.2, 4.1).

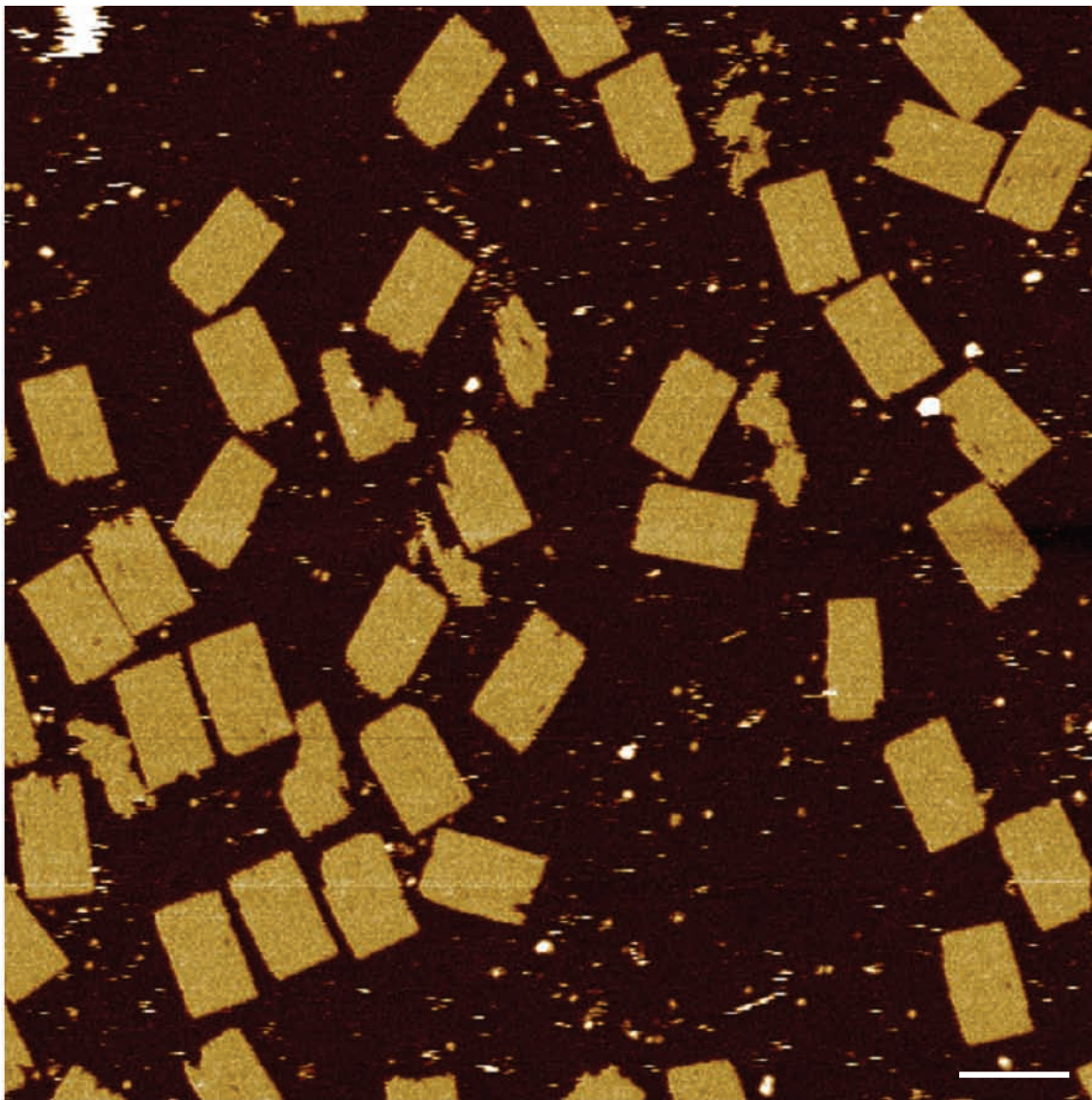
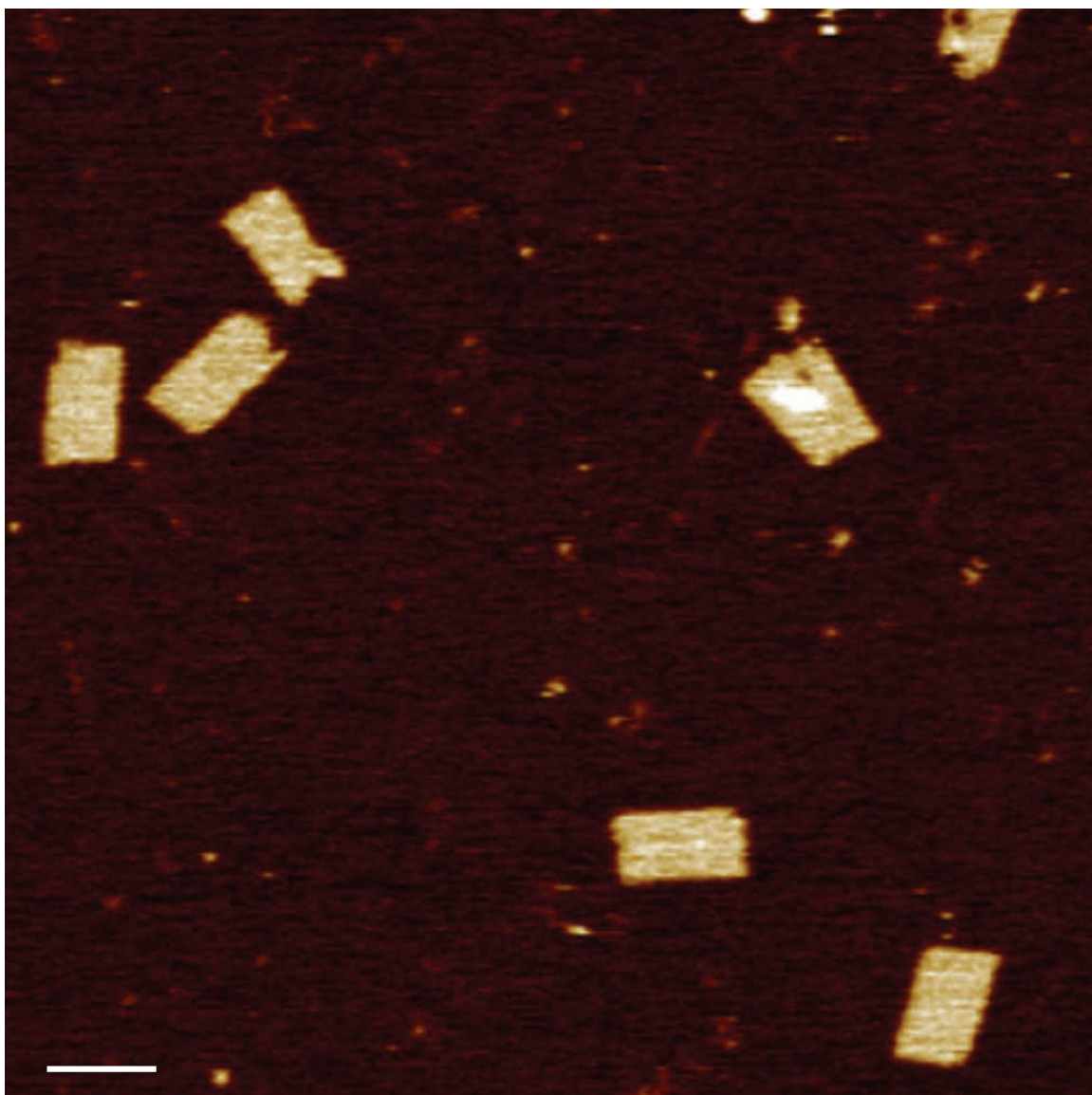
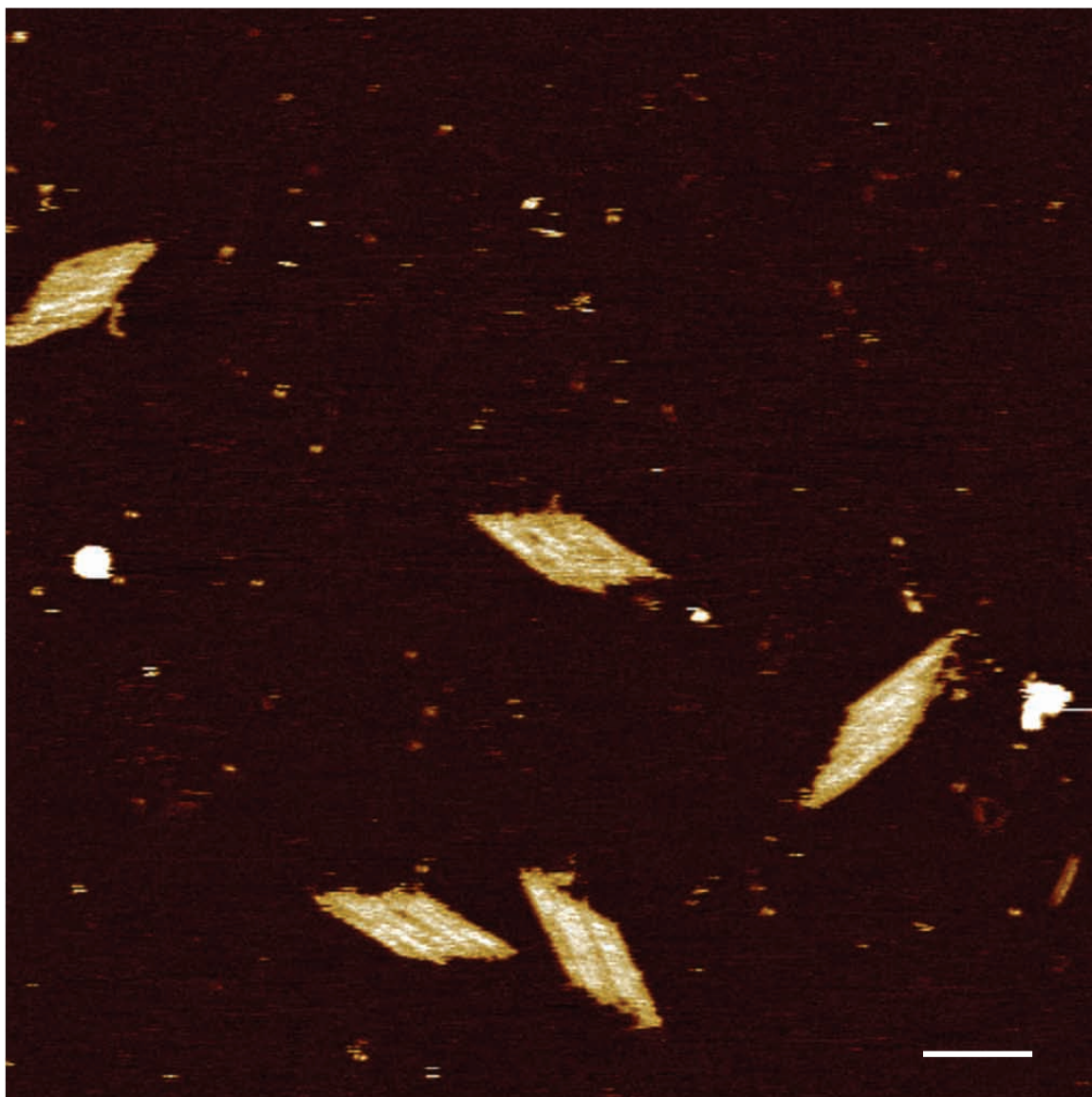


Figure SI42. AFM image of the  $24\text{H}\times 28\text{T}$  structure made from motif 0 (scale bar: 100 nm).



**Figure S143. AFM image of the 24H×29T structure made from motif 1 (scale bar: 100 nm).**



**Figure S144. AFM image of the 24H×29T structure made from motif 3.1 (scale bar: 100 nm).**

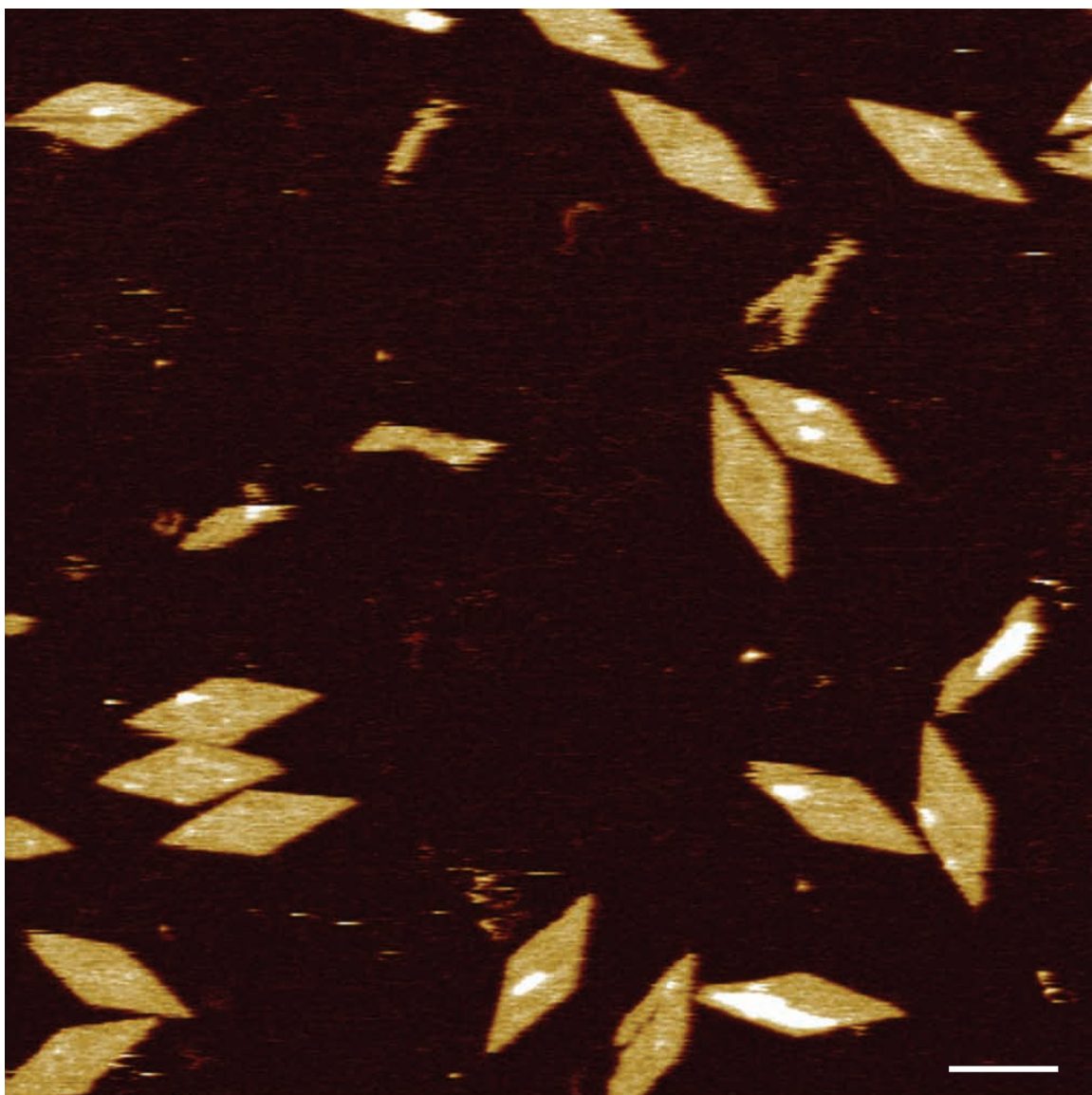


**Figure SI45. AFM image of the 24H×29T structure made from motif 3.2 (scale bar: 100 nm).**

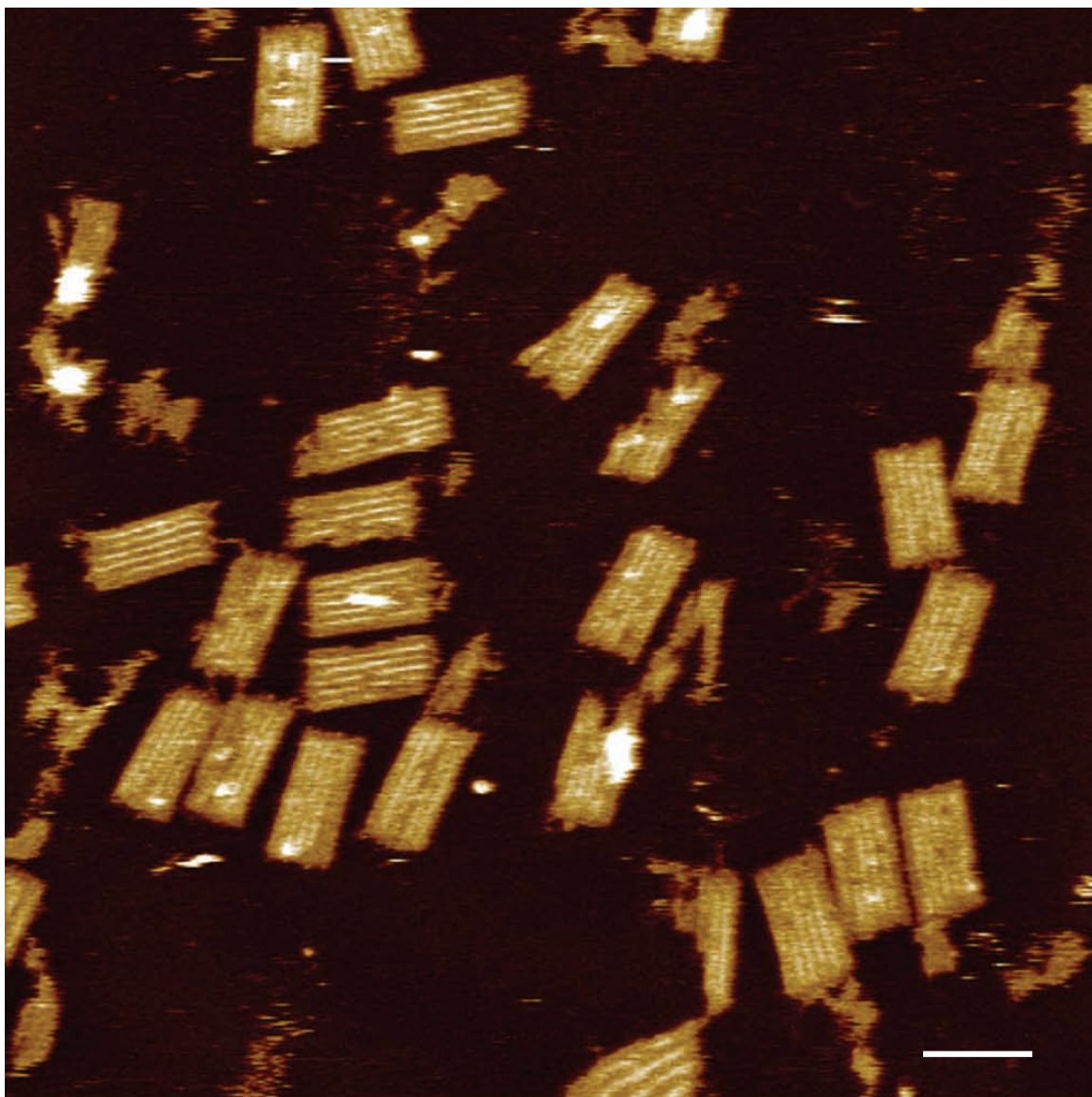


**Figure S146. AFM image of the 24H×29T structure made from motif 4.1 (scale bar: 100 nm).**

## SI2.4 TEM imaging results

Figs. SI47-SI51 show the TEM images of structures made from different motifs with a size of 24H×28T (motif 0) or 24H×29T (motifs 1, 3.1, 3.2 and 4.1).

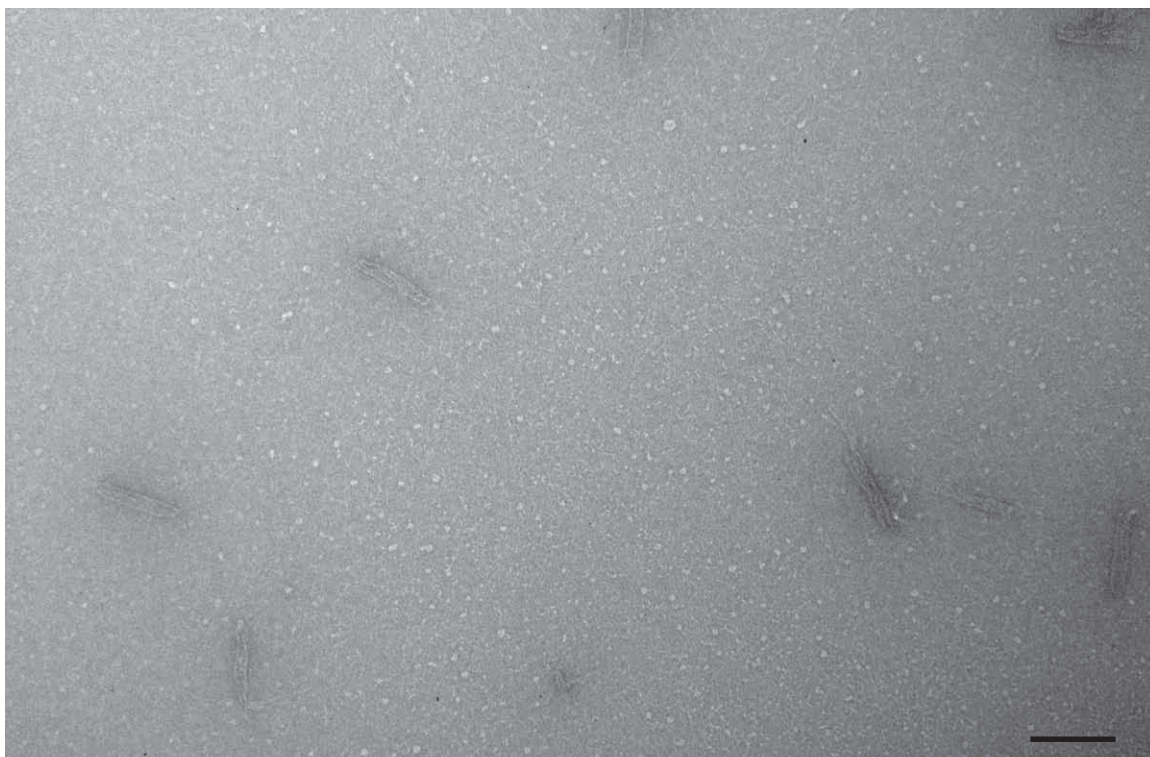


**Figure SI47. TEM image of the 24H×28T structure made from motif 0** (scale bar: 100 nm).

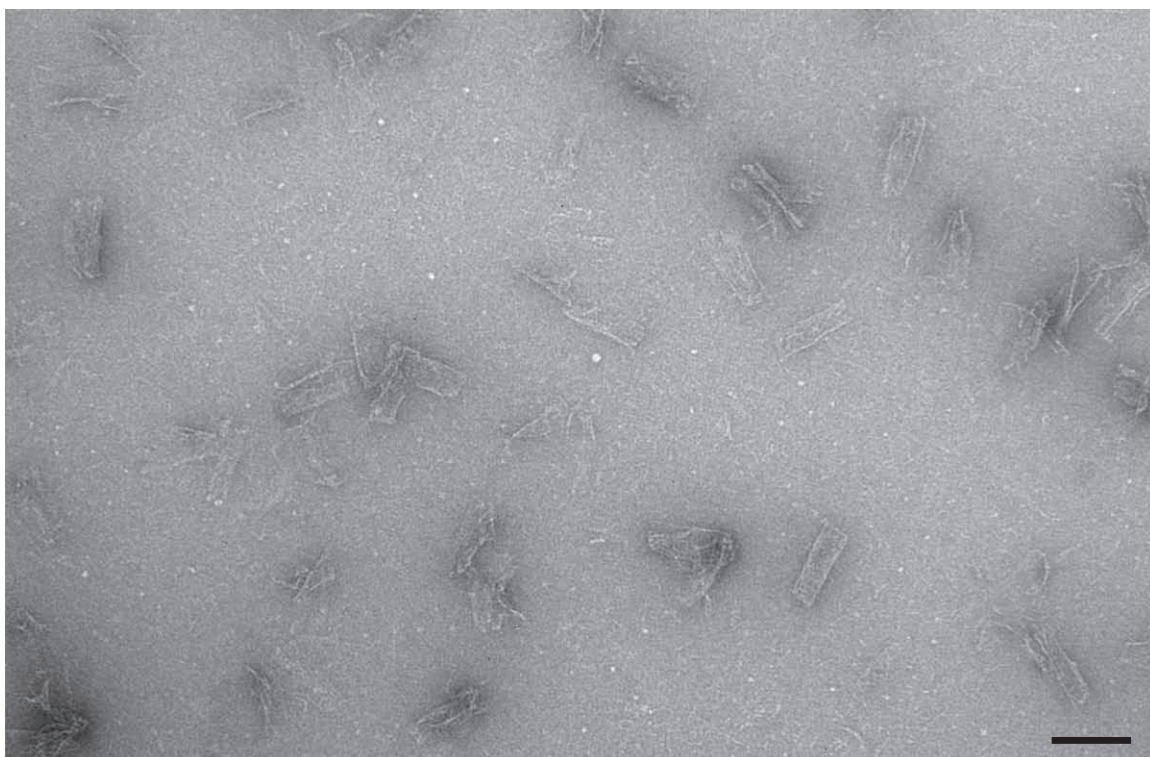


**Figure SI48. TEM image of the 24H×29T structure made from motif 1** (scale bar: 100 nm).

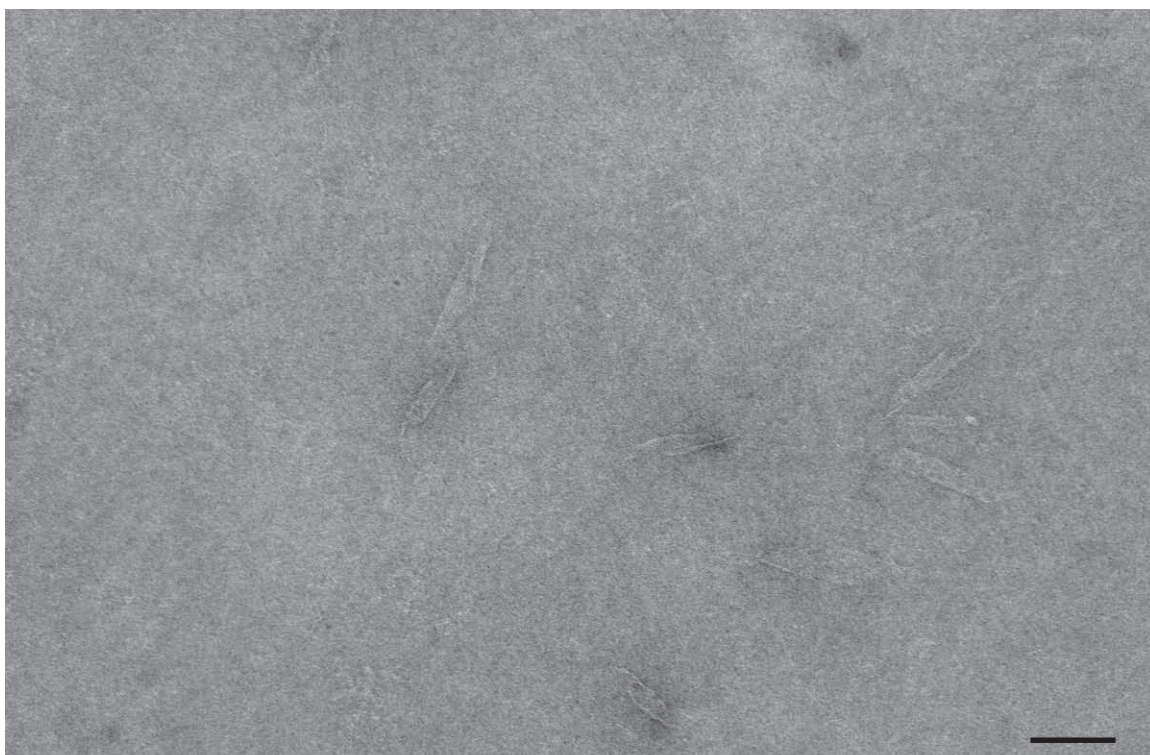


**Figure SI49. TEM image of the 24H×29T structure made from motif 3.1 (scale bar: 100 nm).**

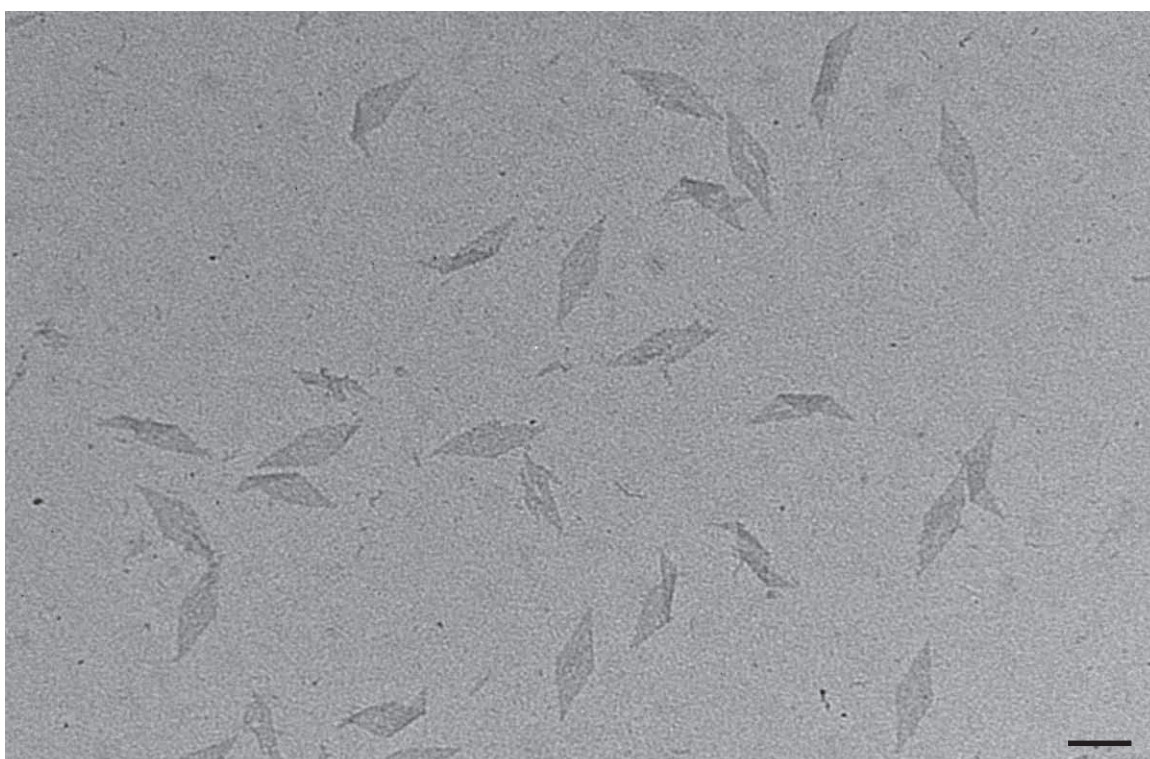


**Figure SI50. TEM image of the 24H×29T structure made from motif 3.2 (scale bar: 100 nm).**

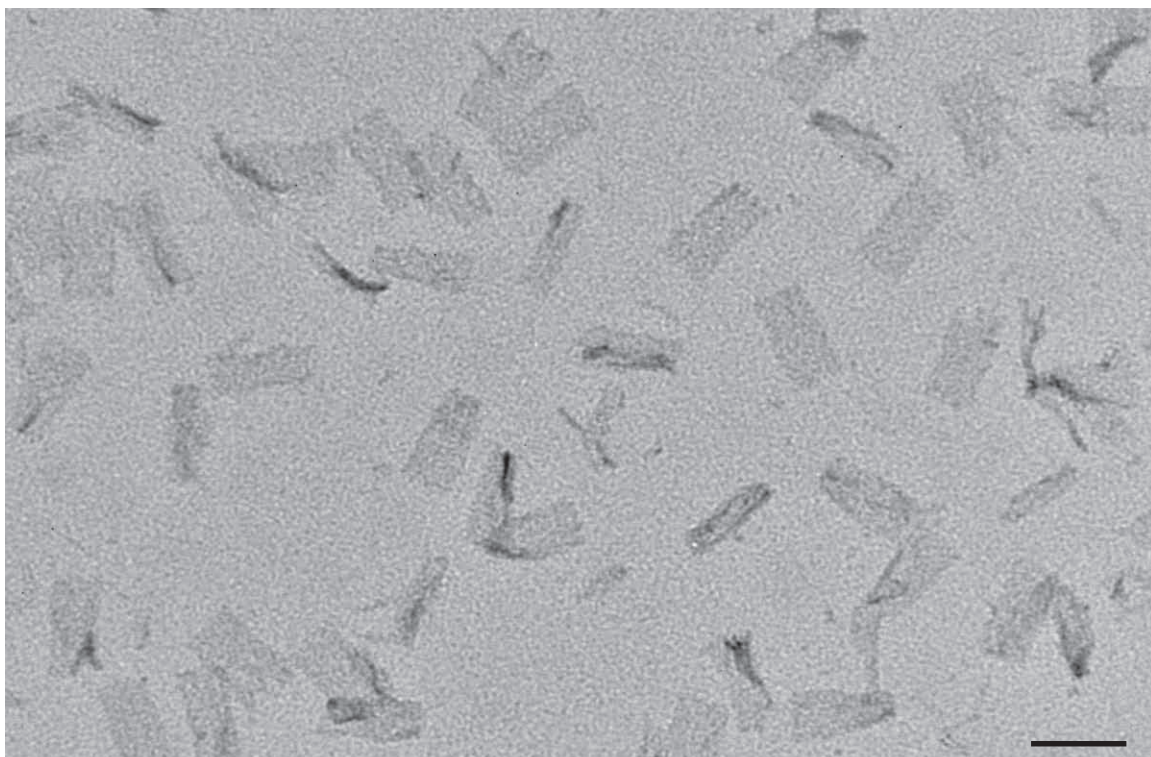


**Figure SI51. TEM image of the 24H×29T structure made from motif 4.1 (scale bar: 100 nm).**

## SI2.5 AFM-based landing assay results

Figs. SI52-SI56 show the results of the AFM-based landing assays for structures made from different motifs with a size of  $24\text{H} \times 28\text{T}$  (motif 0) or  $24\text{H} \times 29\text{T}$  (motifs 1, 3.1, 3.2 and 4.1).

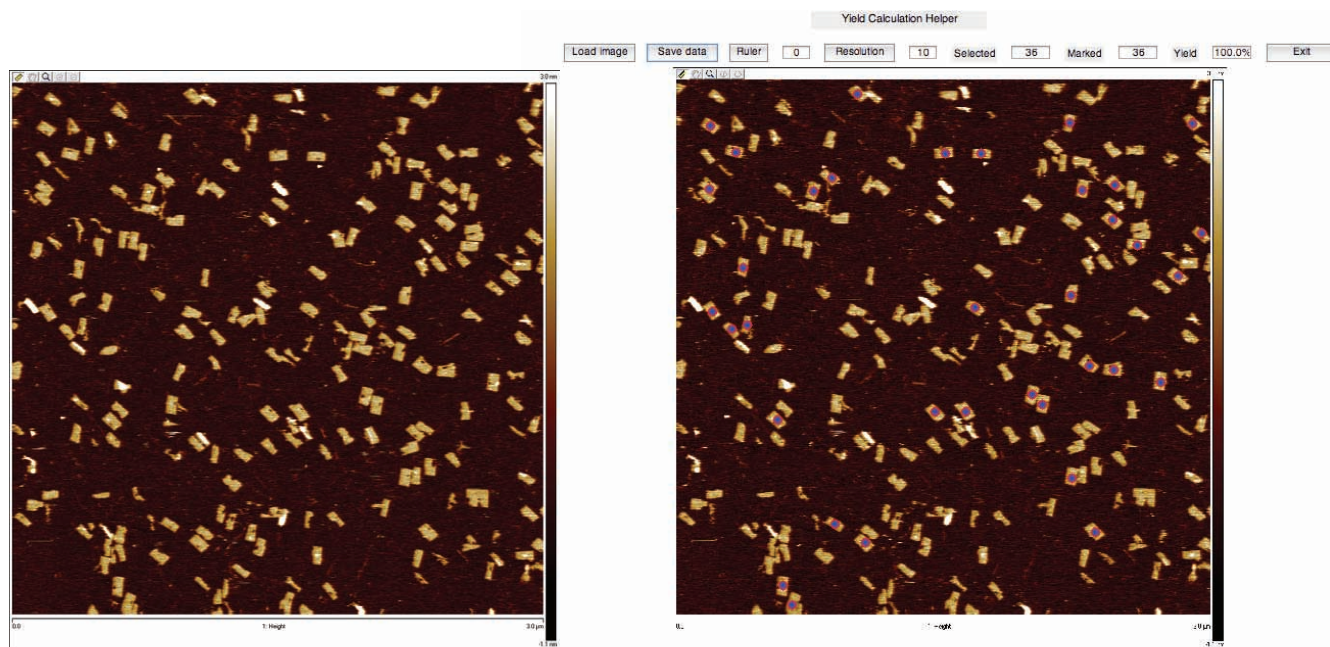


**Figure SI52. AFM-based landing assay for the  $24\text{H} \times 28\text{T}$  structure made from motif 0** (scanning size:  $3\ \mu\text{m} \times 3\ \mu\text{m}$ ). **a**, The original AFM image. **b**, The result of the AFM-based landing assay. A structure facing up was marked with a red circle filled with blue color; a structure facing down was marked with an empty red circle. The percentage of the structures facing up (100%) was calculated as a metric for the flatness of the structure.

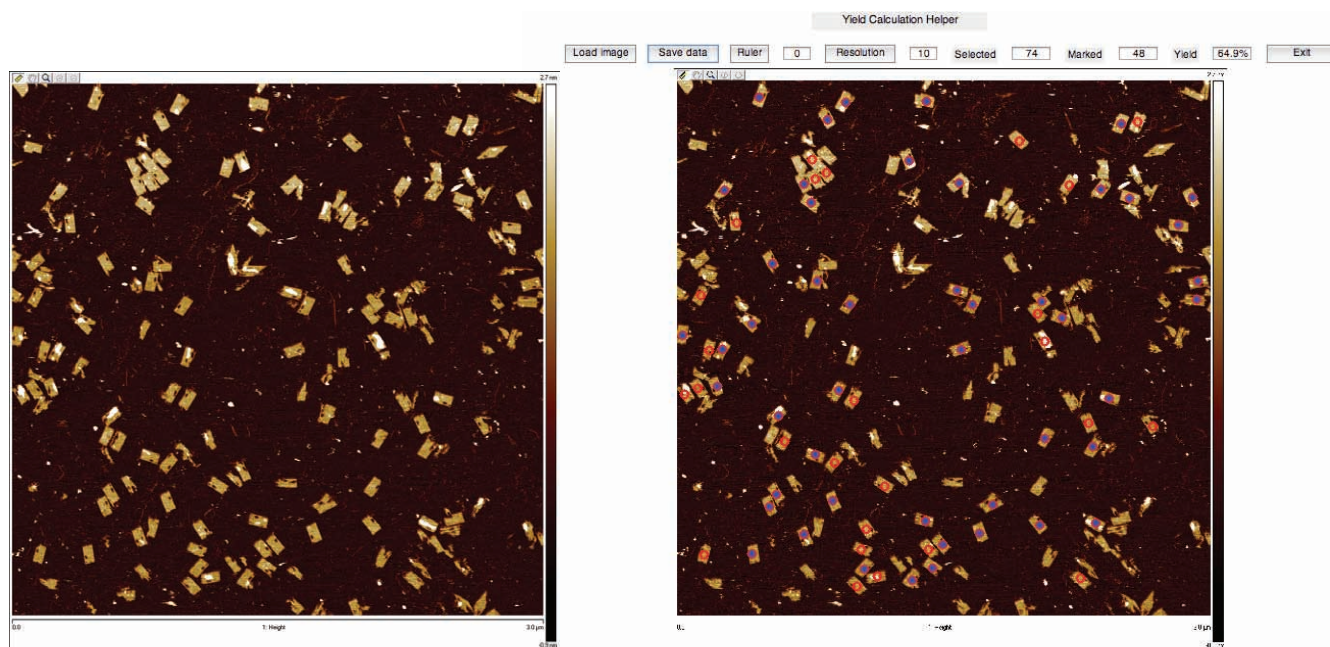


**Figure SI53. AFM based landing assay for the  $24\text{H} \times 29\text{T}$  structure made from motif 1** (scanning size:  $3\ \mu\text{m} \times 3\ \mu\text{m}$ ). **a**, The original AFM image. **b**, The result of the AFM-based landing assay. A structure facing up was marked with a red circle filled with blue color; a structure facing down was marked with an empty red circle. The percentage of the structures facing up (65%) was calculated as a metric for the flatness of the structure.

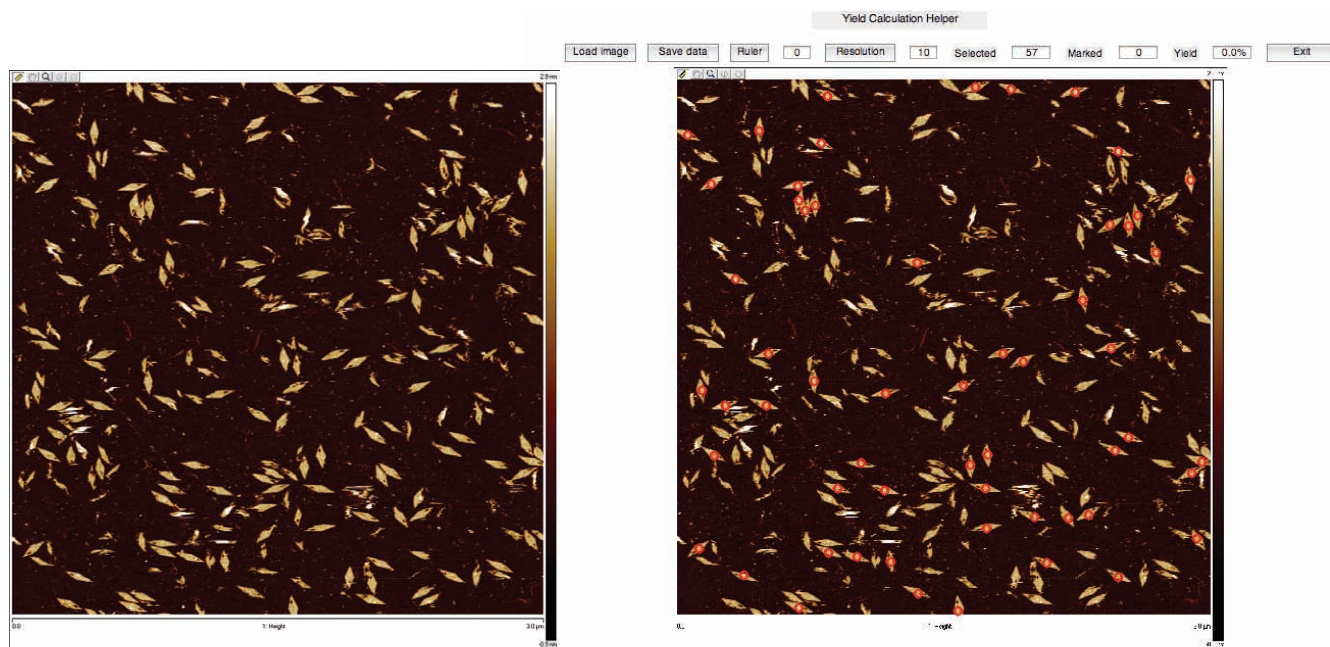


**Figure SI54.** AFM based landing assay for the  $24H \times 29T$  structure made from motif 3.1 (scanning size:  $3 \mu\text{m} \times 3 \mu\text{m}$ ). **a**, The original AFM image. **b**, The result of the AFM-based landing assay. A structure facing up was marked with a red circle filled with blue color; a structure facing down was marked with an empty red circle. The percentage of the structures facing up (0%) was calculated as a metric for the flatness of the structure.

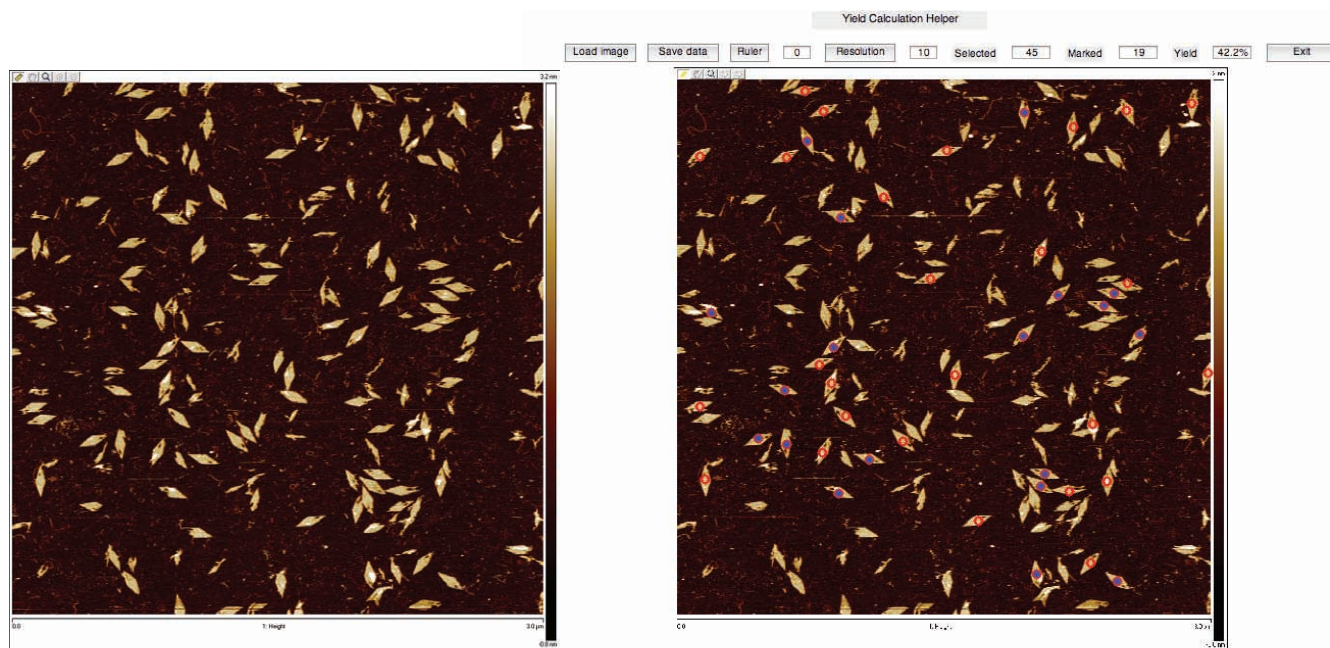


**Figure SI55.** AFM based landing assay for the  $24H \times 29T$  structure made from motif 3.2 (scanning size:  $3 \mu\text{m} \times 3 \mu\text{m}$ ). **a**, The original AFM image. **b**, The result of the AFM-based landing assay. A structure facing up was marked with a red circle filled with blue color; a structure facing down was marked with an empty red circle. The percentage of the structures facing up (42%) was calculated as a metric for the flatness of the structure.

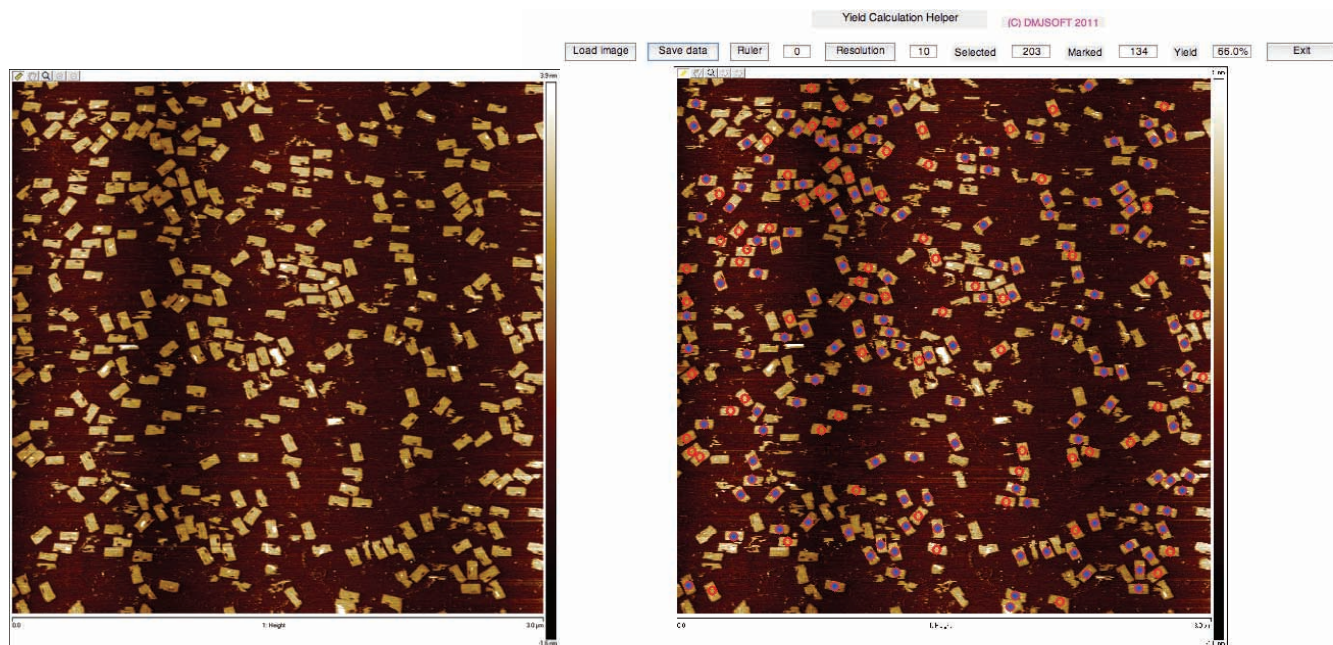


**Figure SI56. AFM based landing assay for the 24H×29T structure made from motif 4.1** (scanning size:  $3\ \mu\text{m} \times 3\ \mu\text{m}$ ). **a**, The original AFM image. **b**, The result of the AFM-based landing assay. A structure facing up was marked with a red circle filled with blue color; a structure facing down was marked with an empty red circle. The percentage of the structures facing up (66%) was calculated as a metric for the flatness of the structure.

## SI2.6 Summary

Fig. SI57 summaries results from different assays of curvature characterization.

	Predicted overall curvature (°)	Predicted curvature per double helix (°)	Width under TEM (nm)	Front side percentage in landing assay	Width under super-resolution imaging (nm)
Motif 0	720	30	16±2 (N=10)	100%	0
Motif 1	-96	-8	38±4 (N=10)	65%	27
Motif 3.1	-408	-17	23±2 (N=10)	0	31
Motif 3.2	0	0	54±2 (N=10)	42%	45
Motif 4.1	0	0	56±1 (N=10)	66%	45

Figure SI57. Summary of curvature characterization.

## SI3 Twist analysis

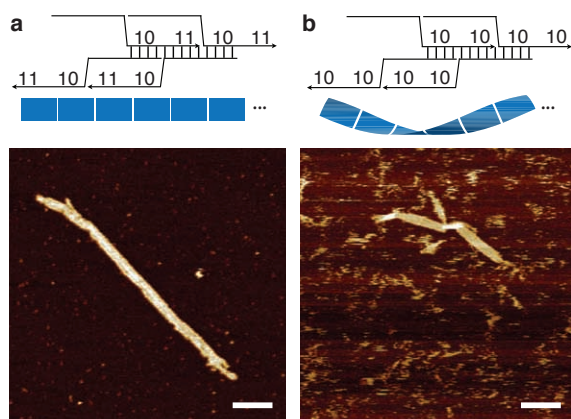
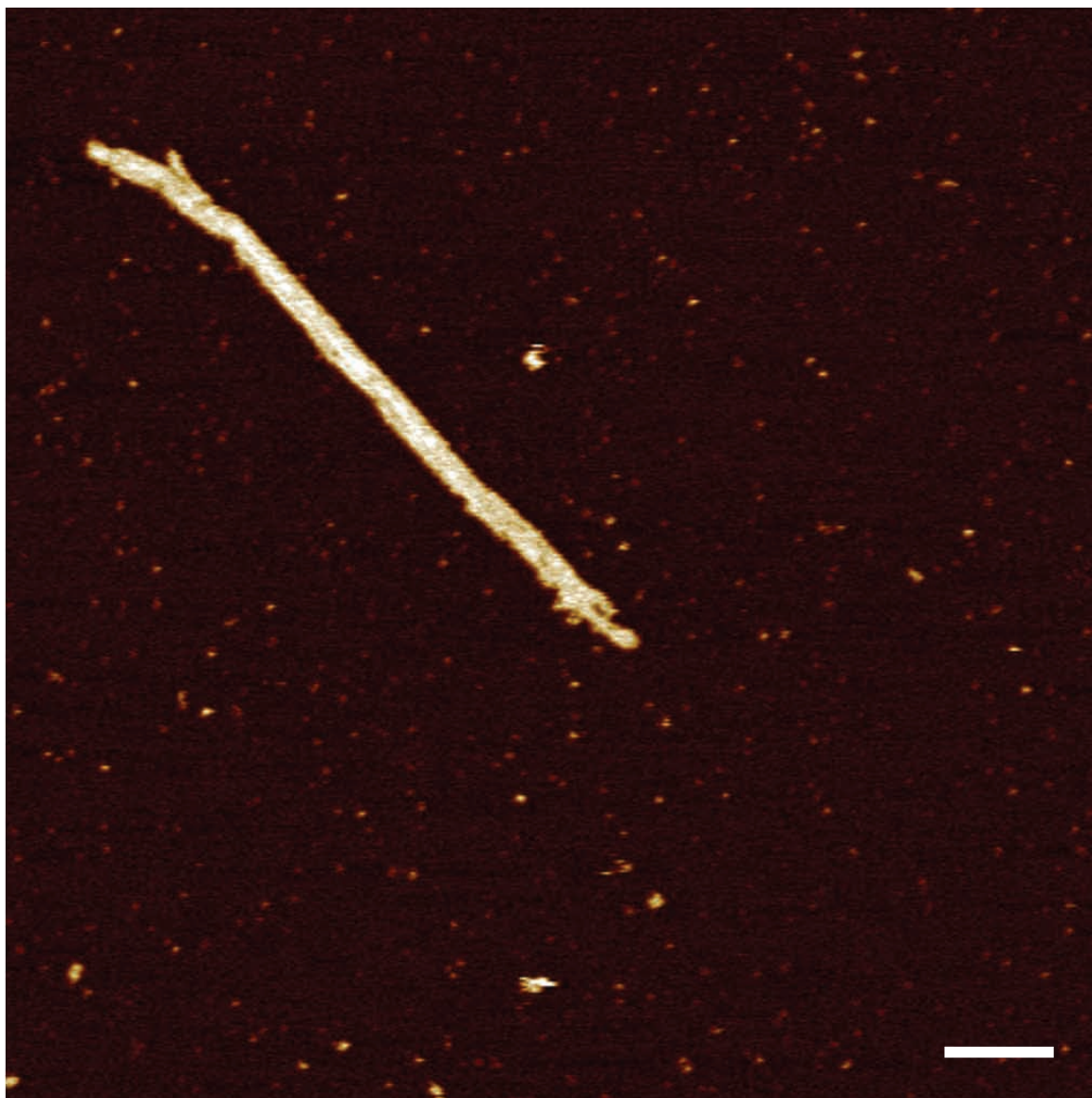


Figure SI58. Characterization of the twist of structures. (a and b) show twist-free polymers made from motif 4.1 and twisted polymers from motif 4.2, respectively. Top panel: schematics of the extended polymer structure. Bottom panel: AFM image. Scale bar: 50 nm.

### SI3.1 AFM imaging results

Figs. SI59-SI60 show the AFM images for polymer made from motifs 4.1 and 4.2, respectively.



**Figure S159.** AFM image of extension along helical axis direction for the  $10H \times 11T$  structure made from motif 4.1 (scale bar: 100 nm).

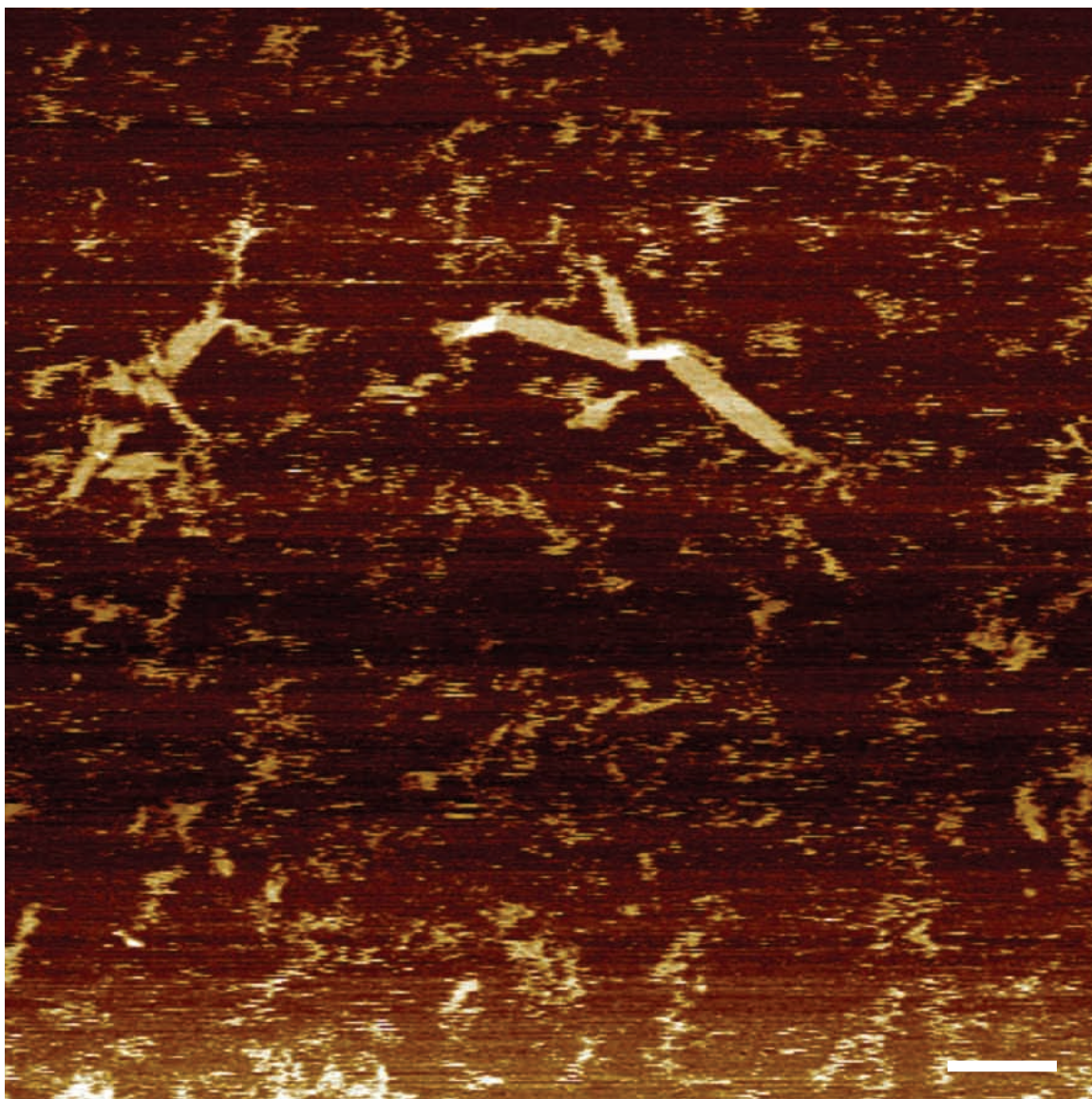


**Figure S160.** AFM image of extension along helical axis direction for 10H×11T structure made from motif 4.2 (scale bar: 100 nm).

### SI3.2 TEM imaging results

Figs. SI61-SI62 show the TEM images for polymer made from the structures formed from motifs 4.1 and 4.2 respectively.

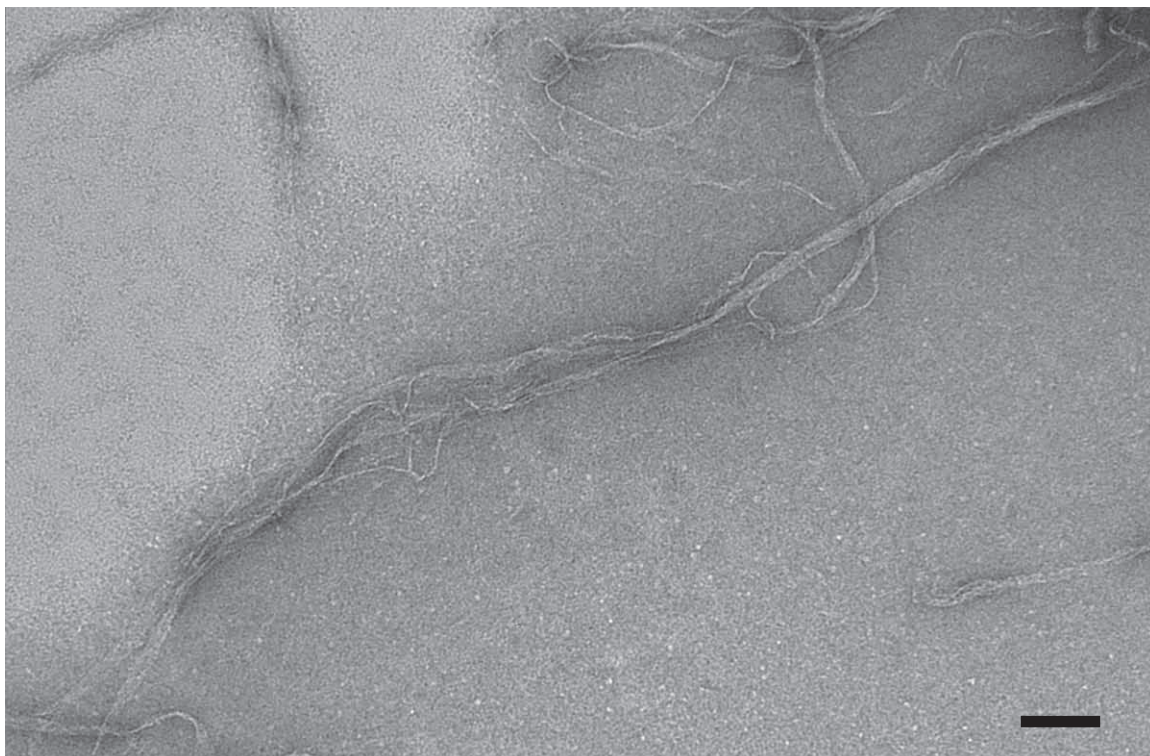


**Figure SI61. TEM image of extension along helical axis direction for 10H×11T structure made from motif 4.1 (scale bar: 100 nm).**

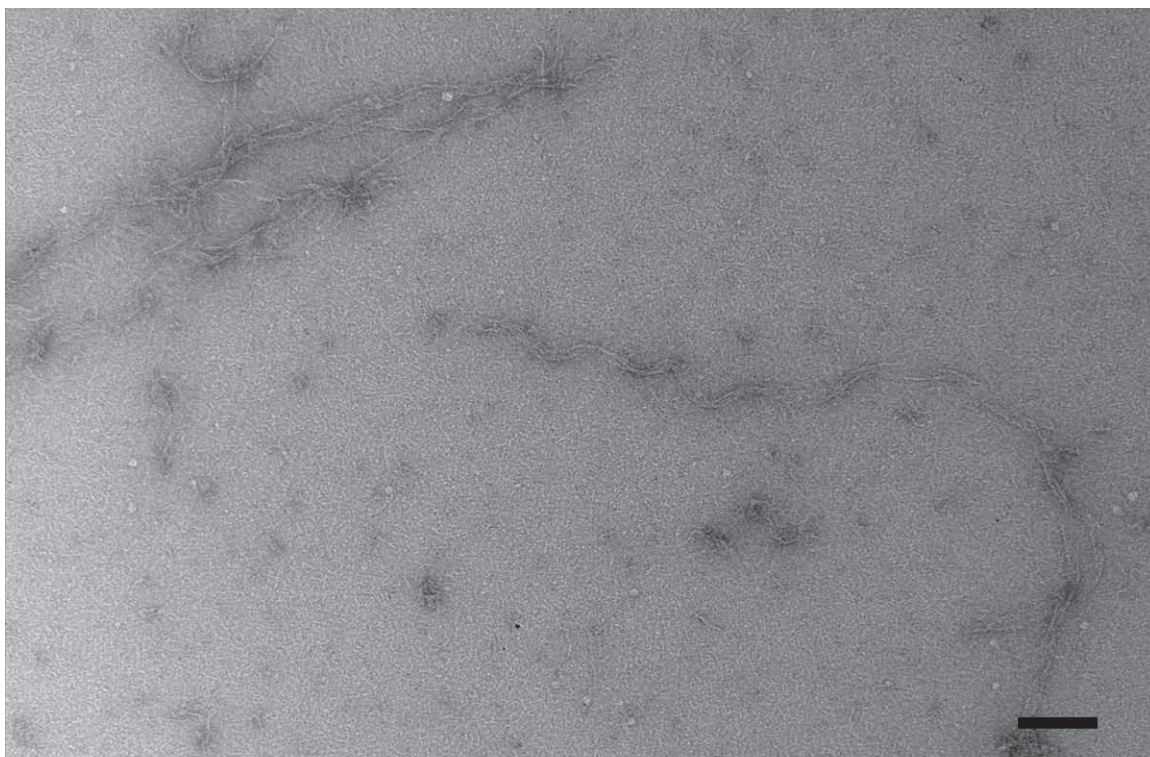


**Figure SI62. TEM image of extension along helical axis direction for 10H×11T structure made from motif 4.2 (scale bar: 100 nm).**